



Dissertation

Quasiparticle description of the hot and dense quark-gluon plasma

ausgeführt zum Zwecke der Erlangung des akademischen Grades
eines Doktors der technischen Wissenschaften unter der Leitung von

Ao. Univ.-Prof. Dr. Anton Rebhan
Institutsnummer: E 136
Institut für Theoretische Physik

eingereicht an der Technischen Universität Wien
Fakultät für Technische Naturwissenschaften und Informatik

von

Dipl.-Ing. Paul Romatschke
Matrikelnummer: 9625501
Pilgramgasse 13/28, A-1050 Wien

5.11.2003

Datum

A handwritten signature in black ink, appearing to read 'Paul Romatschke', written over a horizontal line.

Unterschrift

For my Parents

Deutsche Kurzfassung

Elementarteilchen, die sich in einem Plasma bewegen, haben aufgrund ihrer Wechselwirkung mit dem Medium Eigenschaften, die sich von jenen im Vakuum unterscheiden: man spricht von Quasiteilchen oder allgemeiner von kollektiven Moden des Plasmas. Ähnlich wie die Elementarteilchen im Vakuum sind die Quasiteilchenanregungen für ein Medium charakteristisch und erlauben die Beschreibung einer Vielzahl seiner Eigenschaften. In dieser Arbeit werden die kollektiven Moden der Quantentheorie der starken Wechselwirkung (Quantenchromodynamik) bei Temperaturen und Dichten, die über deren Phasenübergang liegen, analysiert. Auf die dadurch gewonnenen Erkenntnisse basierend werden Modelle zur Beschreibung verschiedener Observablen konstruiert und die Aussagen dieser Modelle mit anderen Methoden (soweit vorhanden) verglichen. Im Speziellen werden sowohl isotrope Systeme wie auch solche mit einer Anisotropie im Impulsraum im Rahmen der Hard-Thermal-Loop (HTL)-Näherung studiert und darauf basierend thermodynamische Größen und deren mögliche Anwendung im isotropen, sowie der Stoß-Energieverlust sowohl im isotropen als auch im anisotropen Fall, berechnet.

Für isotrope Systeme werden insbesondere Aussagen bei endlichen Dichten (bzw. nichtverschwindendem chemischen Potential der Quarks) basierend auf einer phenomenologischen Beschreibung der Resultate von Gitterrechnungen bei verschwindenden Dichten untersucht und diese mit anderen Methoden verglichen. Es zeigt sich, dass die Resultate für den thermodynamischen Druck und die Entropie sowie für die Quark-Suszeptibilitäten gut mit anderen Gitterrechnungen übereinstimmen und auch der Plasmon-Effekt – welcher verheerende Wirkung für die Konvergenz von strikt störungstheoretischen Rechnungen hat – im Falle von Quasiteilchenmodellen zu numerisch kleinen Korrekturen führt. Als mögliche Anwendungen dieser Resultate werden die Massen-Radien Beziehungen von sogenannten Quark-Sternen sowie die hydrodynamische Expansion eines Quark-Gluon-Plasmas nach einer Schwerionenkollision im Rahmen des Bjorken-Modells berechnet.

Bei Systemen mit anisotropen Impulsverteilungen zeigt sich, dass außer den stabilen Quasiteilchenmoden noch weitere, instabile Moden auftreten, die für die dynamische Entwicklung eines unvollständig thermalisierten Quark-Gluon-Plasmas potentiell von großer Bedeutung sind, da diese exponentiell anwachsen-

den Feldamplituden entsprechen. Es wird in der Folge gezeigt, dass solche Instabilitäten durch die damit einhergehenden Singularitäten im Propagator in der störungstheoretischen Berechnung von Streuamplituden zu Divergenzen führen, was den Zusammenbruch solcher Rechnungen signalisiert. Andererseits wird explizit gezeigt, dass zumindest eine Observable, nämlich der Stoß-Energieverlust, frei von diesen Divergenzen ist. Dies ermöglicht dessen Berechnung auch für anisotrope Systeme, wie analytisch für schwache und extrem starke Anisotropien bewiesen wird. Ein Vergleich der Resultate für den Stoß-Energieverlust von isotropen und anisotropen Systemen zeigt, dass dieser in anisotropen Systemen eine zum Teil stark nichttriviale Richtungsabhängigkeit besitzt, was zu möglicherweise beobachtbaren Effekten führen kann.

Abstract

The collective modes of QCD at temperatures and densities above its phase-transition are analyzed; models for various observables based on the knowledge gained from this analysis are constructed, and the results derived are compared to those of other methods, where available. Specifically, isotropic systems as well as systems having an anisotropy in momentum-space are investigated using the Hard-Thermal-Loop (HTL) approximation. Several observables are calculated, ranging from thermodynamic quantities and their application in the isotropic case to the collisional energy loss in the isotropic as well as the anisotropic case.

For isotropic systems, results at finite densities (or non-vanishing quark chemical potential) based on a phenomenological description of lattice calculations at vanishing densities are derived and compared to those following from different methods. It is shown that results for the thermodynamic pressure and entropy as well as those for the quark-number susceptibilities agree well with independent lattice calculations, and it is demonstrated that the plasmon effect leads to numerically small contributions, in contrast to what is found in strictly perturbative approaches. As possible applications of the resulting equation of state the mass-radius relationship of so-called quark-stars as well as the hydrodynamic expansion in the Bjorken model of the quark-gluon plasma created through a heavy-ion collision are calculated.

It is shown that systems with anisotropic momentum-space distributions contain unstable modes in addition to the stable quasiparticle modes, which – since they correspond to exponentially growing field amplitudes – may be of great importance for the dynamical evolution of an incompletely thermalized quark-gluon plasma. Moreover, the presence of such instabilities and the corresponding singularities in the propagator lead to divergences of scattering amplitudes in a perturbative framework, signalling the breakdown of the latter. However, it is demonstrated that at least one observable, namely the collisional energy loss, is protected from these divergencies. This permits its calculation also for anisotropic systems, as can be shown analytically both for very weak as well as for extremely strong anisotropies. A subsequent comparison of results from isotropic and anisotropic systems exhibits a possibly strong directional dependence of the energy loss for the latter, which might lead to effects that can be verified experimentally.

Acknowledgements

This dissertation in its present form would not have been possible without the help and support I received from several people, to some of whom I would like to express my gratitude here. First of all I want to thank my parents Kurt and Helga who made my doctoral studies possible in the first place through their continuous moral and financial support and to whom I have dedicated this dissertation. Also, I want to warmly thank my supervisor Anton Rebhan and my collaborator Mike Strickland who's suggestions and help never failed me when lengthy equations stubbornly obscured the physics instead of revealing it. Moreover, I'd like to thank my colleagues and friends Jean-Paul Blaizot, Andreas Gerhold, Edmond Iancu, Andreas Ipp, Urko Reinoso and Dominik Schwarz for countless interesting discussions and help on various problems. Last but not least, I'd like to thank my girlfriend Ulli for her love and understanding during the past months when I was either physically abroad at a conference or mentally absent when figuring out an integral. Finally I want to apologize to all the friends and colleagues not named here explicitly and assure them of my warmest gratitude, as well as to all those people I have failed to call back in the last months and who still miraculously seem to be talking to me.

PAUL ROMATSCHKE, Vienna 2003

Contents

Deutsche Kurzfassung	v
Abstract	vii
Acknowledgements	ix
1 Introduction	1
1.1 Quantum chromodynamics	1
1.2 The deconfinement transition	3
1.3 The quark-gluon plasma	4
1.4 The QCD pressure	5
1.4.1 Vanishing chemical potential	5
1.4.2 Finite chemical potential	8
1.5 Anisotropic systems	9
1.6 Outline of this work	10
2 QCD Quasiparticles	11
2.1 The gluon propagator in the HTL approximation	11
2.2 The fermion propagator in the HTL approximation	14
2.3 Simple quasiparticle model for the EOS	15
2.3.1 Properties of the flow equation	17
2.4 Summary	18
3 The HTL quasiparticle model	19
3.1 The entropy of the QCD plasma	19
3.1.1 Approximately self-consistent solutions	21
3.2 The HTL quasiparticle model	22
3.3 Modeling the lattice entropy and pressure	23
3.4 Solving the flow equation	25
3.5 The pressure at finite chemical potential	27
3.6 Summary	29

4	The QCD EOS for arbitrary μ and completion of plasmon effect	31
4.1	NLO quasiparticle models	32
4.2	Fitting lattice data at $\mu = 0$	33
4.3	Results for small chemical potential	35
4.3.1	Susceptibilities	35
4.3.2	Lines of constant pressure	36
4.4	Large chemical potential	38
4.4.1	EOS for cold deconfined matter	39
4.5	Application 1: Quark stars	40
4.6	Application 2: Expansion of the quark-gluon plasma	41
4.7	Summary	43
5	Results independent of the lattice	45
5.1	Setup	45
5.2	Results	46
5.2.1	Notes on changing $T_c/\Lambda_{\overline{\text{MS}}}$	48
5.3	Summary	49
6	The anisotropic quark-gluon plasma	51
6.1	Gluon self-energy in an anisotropic system	51
6.1.1	Tensor decomposition	54
6.1.2	Self-energy structure functions	55
6.1.3	Evaluation of the structure functions	57
6.1.4	The quark propagator in an anisotropic system	58
6.2	Collective modes of an anisotropic quark-gluon plasma	58
6.2.1	Static limit	58
6.2.2	Stable modes	60
6.2.3	Unstable modes	61
6.3	Small ξ limit	62
6.3.1	Static Limit	63
6.3.2	Collective modes	63
6.4	Large ξ limit	63
6.5	$\xi \rightarrow -1$ limit	65
6.6	Discussion of instabilities	66
6.7	Summary	67
7	Energy loss of a heavy parton	69
7.1	Soft contribution and effect of instabilities	70
7.1.1	Dynamical shielding of instabilities	71
7.1.2	Application of dynamical shielding	73
7.1.3	Behavior of the soft part	74
7.2	Hard Contribution	76
7.2.1	Behavior of the hard part	78

CONTENTS

xiii

7.3	Isotropic results	79
7.3.1	Limitations	80
7.4	Anisotropic results	80
7.5	Effects of finite chemical potential	81
7.6	Summary	82
8	Conclusions and outlook	83
A	Coefficients for the HTL coupling flow equation	87
B	Analytic expressions for structure functions	89
	Bibliography	91
	Curriculum vitae	100

There is a theory which states that if ever anyone discovers exactly what the Universe is for and why it is here, it will instantly disappear and be replaced by something even more bizarre and inexplicable.

There is another theory which states
that this has already happened.

DOUGLAS ADAMS, *The Hitch Hiker's Guide to the Galaxy II*

Chapter 1

Introduction

1.1 Quantum chromodynamics

Today, quantum chromodynamics (QCD) is accepted to be the established theory of strong interactions. It has been formulated along the lines of the theory of quantum electrodynamics (QED), which – as the unification of quantum theory and electrodynamics – is certainly one of the most successful and accurate theories in modern physics. Consequently, QCD bears several similarities but also exhibits some striking differences with respect to QED, as will be briefly illustrated in the following. Both theories are gauge field theories, but whereas QED is an Abelian gauge theory with the gauge group $U(1)$, quantum chromodynamics is non-Abelian in nature, having the color group $SU(3)$ as a gauge group. The gauge boson associated with the $U(1)$ group of QED is the well-known *photon*, while for the color group $SU(3)$ there are 8 associated gauge bosons called *gluons*. In contrast to the photon which is uncharged, the gluons do carry color charges which are the QCD equivalents of the electromagnetic charge. For QED, the matter particles are the *electron*, *muon* and *tauon* while for QCD there are the six quark species *up*, *down*, *strange*, *charm*, *beauty* and *top*, which are all spin 1/2 fields or fermions; those quark species (or flavors) with masses much smaller than the energy scale under consideration are referred to as *active* or light flavors and their number is usually denoted by N_f .

Both QED and QCD are renormalizable field theories and as a consequence their coupling “constants” are functions of the energy scale Q . In Abelian gauge theories (as QED) the coupling increases for larger energy scales, whereas for low energies it turns out to be small, allowing a valid (and indeed extremely accurate) description of our (low energy) everyday world using perturbation theory.

However, unlike in Abelian gauge theories, the non-Abelian nature of QCD makes its coupling constant $\alpha_s(Q)$ *decrease* as Q becomes large, a property that is known as asymptotic freedom. Consequently, at very high energies one may hope that perturbation theory offers a valid description of QCD since the coupling

constant gets tiny. On the other hand, when the energy scale gets smaller and the coupling constant rises, calculating observables in QCD becomes very hard in general, since one has to deal with a strongly coupled theory and perturbation theory breaks down. Therefore, one obviously needs non-perturbative methods to describe the theory and explain the experimental fact that at very low energies quarks and gluons cannot roam freely but are *confined* into hadrons from which they do not escape.

While at low temperatures quarks and gluons are thus locked up mainly inside *protons* and *neutrons*, one expects them to propagate freely in a state that has been dubbed the *quark-gluon plasma* at very high temperatures. The exact nature of this transition between the confined phase and the quark-gluon plasma phase (whether it is a first or second order phase transition or a crossover) is still a matter of active research.

Several theoretical methods have been proposed to study the physics of QCD, each most apt for a certain energy range, the most popular being:

- Effective models based on the QCD Lagrangian that allow to calculate the low-energy behavior of the theory. Perhaps the most interesting of these is chiral perturbation theory, based on the effective chiral Lagrangian (see GASSER's and LEUTWYLER's original articles on this subject [1, 2] or [3] for a pedagogical review).
- Monte-Carlo simulations of QCD on a lattice, which so far is the only method to provide quantitative results for the intermediate energy range near the deconfinement transition. Since simulations with dynamical quarks are much more time consuming than those without, the situation best studied in lattice QCD is that of a pure gauge theory. Nevertheless, there has also been considerable progress for systems with quarks and recently even for non-vanishing chemical potential. The latter in general poses a major problem for lattice calculations because of the *sign problem*, which prohibits the use of conventional numerical algorithms (see KARSCH [4] for a pedagogical review).
- Perturbative approaches, which are expected to be most accurate for very high energies. For instance, there exist several methods to calculate the equation of state for the quark-gluon plasma phase; a short review on this subject will be given in section 1.4.

On the experimental side, the main earth-based tool to investigate QCD near or above the phase transition is ultrarelativistic particle collisions. The study of these makes huge collider facilities necessary, such as those of CERN (*Centre Européenne pour la Recherche Nucléaire*) in Switzerland/France and BNL (*Brookhaven National Laboratory*) in the U.S.A. While the SPS (*Super Proton Synchrotron*) collider at CERN produced the first experimental indication of the

existence of the quark-gluon plasma phase, it has currently been dismantled to make way for the next generation collider LHC (*Large Hadron Collider*), which will allow to probe energies well above the phase transition and is due to become operational in 2007. Since 1999, RHIC (*Relativistic Heavy Ion Collider*) is the collider operational at BNL, which has already produced a wealth of new data bringing the study of nucleus-nucleus collisions carried out at SPS to a new energy regime.

Finally, indirect studies of QCD may be possible through astrophysical observations and cosmology [5].

1.2 The deconfinement transition

Our current understanding of QCD is such that whenever the system under consideration becomes sufficiently hot and/or dense, hadrons dissolve into a gas of almost free quarks and gluons, the quark-gluon plasma. More precisely, either the temperature T , or the quark chemical potential μ , or a combination of both, has to be big enough so that the system undergoes a transition to the deconfined state of matter. In a slight abuse of terminology, one refers to the temperature and chemical potential, for which the system undergoes the transition, as critical temperature T_c and critical chemical potential μ_c , regardless of the exact nature of the transition (first/second order phase transition or crossover).

At vanishing chemical potential, lattice studies of QCD tell us that the critical temperature is on the order of a few hundred MeV, which is much smaller than the masses of the charm, beauty and top quark. For this reason, those heavy quarks do not play a role in the description of the physics near the deconfinement transition, so it is useful to limit the number of active (=light) quark flavors to $N_f = 3$. Moreover, since the up and down quark masses are so small compared to the energy scale of the deconfinement transition, these quarks may be taken to be massless. The strange quark, finally, is neither much heavier nor much lighter than the deconfinement scale, so the number of active quark flavors near the deconfinement transition is between two and three, also sometimes denoted as $N_f = 2 + 1$.

Based on universality arguments, it is possible to show that for a pure gauge theory ($N_f = 0$, corresponding to infinitely heavy up, down and strange quarks) as well as for three and more active flavors ($N_f \geq 3$, corresponding to zero up, down and strange quark masses) the deconfinement transition should be a first-order phase transition. For $N_f = 2$, the transition is probably a second order phase transition, but the situation is not entirely clear [6]. Fig. 1.1 shows a cartoon of our current knowledge about the nature of the deconfinement transition at vanishing chemical potential, indicating that for light up and down quarks and a moderately heavy strange quark the transition is probably a second order phase transition, though a cross-over cannot be ruled out either.

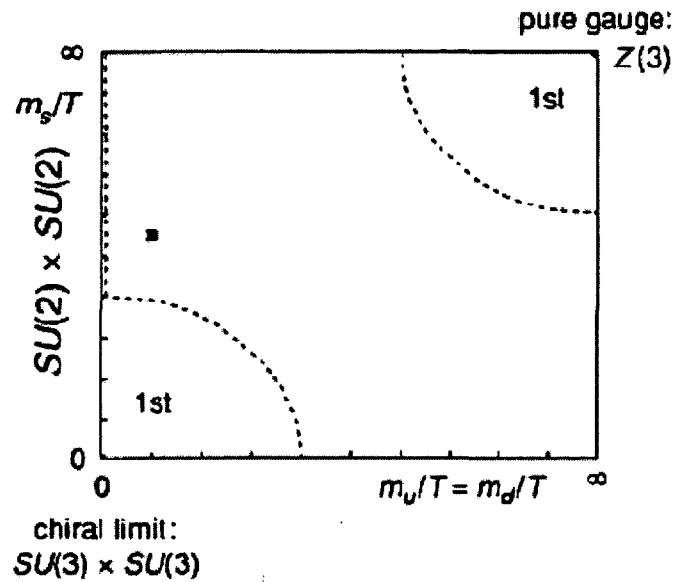


Figure 1.1: Character of the transition as a function of the light quark masses $m_u = m_d$ and the strange quark mass m_s . The dot represents the physical values of the parameters. From [6].

The value of the critical temperature has been studied intensively in lattice QCD calculations at $\mu = 0$, giving [7, 4]

- $T_c = 271 \pm 2$ MeV for $N_f = 0$
- $T_c = 171 \pm 4$ MeV and $T_c = 173 \pm 8$ MeV for $N_f = 2$, depending on whether one uses Wilson or staggered fermion lattice implementations
- $T_c = 154 \pm 8$ MeV for $N_f = 3$.

1.3 The quark-gluon plasma

The quark-gluon plasma phase is unlike any of the other phases we know of in nature: it is a new state of matter, on equal footing with solid, fluid, gaseous and the electromagnetic plasma, which makes its study interesting from a conceptual point of view already. Furthermore, from standard cosmology we expect that the quark-gluon plasma was the prevailing form of matter until about 10^{-5} seconds after the Big Bang, which could have interesting implications on the universe. Nowadays, it is expected to be produced only in ultrarelativistic heavy-ion collisions, and perhaps reside in the core of heavy neutron stars, which might have interesting astrophysical consequences. For these reasons, one would like to know more about the properties of this state of matter, especially since ultrarelativistic

heavy-ion collision measurements in the next decade may allow to verify these predictions experimentally.

One of these properties is the equation of state (EOS) of the quark-gluon plasma; once the latter is created through the collision of two ultrarelativistic nuclei, the expansion of the "fireball" is controlled mainly by the EOS. Also, the EOS specifies the mass-radius relation of so-called quark-stars through the Tolman-Oppenheimer-Volkoff equations.

The EOS itself follows from the pressure $p(T, \mu)$ (which is related to the thermodynamic potential $\Omega = -pV$) through the standard thermodynamic equations

$$s = \frac{dp}{dT}, \quad n = \frac{dp}{d\mu}, \quad \epsilon = -p + sT + n\mu, \quad (1.1)$$

where s , n and ϵ are the entropy, number and energy density, respectively; from these, the energy density is given as a function of the pressure only, $\epsilon = \epsilon(p)$, which is one representation of the EOS. As a consequence, knowledge of the pressure for arbitrary temperature and chemical potential automatically implies the EOS.

1.4 The QCD pressure

Since the QCD coupling becomes small because of asymptotic freedom, one could expect that weak coupling calculations at high temperature T or chemical potential μ lead to reasonable estimates of the thermodynamic pressure of QCD. To zeroth order in the coupling (where the quark-gluon plasma would correspond to an ideal gas of quarks and gluons), the pressure takes the form

$$p_0 = \frac{(N^2 - 1)\pi^2 T^4}{45} + NN_f \left(\frac{7\pi^2 T^4}{180} + \frac{\mu^2 T^2}{6} + \frac{\mu^4}{12\pi^2} \right), \quad (1.2)$$

where N_f is the number of massless quark-flavors and $N = 3$ is the number of colors [8]. The first correction to this result (which itself corresponds to black-body radiation in electrodynamics) is of first order in α_s and given by

$$p_2 = -N(N^2 - 1) \frac{\alpha_s \pi T^4}{36} - (N^2 - 1) N_f \frac{\alpha_s (N^2 - 1) \pi}{144} \left(5T^4 + 18 \frac{m u^2 T^2}{\pi^2} + \frac{9\mu^4}{\pi^2} \right). \quad (1.3)$$

1.4.1 Vanishing chemical potential

To simplify the argument, consider the chemical potential to be zero for the moment, so that the pressure is proportional to T^4 and all the non-trivial temperature behavior of p/T^4 resides in the temperature dependence of the strong

coupling α_s . The standard procedure is to take the solution for the running coupling from the renormalization group equation, which to lowest (1-loop) order is given by

$$\alpha_s(\bar{\mu}) = \frac{12\pi}{(11N - 2N_f) \ln \bar{\mu}^2 / \Lambda_{\overline{\text{MS}}}^2}, \quad (1.4)$$

and put the renormalization point $\bar{\mu}$ proportional to the first Matsubara frequency, $\bar{\mu} = c_{\bar{\mu}} 2\pi T$, which for massless quarks is the only dimensionfull quantity inherent to the theory. The parameter $c_{\bar{\mu}}$ expresses our ignorance about the ideal renormalization point and is usually varied by a factor of two to obtain an estimate of how strongly the result depends on this chosen renormalization point; obviously, one would prefer the result to have as little dependence as possible on the arbitrary parameter $c_{\bar{\mu}}$. The strong coupling α_s also depends on the scale parameter of the modified minimal subtraction scheme, $\Lambda_{\overline{\text{MS}}}$, which cannot be fixed by theoretical considerations but has to come from experiments. However, α_s is not easily measured at energy scales near the deconfinement transition, so one has to extrapolate measurements down from higher energies. Currently, the official extrapolation value at $\bar{\mu} = 2 \text{ GeV}$ is given by [9]

$$\alpha_s(\bar{\mu} = 2\text{GeV}) = 0.2994; \quad (1.5)$$

since from the choice of $\bar{\mu} \simeq 2\pi T$ this corresponds to a temperature where one expects up, down and strange quarks to be effectively massless ($N_f = 3$), this would fix $\Lambda_{\overline{\text{MS}}}^{(3)} \simeq 194 \text{ MeV}$. However, by using a higher order correction to the running coupling (2-loop),

$$\alpha_s(\bar{\mu}) = \frac{12\pi}{(11N - 2N_f)\bar{L}(\bar{\mu})} \left(1 - \frac{(34N^2 - 13NN_f + 3N_f/N) \ln \bar{L}(\bar{\mu})}{6(11N - 2N_f)^2 \bar{L}(\bar{\mu})} \right) \quad (1.6)$$

where $\bar{L}(\bar{\mu}) = \ln \bar{\mu}^2 / \Lambda_{\overline{\text{MS}}}^2$, the value of $\Lambda_{\overline{\text{MS}}}$ changes to $\Lambda_{\overline{\text{MS}}}^{(3)} \simeq 378 \text{ MeV}$ and adopting a 3-loop running coupling, one finds $\Lambda_{\overline{\text{MS}}}^{(3)} \simeq 344 \text{ MeV}$. One could still improve on this result by taking into account matching conditions between the different quark mass scales [10] as well higher order (e.g. 4-loop [11]) beta-functions for the running coupling; however, being interested in a rough estimate only, one can naively use the critical temperature $T_c \sim 154 \text{ MeV}$ for $N_f = 3$ to obtain the ratio $T_c / \Lambda_{\overline{\text{MS}}}^{(3)} \sim 0.45$, which turns out to be reasonably close to the value for two active flavors advocated by GUPTA [12],

$$\frac{T_c}{\Lambda_{\overline{\text{MS}}}^{(2)}} = 0.49. \quad (1.7)$$

Therefore, I will adopt this ratio for all the two-flavor calculations in the following. Clearly, if a different value is adopted, some quantitative results in

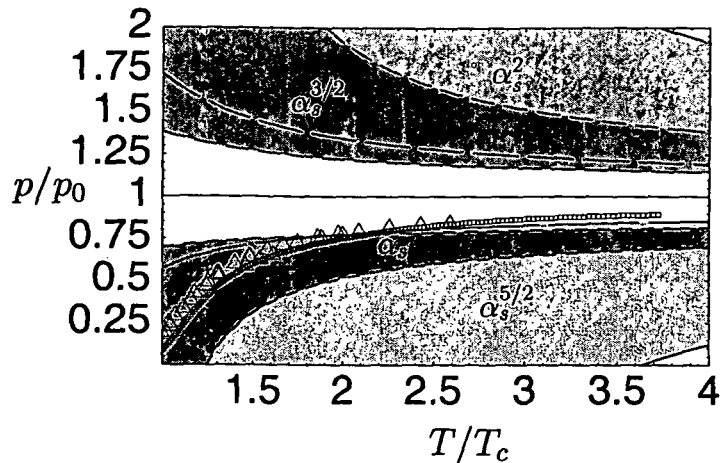


Figure 1.2: Strictly perturbative results for the thermal pressure of $N_f = 2$ QCD, normalized to the ideal-gas value p_0 , as a function of T/T_c (assuming $T_c/\Lambda_{\overline{\text{MS}}} = 0.49$). The various gray bands bounded by differently dashed lines show the perturbative results to order α_s , $\alpha_s^{3/2}$, α_s^2 and $\alpha_s^{5/2}$, with the $\overline{\text{MS}}$ renormalization point $\bar{\mu}$ varied between πT and $4\pi T$ [16]. The boxes and triangles show the estimated continuum-extrapolated lattice results from [17, 18].

this work will change somewhat, but the qualitative picture remains the same and the modifications to the results should be straightforward (I will also give the trend of the modified result in chapter 5).

Having determined the temperature dependence of the coupling one can proceed to evaluate the perturbative pressure; indeed, explicit calculations of higher order contributions to the pressure have been pushed to $\alpha_s^{5/2}$ [13, 14] and even to $\alpha_s^3 \log \alpha_s$ in a recent heroic effort [15]. The result, however, is rather depressing: instead of showing any sign of convergence, adding successive orders gives a total pressure that is sometimes below, sometimes above the free pressure p_0 , jumping in an nearly unpredictable fashion (see Fig. 1.2). Perhaps worse, the ambiguity introduced by the constant $c_{\bar{\mu}}$ seems to increase for every order added to the pressure, signalling a complete loss of predictive power.

Various mathematical extrapolation techniques have been tried, such as Padé approximants and Borel resummation [19, 20, 21, 22, 23]. The resulting expressions are indeed better behaved than polynomial approximations truncated at order $\alpha_s^{5/2}$ or lower, showing a weaker dependence on the renormalization scale. However, while these methods do improve the situation somewhat, it is fair to say that they offer little physical insight on the source of the difficulty.

However, in recent years resummations based on the hard-thermal-loop (HTL) effective action [24] have been proposed, alternatively in the form of so-called HTL perturbation theory [25, 26] or based upon the 2-loop Φ -derivable approximation

[27, 28, 29] (see also PESHIER [30])¹. The latter approach, which assumes weakly interacting quasiparticles as determined by the HTL propagators and NLO corrections thereof, leads to results which agree remarkably well with lattice data²; more details about this approach will be given later on. Recently, it has also been shown that the results from the HTL quasiparticle models are in fact consistent with those obtained in high-order perturbation theory if the latter is organized through an effective (dimensionally reduced) field theory according to [34] and effective-field-theory parameters are kept without further expanding in powers of the coupling [16], as already advocated in Ref. [15].

1.4.2 Finite chemical potential

In contrast to vanishing chemical potential, where lattice studies seem to be quite capable of calculating the EOS for a quark-gluon plasma near the deconfinement transition, this task is by far more difficult at finite (and especially large) chemical potential. The reason for this is that the quark determinant becomes complex at finite chemical potential μ , so Monte-Carlo simulations cease to be directly applicable [35]; this is known as the sign problem. Recently however, there has been important progress also for lattice calculations³ at non-vanishing μ [37, 38, 39, 35, 40, 41], which circumvent the problem of a complex quark determinant by either a Taylor expansion in μ of the observables at vanishing chemical potential or an analytic continuation of observables calculated at purely imaginary μ . Unfortunately, all these calculations are limited to the case of small chemical potential ($\mu/T \ll 1$) for now, so an EOS for cold dense matter, which is of importance in astrophysical situations [42, 43, 44, 45]) is currently beyond the reach of lattice calculations. Moreover, a recent result for a model of QCD with an infinite number of flavors ($N_f \rightarrow \infty$) indicates that extrapolation of results obtained at $\mu = 0$ breaks down rather abruptly for $\mu/T \gtrsim \pi$, pointing presumably towards a generic obstruction for extrapolating data from small to large chemical potential [46].

As a remedy for this situation, PESHIER *et al.* [42, 43] proposed a method which can be used to map the available lattice data for $\mu = 0$ to finite μ and small temperatures by describing the interacting plasma as a system of massive quasiparticles. Since this procedure does not involve any direct extrapolation, the model proposed by PESHIER and its hard-thermal-loop (HTL) extension which

¹For recent progress with higher-loop Φ -derivable approximations in scalar field theory see Refs. [31, 32, 33].

²This is in fact not the case for 2-loop HTL perturbation theory [26]. However a dimensionally reduced variant [16] of this form of improved perturbation theory (which is perturbatively equivalent and moreover much simpler) has recently been shown to agree well with the results of Refs. [27, 28, 29] and correspondingly also with lattice data.

³A perturbative expansion of the pressure for small chemical potential has also been calculated recently [36].

will be considered later on are generally capable of calculating the EOS for the quark-gluon plasma for any (i.e. also large) value of μ/T , given that the models stay reliable for all temperatures and densities. Accordingly, such quasiparticle models⁴ are a valuable complementary method to e.g. lattice calculations at small chemical potential, and they turn out to give quite robust quantitative predictions on the EOS for cold dense QCD matter as well as on the critical chemical potential.

I will give a detailed discussion of the results for the EOS obtained by these quasiparticle models and also compare with results from other approaches [49, 50, 44, 45].

1.5 Anisotropic systems

So far, all the discussion has been limited to homogeneous and isotropic systems. However, considering that the system created through a collision of two heavy ions propagating essentially at the speed of light is certainly not homogeneous and isotropic, one has to ask whether a description through *equilibrium* field theory actually constitutes a valid treatment of this system. This question can be restated in the form of whether the system *thermalizes* fast enough so that at least at a local scale it can be described by equilibrium field theory. The advent of "bottom-up" thermalization by BAIER, MÜLLER, SCHIFF and SON [51] was a big step towards answering this question, although there are indications that this scheme probably will have to be modified because of more recent developments discussed below.

Despite continuous progress [52, 53, 54, 55], an out-of equilibrium study of QCD has not been achieved yet; however, one may try to learn more about out-of-equilibrium situations by studying systems that are close to equilibrium. For instance, one can consider the effects that an anisotropic momentum-space distribution function has on the thermalization, or more precisely isotropization of a quark-gluon plasma. As has been pointed out first by MRÓWCZYŃSKI [56, 57, 58], such a system possesses instabilities that correspond to so-called Weibel or filamentation instabilities in electrodynamics [59]. WEIBEL showed that unstable transverse modes exist in electrodynamic plasmas with anisotropic momentum distributions and derived their growth rate in linear response theory. In plasma physics, it has been shown that these instabilities generate strong magnetic fields resulting in the filamentation of the electron current by simulations and recently also experimentally [60]. The effects of these instabilities are much less clear, but they may potentially be very important for the quark-gluon plasma evolution at RHIC or LHC due to the large amount of momentum-space anisotropy in the gluon distribution functions at $\tau \sim 1$ fm/c.

⁴See also the model in Ref. [47] which has been extended to finite chemical potential in Ref. [48].

MRÓWCZYŃSKI and RANDRUP recently performed phenomenological estimates of the growth rate of the instabilities for two types of anisotropic distribution functions [61], finding that the degree of amplification of the Weibel instability is not expected to dominate the dynamics of a QGP, but instead is comparable to the contribution from elastic Boltzmann collisions. However, if a large number of the unstable modes could be excited then it is possible that their combined effect on the overall dynamics could be significant.

Moreover, ARNOLD, LENAGHAN and MOORE [62] argued that the presence of instabilities giving rise to large gauge fields necessarily change the first stage of the bottom-up thermalization scenario qualitatively, making a revision of the original scheme unavoidable.

In this work, I will perform a detailed study of the HTL quasiparticles and unstable modes in an anisotropic quark-gluon plasma and discuss their effects on the properties of such a system with respect to an isotropic quark-gluon plasma.

1.6 Outline of this work

In chapter 2, which is still of introductory character, I will give a definition of what I will refer to as quasiparticles and also introduce a simple quasiparticle model for the QCD pressure of the isotropic quark-gluon plasma. In chapter 3, I will introduce resummed perturbation theory based on the 2PI effective action and an extension of the simple quasiparticle model that follows from it. In chapter 4, I will discuss the results one obtains from mapping lattice data from zero to arbitrary chemical potential, including two possible applications. In chapter 5, I will investigate to what extent these results are modified when one limits the input to only the value of $T_c/\Lambda_{\overline{\text{MS}}}$. In chapter 6, I will calculate the HTL resummed gluon self-energy of an anisotropic quark-gluon plasma, identify all stable and unstable collective modes of the system, and consider their effect on the partonic energy loss with respect to an isotropic system in chapter 7. Finally, I will give my conclusions in chapter 8.

Chapter 2

QCD Quasiparticles

When elementary particles propagate through a medium, their vacuum properties are changed through the effect of their interactions, which is also referred to as “dressing”. In the simplest case, a quasiparticle is then just an elementary particle which had e.g. its vacuum mass changed to an effective mass by the medium.

However, in general a medium is characterized by a whole set of collective modes or quasiparticles (I will use the terms interchangeably), some of which correspond to elementary particles in the vacuum and others which do not. Loosely speaking, a quasiparticle is an in-medium excitation that behaves as if it was an elementary particle, although it might not correspond to one in the vacuum.

Generally, quasiparticles possess a dispersion law $E(k)$ that gives their energy E as a function of their momentum k and – since their lifetime may not be infinite – a decay or damping rate $\gamma(k)$. Both the dispersion relation as well as the decay rate are linked to the peak and width of the spectral densities; in the simple cases considered in the following the spectral densities can be assumed to have a Breit-Wigner form so that the dispersion relations and decay rate are linked to a simple pole of the propagator.

2.1 The gluon propagator in the HTL approximation

The gluon propagator $G^{\mu\nu}$ is related to the gluon self-energy $\Pi^{\mu\nu}$ through the Dyson-Schwinger equation

$$G_{\mu\nu}^{-1} = G_{\mu\nu,0}^{-1} + \Pi_{\mu\nu}. \quad (2.1)$$

Using a tensor decomposition of the self-energy and restricting to the HTL approximation [63, 28] and the temporal axial gauge¹ one finds

$$\begin{aligned}\Pi_{ij}(\omega, k) &= \left(\delta_{ij} - \frac{k_i k_j}{k^2} \right) \Pi_T(\omega, k) - \frac{k_i k_j}{k^4} \Pi_L(\omega, k), \\ \Pi_{00}(\omega, k) &= -\Pi_L(\omega, k), \quad \Pi_{0i}(\omega k) = -\frac{\omega k_i}{k^2} \Pi_L(\omega, k),\end{aligned}\quad (2.2)$$

where the longitudinal and transversal parts of the self-energy are given by

$$\Pi_L(\omega, k) = m_D^2 \left[1 - \frac{\omega}{2k} \ln \frac{\omega + k}{\omega - k} \right], \quad \Pi_T(\omega, k) = \frac{1}{2} \left[m_D^2 + \frac{\omega^2 - k^2}{k^2} \Pi_L \right], \quad (2.3)$$

and

$$m_D^2 = 4\pi\alpha_s \left(\frac{2N + N_f}{6} T^2 + \frac{N_f \mu^2}{2\pi^2} \right) \quad (2.4)$$

is the QCD Debye mass squared. In the temporal axial gauge the gluon propagator then reads

$$G_{ij}(\omega, k) = \left(\delta_{ij} - \frac{k_i k_j}{k^2} \right) G_T(\omega, k) + \frac{k_i k_j}{k^2} \frac{k^2}{\omega^2} G_L(\omega, k), \quad (2.5)$$

where

$$G_L(\omega, k) = \frac{-1}{k^2 + \Pi_L(\omega, k)}, \quad G_T(\omega, k) = \frac{-1}{\omega^2 - k^2 - \Pi_T(\omega, k)}. \quad (2.6)$$

The poles ω of the gluon propagator then fall into two branches, corresponding to a longitudinal ($G_L^{-1}(\omega_L(k), k) = 0$) and a transversal ($G_T^{-1}(\omega_T(k), k) = 0$) mode. The dispersion relations $E_L(k)$, $E_T(k)$ and associated damping rates $\gamma_L(k)$, $\gamma_T(k)$ are simply given by the real and imaginary part of the poles, respectively,

$$\omega_L(k) = E_L(k) - i\gamma_L(k), \quad \omega_T(k) = E_T(k) - i\gamma_T(k), \quad (2.7)$$

or more specific for the above modes,

$$\begin{aligned}0 &= k^2 + \text{Re}\Pi_T(E_L(k), k), \quad E_T^2(k) = k^2 + \text{Re}\Pi_T(E_T(k), k), \\ 0 &= \text{Im}\Pi_L(E_L(k) + i\gamma_L(k), k), \quad \gamma_T(k) = -\frac{1}{2E_T(k)} \text{Im}\Pi_T(E_T(k) + i\gamma_T(k), k).\end{aligned}\quad (2.8)$$

In Fig. 2.1, a plot of the dispersion relations in quadratic scale is shown: there are propagating modes above a common plasma frequency $\omega > \omega_{pl} = \sqrt{m_D^2/3}$, which for the transverse branch tend to a mass hyperboloid with asymptotic mass squared

$$m_\infty^2 = \frac{m_D^2}{2}, \quad (2.9)$$

¹This particular gauge is chosen for convenience only; a proof of the gauge independence of the dispersion relations below can be found in [64].

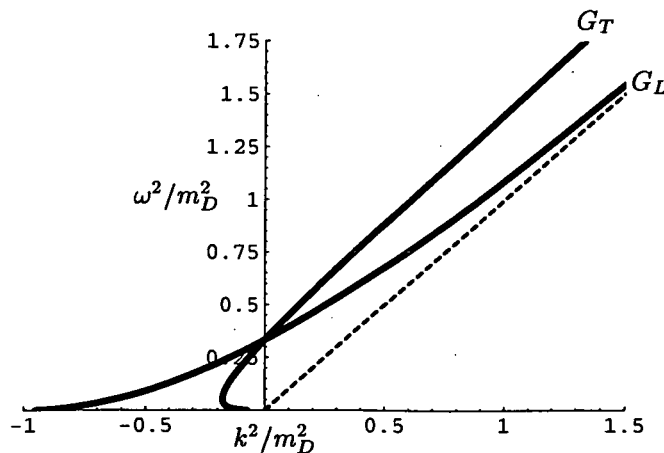


Figure 2.1: Dispersion relations for the transversal (G_T) and longitudinal (G_L) part of the gluon propagator in quadratic scales. Positive values of k^2 correspond to propagating modes (mass hyperboloids show as straight lines parallel to the light cone indicated by the dashed line) whereas negative values show screening phenomena.

whereas the longitudinal branch approaches the light-cone exponentially with a residue that is exponentially suppressed. Indeed, this last mode (which is sometimes called the longitudinal plasmon) does not have a vacuum analogue and disappears from the spectrum at $k \rightarrow \infty$. The transverse mode, however, represents an in-medium version of the physical gauge boson polarization.

For $\omega < \omega_{pl}$, k turns out to be imaginary which corresponds to the phenomenon of screening; in QCD, there is magnetic (transversal mode) as well as electric (longitudinal mode) screening with a screening length given by $1/|k|$ as long as $\omega > 0$.

In the static limit $\omega = 0$, the self-energies become $\Pi_L(0, k) = m_D^2$ and $\Pi_T(0, k) = 0$, respectively. Accordingly, whereas the longitudinal branch predicts screening in the electrostatic sector with inverse screening length $|k| = m_D$, the solution to the transverse branch, $k = 0$, signals the absence of magnetostatic screening. In fact, in Abelian gauge theories there are strong arguments that the absence of a magnetic screening mass is required by gauge invariance of the theory [65]. However, in non-Abelian gauge theories this absence is not guaranteed and indeed lattice QCD simulations do find a screening behavior in the transverse sector [66]. Note that also analytically one can find a nontrivial magnetostatic behavior if one no longer requires the system to be isotropic; the result for the magnetic screening mass, however, is somewhat unexpected and this case will be described in more detail in chapter 6.

To leading order, the imaginary part of the gluon self-energy vanishes for $\omega^2 > k^2$. Accordingly, the damping rates of the quasiparticles are zero to this

order of the coupling. However, there is a contribution at order α_s , which has been calculated by BRAATEN and PISARSKI [67] in the zero momentum limit after several incomplete attempts by various authors in the 1980's (see [63] for a collection of published values). For nonzero momentum the damping rates have an apparent logarithmic singularity that is cut off by the magnetostatic mass [68], which has to be calculated non-perturbatively; only the zero momentum result seems to be protected from this effect, although there may be different problems arising at next-to-leading order [69].

Finally, in the region with $\omega^2 < k^2$ the imaginary part of the gluon self-energy is large ($\sim \alpha_s T^2$); this corresponds to the possibility of Landau damping, which is the dissipation of energy in the plasma [6] (see also chapter 7 where the energy loss of a heavy parton is calculated).

2.2 The fermion propagator in the HTL approximation

The fermion propagator S (suppressing Lorentz indices) fulfills a Dyson-Schwinger equation similar to the gluon propagator

$$S^{-1} = S_0^{-1} + \Sigma, \quad (2.10)$$

where Σ is the fermionic self-energy. The most general form of Σ compatible with the rotational and chiral symmetries is

$$\Sigma(\omega, k) = a(\omega, k)\Gamma^0 + b(\omega, k)\hat{\mathbf{k}} \cdot \mathbf{\Gamma}, \quad (2.11)$$

where $\mathbf{\Gamma}$ are the Dirac matrices. This can be rewritten as

$$\Gamma_0 \Sigma(\omega, k) = \Sigma_+(\omega, k)\Lambda_+(\hat{\mathbf{k}}) - \Sigma_-(\omega, k)\Lambda_-(\hat{\mathbf{k}}), \quad (2.12)$$

where $\Sigma_{\pm}(\omega, k) = b(\omega, k) \pm a(\omega, k)$ and the spin matrices

$$\Lambda_{\pm}(\hat{\mathbf{k}}) \equiv \frac{1 \pm \Gamma^0 \mathbf{\Gamma} \cdot \hat{\mathbf{k}}}{2}, \quad \Lambda_+ + \Lambda_- = 1, \quad \Lambda_{\pm}^2 = \Lambda_{\pm}, \quad (2.13)$$

$$\Lambda_+ \Lambda_- = \Lambda_- \Lambda_+ = 0, \quad \text{Tr} \Lambda_{\pm} = 2, \quad (2.14)$$

project onto spinors whose chirality is equal (Λ_+), or opposite (Λ_-), to their helicity. Using $S_0^{-1} = -\not{k} + \Sigma$ one can decompose the propagator

$$S(\omega, k)\Gamma_0 = \Delta_+(\omega, k)\Lambda_+ + \Delta_-(\omega, k)\Lambda_-, \quad (2.15)$$

with $\Delta_{\pm}^{-1} \equiv -[\omega \mp (k + \Sigma_{\pm})]$. Accordingly, there are also two fermionic pole branches corresponding to $\Delta_+^{-1} = 0$ and $\Delta_-^{-1} = 0$, where the latter one is occasionally referred to as plasmino branch. Using the result for the fermion self-energy in the HTL approximation,

$$\Sigma_{\pm}(\omega, k) = \frac{M^2}{k} \left(1 - \frac{\omega \pm k}{2k} \ln \frac{\omega + k}{\omega - k} \right), \quad (2.16)$$

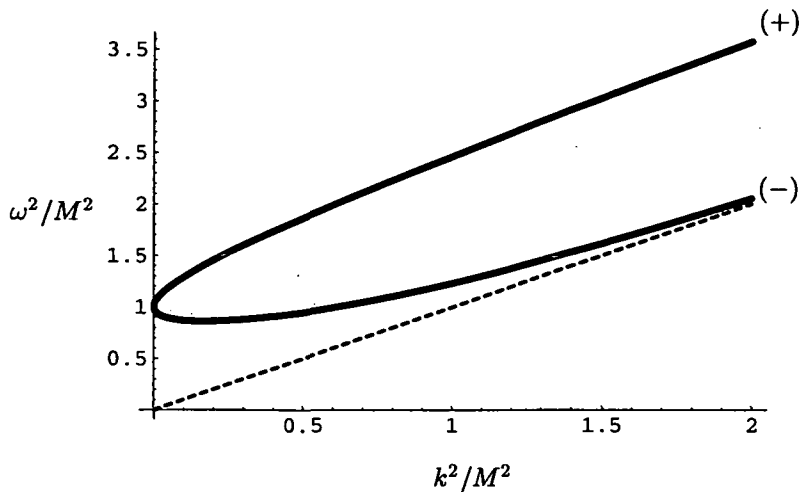


Figure 2.2: Dispersion relations for the fermionic quasiparticles in quadratic scale. Shown are the regular (+) and plasmino (-) branch, together with the light cone (dashed-line).

where M^2 is the plasma frequency for fermions,

$$M^2 = \frac{4\pi\alpha_s(N^2 - 1)}{16N} \left(T^2 + \frac{\mu^2}{\pi^2} \right), \quad (2.17)$$

one can proceed to plot the dispersion relations $E_+(\omega)$, $E_-(\omega)$ for the fermionic modes, shown in Fig. 2.2.

The plasmino branch shows an interesting minimum of ω at $\omega/M \simeq 0.93$, $k/M \simeq 0.41$ and approaches the light-cone for large momenta with exponentially vanishing residue; the regular branch tends to a mass hyperboloid with asymptotic mass squared

$$M_\infty^2 = 2M^2. \quad (2.18)$$

The damping rates also vanish to leading order but there is a contribution to order α_s , as was the case for the gluonic modes [68].

2.3 Simple quasiparticle model for the EOS

The main building block one uses in the derivation of the HTL approximation is that the principal contribution for the loop integral in e.g. the self-energies comes from momenta which are of order $k \sim T$, dubbed “hard” (hence the name hard-thermal-loop). Therefore, for weak coupling α_s , when momenta of order $k \sim \alpha_s^{1/2}T$ (dubbed “soft”) are much smaller than hard momenta, the thermodynamic behavior of the system is dominated by the hard excitations. However, the relevant collective modes at large momenta have already been identified in the previous sections: while the longitudinal plasmon as well as the plasmino

mode are exponentially suppressed, the transverse gluonic and positive fermionic branches represent particle excitations that propagate predominantly on simple mass shells with dispersion relations

$$E_T(k)^2 = m_\infty^2 + k^2, \quad E_+(k)^2 = M_\infty^2 + k^2, \quad (2.19)$$

with the asymptotic masses m_∞ and M_∞ given above. It is therefore straightforward to model the thermodynamic pressure as a gas of weakly interacting massive particles with residual mean-field interaction B [70, 42],

$$p(T, \mu) = p_g(T, m_\infty^2) + p_q(T, \mu, M_\infty^2) - B(m_\infty^2, M_\infty^2), \quad (2.20)$$

where

$$p_g(T, m_\infty^2) = -2(N^2 - 1) \int \frac{d^3k}{(2\pi)^3} \ln(1 - e^{-E_T(k)/T}), \quad (2.21)$$

$$p_q(T, \mu, M_\infty^2) = 2NN_f \int \frac{d^3k}{(2\pi)^3} \ln(1 + e^{-(E_+(k)-\mu)/T}) + (\mu \rightarrow -\mu) \quad (2.22)$$

represent the partial pressure from gluons (g) and quarks (q). Using the stationarity of the thermodynamic potential under variation of the self-energies one finds

$$\frac{\partial B}{\partial m_\infty^2} = \frac{\partial p_g(T, m_\infty^2)}{\partial m_\infty^2}, \quad \frac{\partial B}{\partial M_\infty^2} = \frac{\partial p_q(T, \mu, M_\infty^2)}{\partial M_\infty^2}, \quad (2.23)$$

implying

$$s = \frac{dp}{dT} = \frac{\partial[p_g(T, m_\infty^2) + p_q(T, \mu, M_\infty^2)]}{\partial T}, \quad n = \frac{dp}{d\mu} = \frac{\partial p_q(T, \mu, M_\infty^2)}{\partial \mu} \quad (2.24)$$

for the entropy and number density, s and n , respectively.

If one expands Eq.(2.20) in powers of the coupling α_s , the leading order perturbative result $p_0 + p_2$ given in Eqs.(1.2,1.3), and part of the higher order correction is reproduced. Unexpanded, however, Eq.(2.20) represents a thermodynamically consistent resummation of terms in all orders of α_s , suggesting also a possible applicability of the model in the strong coupling regime. Indeed, by introducing an ansatz for the strong coupling (inspired by the running coupling Eq.(1.4)) that contains two phenomenological parameters λ and T_s at $\mu = 0$,

$$\alpha_{s,\text{eff}}(T, \mu = 0) = \frac{12\pi}{(11N - 2N_f) \ln[\lambda(T + T_s)/T_c]^2}, \quad (2.25)$$

it turns out that one can accurately describe lattice data for the entropy and eventually the pressure (see chapter 3 for details).

Moreover, for non-vanishing chemical potential, one obtains a flow equation for the coupling: since the quasiparticle masses depend on T and μ explicitly

as well as implicitly through the coupling $\alpha_s(T, \mu)$, Maxwell's relation $ds/d\mu = dn/dT$ implies a partial differential equation for α_s which takes the form

$$a_T \frac{\partial \alpha_s}{\partial T} + a_\mu \frac{\partial \alpha_s}{\partial \mu} = b, \quad (2.26)$$

where the coefficients a_T , a_μ and b depend on T , μ and α_s . Given a valid boundary condition, a solution for $\alpha_s(T, \mu)$ can be found by solving the above flow equation by the method of characteristics; once α_s is thus known in the T, μ plane, the quasiparticle partial pressures p_g and p_q are also fixed completely. Finally, the residual interaction B is then given by the integral

$$B = \int \sum_{i=g,q} \frac{\partial p_i}{\partial m_i^2} \left(\frac{\partial m_i^2}{\partial \mu} d\mu + \frac{\partial m_i^2}{\partial T} dT \right) + B_0, \quad (2.27)$$

where B_0 is an integration constant that has to be fixed either through lattice data or through matching the pressure on to a low-energy effective theory. In chapter 3 the details of this calculation and also an interpretation of the results will be given.

2.3.1 Properties of the flow equation

When calculating the coefficients a_T , a_μ and b of Eq.(2.26), one finds that in particular a_T and a_μ obey [43]

$$a_T(T, \mu \rightarrow 0) = 0, \quad a_\mu(T \rightarrow 0, \mu) = 0, \quad (2.28)$$

while the respective other coefficient does not vanish in these limits. The characteristic equations following from Eq.(2.26),

$$a_\mu dT = a_T d\mu, \quad a_\mu d\alpha_s = b d\mu, \quad (2.29)$$

then imply that the characteristics are perpendicular to both the T and the μ axes. Therefore, specifying the coupling α_s on some interval on the T or μ axes represents a valid boundary condition for the flow equation (2.26).

In the limit of vanishing coupling $\alpha_s \rightarrow 0$ it can be shown that the coefficient b vanishes. The coupling is then constant along the characteristics, which become ellipses in the variables T^2 and μ^2 [42], given by

$$\frac{4N + 5N_f}{9N_f} T^4 + 2T^2 \frac{\mu^2}{\pi^2} + \left(\frac{\mu}{\pi} \right)^4 = \text{const.} \quad (2.30)$$

Note that for nonzero coupling this is still true approximately.

However, the solution to the flow equation is not forcibly unique everywhere, since the characteristics may turn out to be intersecting for certain regions in the T, μ -plane. This ambiguity as well as its resolution will be treated in more detail in chapter 3.

2.4 Summary

In this chapter I have defined and characterized the leading-order gluonic and fermionic quasiparticle excitations relevant for QCD. From the respective self-energies the dispersion relations were calculated and it was found that for hard momenta two of these excitations vanish exponentially while the remaining two propagate approximately on simple mass shells. Following GORENSTEIN and PESHIER [70, 42], I argued that the thermodynamic pressure of QCD can be modeled by that of a free gas of massive particles together with some residual interaction, which itself is determined by requiring stationarity of the pressure with respect to the self-energies. Anticipating that by using a simple 2-parameter ansatz for an effective strong coupling this model can be used to accurately describe lattice data for the entropy and pressure (which will be done in chapter 3), I showed that by using Maxwell's relation one obtains a flow equation for the coupling, which, once solved, will give an equation of state of deconfined QCD for arbitrary temperature and chemical potential. Finally, I derived the equations for the characteristics of the coupling flow equation and anticipated that they will resemble ellipses in the variables T^2 and μ^2 , with endpoints perpendicular to the T and μ axes.

Chapter 3

The HTL quasiparticle model

In the last chapter I have set up a simple quasiparticle model of the QCD pressure that only takes into account the hard excitations, ignoring longitudinal plasmon and plasmino quasiparticles. A comparison between the strictly perturbative pressure known to order $\alpha_s^{5/2}$ and a perturbative expansion of the simple quasiparticle model shows that – while the leading orders are correctly reproduced – only $1/4/\sqrt{2}$ or about 18% of the order $\alpha_s^{3/2}$ term are included in the simple quasiparticle model. However, it is precisely the inclusion of this term (also called the plasmon term) that makes the result for the pressure go “wild” in the first place, spoiling the convergence of the strictly perturbative expansion as was shown in Fig. 1.2. Consequently, neither does the simple quasiparticle model incorporate a big part of the plasmon effect (which could mean quantitative results are incorrect by an unknown amount) nor is it a priori clear whether an extension including the *full* plasmon term would not go astray as violently as in the strict perturbative case (implying that also qualitatively the results from the simple quasiparticle model would be dubious). Therefore, it is important to consider refinements of the simple quasiparticle model that incorporate more of the physically important plasmon term, so that the above caveats can be settled.

One such refinement, namely that of a quasiparticle model for the QCD thermodynamic pressure that is based on the HTL-resummed entropy [27, 71, 28], will be considered in the following.

3.1 The entropy of the QCD plasma

As a starting point, one uses the result that the thermodynamic potential $\Omega = -pV$ can be written as the following functional of the full gluon and fermion propagators G and S [27]:

$$\frac{1}{T}\Omega[G, S] = \frac{1}{2}\text{Tr} \ln G^{-1} - \text{Tr} \ln S^{-1} - \frac{1}{2}\text{Tr} \Pi G + \text{Tr} \Sigma S + \Phi[G, S], \quad (3.1)$$

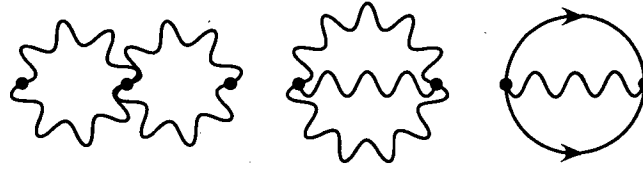


Figure 3.1: Diagrams for Φ at 2-loop order in QCD in the temporal axial gauge. Wiggly lines refer to gluon, plain lines refer to fermions.

where Π and Σ are the gluon and quark self-energies of chapter 2 (related to the full propagators by Dyson's equation (2.1, 2.10)) and Tr includes traces over color indices and also over Lorentz and spinor indices when applicable. $\Phi[G, S]$ is the sum of the 2-particle-irreducible "skeleton" diagrams, which to 2-loop order are shown in Fig. 3.1.

The essential property of the functional $\Omega[G, S]$ is to be stationary under variations of G and S (at fixed G_0 and S_0),

$$\frac{\delta\Omega}{\delta G} = 0, \quad \frac{\delta\Omega}{\delta S} = 0, \quad (3.2)$$

so the physical pressure is then obtained as the value of Ω at its extremum. Note that the stationarity conditions imply

$$\frac{\delta\Phi}{\delta G} = \frac{1}{2}\Pi, \quad \frac{\delta\Phi}{\delta S} = \Sigma, \quad (3.3)$$

which together with the Dyson's equations define the physical propagators and self-energies in a self-consistent way. Accordingly, by selecting a class of skeletons in $\Phi[G, S]$ and calculating Π and Σ from the above relations one obtains a self-consistent approximation of the physical pressure.

Using the temporal axial gauge which preserves rotational invariance and also makes the Faddeev-Popov ghosts decouple from the theory, the gluon and quark propagators can be decomposed as in the previous chapter, so that one can evaluate Eq.(3.1) using standard contour integration techniques. Accordingly, the entropy density $s = -\frac{d\Omega/V}{dT}$ is evaluated to be

$$s = s_g + s_q + s', \quad (3.4)$$

where

$$s_g = -(N^2 - 1) \int \frac{d^4k}{(2\pi)^4} \frac{\partial n(\omega)}{\partial T} \left\{ 2 \left[\text{Im} \ln(-\omega^2 + k^2 + \Pi_T) - \text{Im} \Pi_T \text{Re} D_T \right] \right. \\ \left. + \text{Im} \ln(k^2 + \Pi_L) + \text{Im} \Pi_L \text{Re} D_L \right\},$$

$$s_f = -2NN_f \int \frac{d^4k}{(2\pi)^4} \frac{\partial f(\omega)}{\partial T} \left\{ \text{Im} \ln \Delta_+^{-1} + \text{Im} \ln(-\Delta_-^{-1}) \right\}$$

$$\begin{aligned}
s' = & - \left. \frac{\partial(T/V\Phi[G, S])}{\partial T} \right|_{D, S} + (N^2 - 1) \int \frac{d^4 k}{(2\pi)^4} \frac{\partial n(\omega)}{\partial T} (2\text{Re}\Pi_T \text{Im}D_T - \text{Re}\Pi_L \text{Im}D_L) \\
& + 2NN_f \int \frac{d^4 k}{(2\pi)^4} \frac{\partial f(\omega)}{\partial T} \{ \text{Re}\Sigma_+ \text{Im}\Delta_+ - \text{Re}\Sigma_- \text{Im}\Delta_+ \}. \quad (3.5)
\end{aligned}$$

Here $n(\omega)$ and $f(\omega)$ are the Bose-Einstein and Fermi-Dirac distributions,

$$n(\omega) = \frac{1}{\exp \omega/T - 1}, \quad f(\omega) = \frac{1}{\exp(\omega - \mu)/T + 1} + \frac{1}{\exp(\omega + \mu)/T + 1}, \quad (3.6)$$

and decomposition of the propagators from chapter 2 has been used.

When restricting to an approximation where $\Phi[D, S]$ contains only 2-loop skeletons (shown in Fig. 3.1), one finds the remarkable property that

$$s' = 0, \quad (3.7)$$

which has been shown in Refs. [72, 28] for QED and QCD, respectively. Since in this approximation the self-energies and propagators are to be determined self-consistently by solving "gap-equations" of the form

$$D_T^{-1} = -\omega^2 + k^2 + \Pi_T[D_T, D_L, \Delta_+, \Delta_-], \quad (3.8)$$

where Π_T is given by one-loop self-energy expressions only, the resulting expression for the entropy (3.4) is also effectively one-loop.

This has important consequences: firstly, one has reduced the problem of calculating a two-loop quantity (the free energy or thermodynamic pressure) to a simple integration of an effectively one-loop quantity (the entropy expression from above); secondly, since the term s' has been interpreted as the contribution from the residual interaction of the quasiparticles [28], the result $s' = 0$ means that this contribution vanishes for the QCD entropy in the 2-loop approximation. I will make use of this interpretation in the following.

3.1.1 Approximately self-consistent solutions

Unfortunately, "gap equations" like Eq.(3.8) are non-local, which makes their exact solution prohibitively difficult. Moreover, the gap equations contain UV divergencies and therefore require a renormalization scheme compatible with the self-consistent structure of this non-local equation. Whereas this daunting task has been at least formally resolved in the scalar $\lambda\phi^4$ model [32, 33], the richer structure of QCD along with unresolved problems concerning gauge-dependencies of the two-particle-irreducible scheme at higher orders [73] render a self-consistent renormalization of the gap-equations in QCD an open problem.

Therefore, it is convenient to construct so-called "approximately self-consistent" solutions, which maintain the properties of Eq.(3.3) together with the Dyson's

equations up to and including a given order of α_s , and which are manifestly gauge independent and UV finite. For example, using the HTL results for the self-energies and the resulting full propagators (given in chapter 2) constitutes just one such approximately self-consistent solution; therefore, using the HTL approximation for the self-energies and propagators in Eqs.(3.4,3.5,3.7) gives a gauge-invariant, non-perturbative approximation to the full entropy.

3.2 The HTL quasiparticle model

Similar to the simple quasiparticle model, one can construct a model for the thermodynamic pressure that incorporates the relevant HTL quasiparticle excitations, which I will call the *HTL quasiparticle model* in the following [74]. Since this model should be a refinement of the simple quasiparticle model, two requirements have to be fulfilled: firstly, the HTL model has to incorporate more of the physically important plasmon effect, and secondly, it should constitute a natural extension of the simple quasiparticle model, including its structure in some sense.

The key to the construction of the HTL quasiparticle model lies in the observation that similar to the results in the simple quasiparticle model the entropy in the two-loop Φ -derivable approximation of the previous section is given in terms of HTL quasiparticle excitations only, while the contribution from residual interactions vanishes. One therefore *defines* the HTL quasiparticle model entropy to be given by Eq.(3.5), which is known to be a fairly good approximation to the full entropy of the quark-gluon plasma [28]. Taking all this into account, one is led to the following ansatz for the thermodynamic QCD pressure:

$$p(T, \mu) = p_{g,HTL}(T, m_D^2) + p_{q,HTL}(T, \mu, M^2) - B_{HTL}(m_D^2, M^2), \quad (3.9)$$

with

$$p_{g,HTL} = -2(N^2 - 1) \int \frac{d^3k}{(2\pi)^3} \int_0^\infty \frac{d\omega}{2\pi} n(\omega) [2\text{Im} \ln(-\omega^2 + k^2 + \Pi_T) - 2\text{Im}\Pi_T \text{Re}D_T + \text{Im} \ln(k^2 + \Pi_L) + \text{Im}\Pi_L \text{Re}D_L] \quad (3.10)$$

$$p_{q,HTL} = -4NN_f \int \frac{d^3k}{(2\pi)^3} \int_0^\infty \frac{d\omega}{2\pi} f(\omega) [\text{Im} \ln(k - \omega + \Sigma_+) - \text{Im}\Sigma_+ \text{Re}\Delta_+ + \text{Im} \ln(k + \omega + \Sigma_-) + \text{Im}\Sigma_- \text{Re}\Delta_-], \quad (3.11)$$

obeying the stationarity conditions

$$\frac{\partial p}{\partial m_D^2} = \frac{\partial p}{\partial M^2} = 0. \quad (3.12)$$

Clearly, the model (3.9) fulfills all of the above requirements: the pressure is described by a gas of weakly interacting HTL quasiparticles, which have momentum-dependent dispersion relations that were given in chapter 2. Therefore, the integrations in Eq.(3.11) pick up contributions equal to those of the simple quasiparticle model for large momenta, while for soft momenta the richer structure of

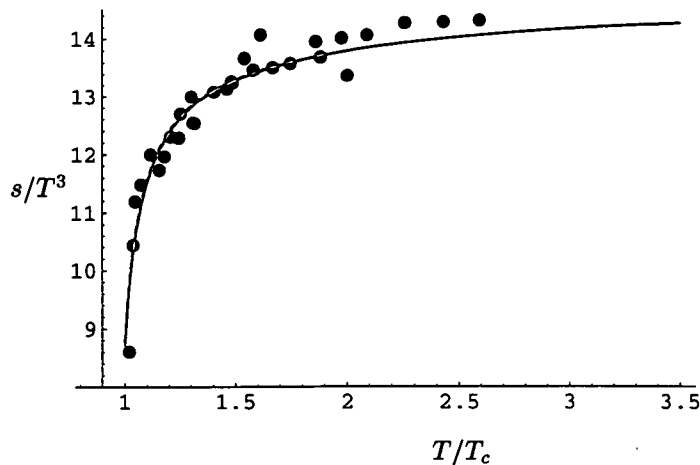


Figure 3.2: Entropy data generated from Ref. [17] vs. fitted model entropy. The HTL and simple quasiparticle model fits are nearly indistinguishable to the naked eye.

the quasiparticle excitations are taken into account. Consequently, when doing a perturbative expansion of Eq.(3.11) at $\mu = 0$ in powers of the coupling α_s , one finds that 25% of the plasmon effect is included in the HTL model, in contrast to 18% for the simple quasiparticle model. Furthermore, the stationarity condition ensures that there is no residual interaction to the entropy ($s' = 0$) and the resulting model entropy is indeed given by $s = s_g + s_f$.

In its setup, the HTL quasiparticle model is very similar to the simple quasiparticle model, so the general discussion of this model in chapter 2 remains valid to a large extent also for the HTL model. Indeed, to tell whether the plasmon effect has a destabilizing effect in these quasiparticle models similar to what happens in strict perturbation theory, one has to compare the results from both models in a standardized procedure, so I will follow the steps from Eq.(2.25) onwards for both models, filling in the details and pointing out the differences.

3.3 Modeling the lattice entropy and pressure

Restricting $\mu = 0$ and using the ansatz (2.25) for the strong coupling α_s , the entropy of the HTL and simple quasiparticle models becomes a function of the temperature T and two fit parameters T_s and λ , $s = s(T, T_s, \lambda)$. Using lattice data for $N_f = 2$ and $N = 3$ from Ref. [17] together with an estimated continuum extrapolation from [43], these two parameters T_s and λ are determined by a least square fit to the data. The numerical values for these fit parameters (which are reproduced in chapter 4) turn out to be quite similar, and the respective fits to the lattice data (shown in Fig. 3.2) are nearly indistinguishable.

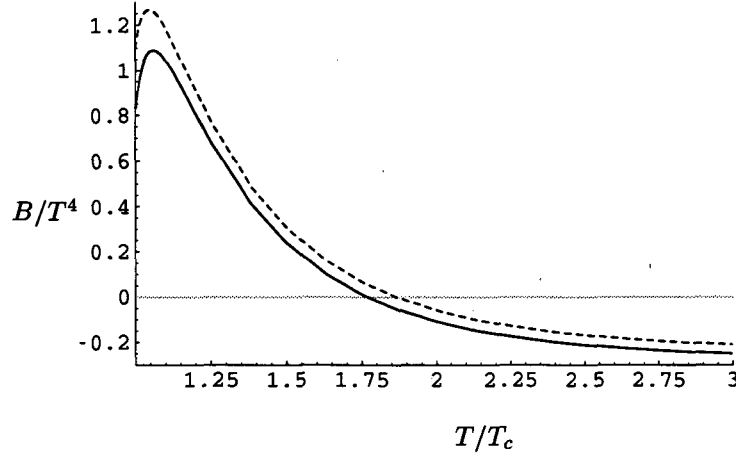


Figure 3.3: Residual interaction B for the HTL (full line) and simple model (dashed-line), respectively.

Once the fit parameters have been fixed, so has $\alpha_{s,\text{eff}}$ at vanishing chemical potential, and consequently also the quasiparticle masses. One can then use Eq.(2.27) together with $d\mu = 0$,

$$B = \int \sum_{i=g,q} \frac{\partial p_i}{\partial m_i^2} \frac{\partial m_i^2}{\partial T} dT + B_0, \quad (3.13)$$

to determine the residual interaction as a function of the temperature up to an integration constant B_0 . This integration constant has been determined by a fit of the lattice pressure with the simple quasiparticle model in [43], obtaining

$$B_0 = B|_{T_c} = 1.1 T_c^4, \quad (3.14)$$

so that the resulting model pressure at T_c becomes

$$p(T_c, \mu = 0) = 0.536(1)T_c^4. \quad (3.15)$$

To facilitate comparison, I fix the HTL model value of B_0 by requiring $p_{HTL}(T_c, \mu = 0) \simeq 0.536 T_c^4$, obtaining $B_{0,HTL} = 0.82 T_c^4$. The resulting residual interactions for the HTL and simple quasiparticle models are plotted in Fig. 3.3; finally, the overall model pressure is compared to the lattice data in Fig. 3.4.

Clearly, both the HTL and the simple quasiparticle model can be used to describe the lattice data very accurately once a 2-parameter fit for the effective coupling is adopted, even close to the deconfinement transition. Furthermore, since the fit parameters turn out to be only slightly different and the resulting fits to the lattice data are nearly indistinguishable, one concludes that (at least at $\mu = 0$) the inclusion of the plasmon effect does not seem to destabilize the

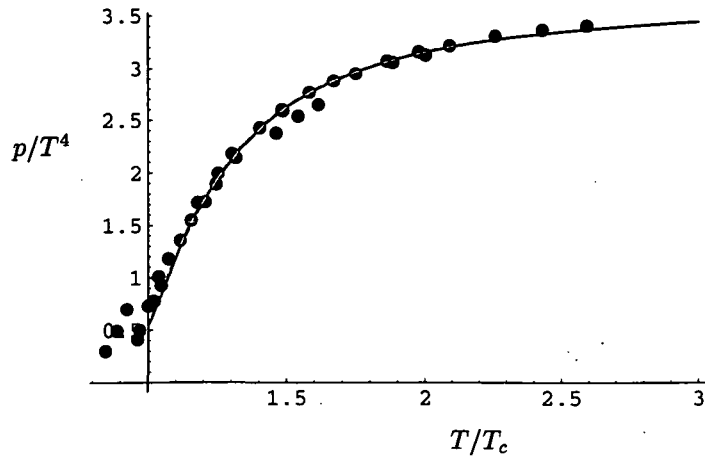


Figure 3.4: Pressure data from Ref. [17] vs. model pressure. HTL and simple model results are indistinguishable for the naked eye.

quasiparticle models; on the contrary, even though the effective coupling gets rather large near $T = T_c$ (see chapter 4 for details), the effects of changing the percentage of the included plasmon effect are rather small. Therefore, one gains some confidence that a phenomenological description of the thermodynamic QCD pressure through quasiparticle models is also applicable in the non-perturbative regime, and in turn may be used to derive results that lie parametrically far from the initial (lattice) data.

3.4 Solving the flow equation

At non-vanishing chemical potential, the models are required to fulfill Maxwell's relation

$$\frac{ds}{d\mu} = \frac{dn}{dT}. \quad (3.16)$$

Since the entropy s as well as the number density n depend on T and μ both explicitly through the Bose-Einstein and Fermi-Dirac distribution functions as well as implicitly through the quasiparticle masses, one has

$$\frac{ds}{d\mu} - \frac{dn}{dT} = \sum_{i=g,q} \frac{\partial s}{\partial m_i^2} \frac{dm_i^2}{d\mu} - \frac{\partial n}{\partial m_i^2} \frac{dm_i^2}{dT}, \quad (3.17)$$

because the explicit derivations of s and n with respect to μ and T cancel, respectively. The quasiparticle masses themselves also depend on T and μ both explicitly and implicitly through the coupling $\alpha_{s,\text{eff}}$, so that e.g. for the Debye mass one finds

$$\frac{dm_D^2}{d\mu} = \frac{N_f}{2\pi^2} 2\mu 4\pi \alpha_s(T, \mu) + \frac{\partial \alpha_s(T, \mu)}{\partial \mu} 4\pi \left(\frac{2N + N_f}{6} T^2 + \frac{N_f \mu^2}{2\pi^2} \right). \quad (3.18)$$

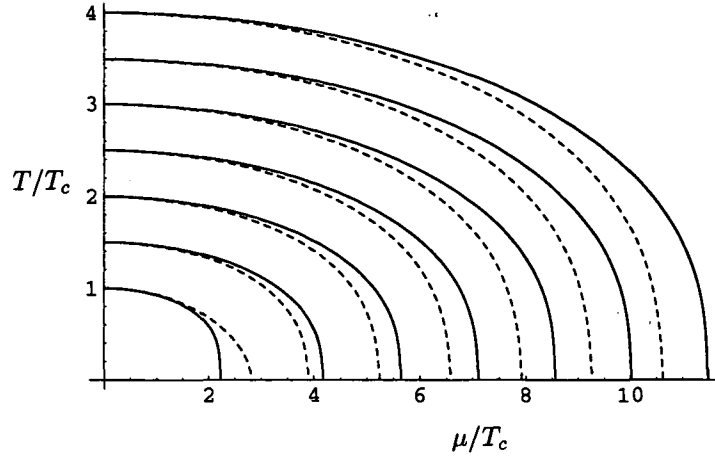


Figure 3.5: Comparison of the shape of the characteristics for the HTL (full lines) and simple quasiparticle model (dashed lines). T_c denotes $T_c|_{\mu=0}$.

Therefore, Eq.(3.17) represents a partial differential equation for the coupling that can be written in the form already anticipated in Eq.(2.26),

$$a_T \frac{\partial \alpha_s}{\partial T} + a_\mu \frac{\partial \alpha_s}{\partial \mu} = b, \quad (3.19)$$

since it takes a considerable amount of algebra to derive the coefficients a_T , a_μ and b in the HTL model, their explicit form may be of use in further studies. However, since their appearance is rather unwieldy, I refrain from reproducing these coefficients in the main text and have relegated them to appendix A.

When evaluating the coefficients numerically and comparing their value for the HTL and simple quasiparticle model, one finds that while a_T and a_μ assume nearly equal values, the coefficient b turns out to differ noticeably which has interesting consequences, as will become clear in the following. The solution to the flow equation (2.26) for the coupling is found by using the initial value condition $\alpha_{s,\text{eff}}(T, \mu = 0)$ and then numerically solving the characteristics of Eq.(2.26),

$$a_\mu dT = a_T d\mu, \quad a_\mu d\alpha_s = b d\mu. \quad (3.20)$$

The shapes of the characteristics are shown in Fig. 3.5 for both the HTL and the simple quasiparticle model; as anticipated in chapter 2, the characteristic curves resemble ellipses in T^2 and μ^2 , which are perpendicular to both the T and the μ axis. Furthermore, for the simple quasiparticle model there is a set of characteristics (those which start at $\mu = 0$ in the interval $[T_c, 1.06T_c]$) that intersect in a narrow region, indicating that there the solution to the flow equation is not unique (see Fig. 3.6). However, when also calculating the pressure along the characteristics it turns out that it becomes negative in the intersection region;

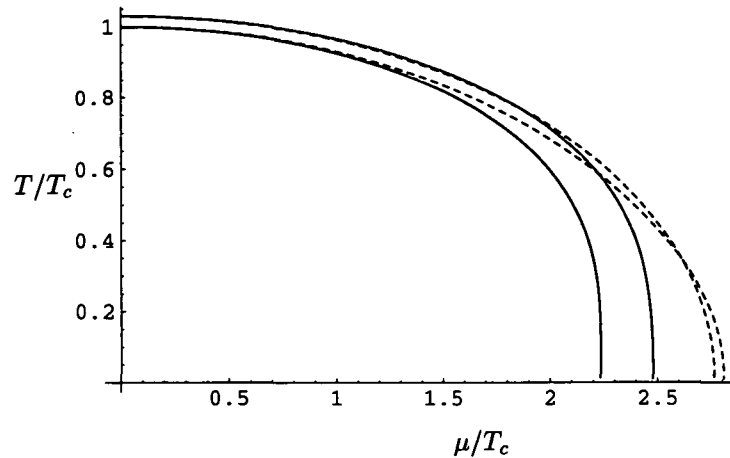


Figure 3.6: Characteristics starting very near T_c : for the simple quasiparticle model (dashed-lines) intersections are occurring, while for the HTL model (full lines) this is not the case.

it has been argued [43] that this implies that a transition to another phase with positive pressure has been occurring somewhere outside this region, which therefore means that the quasiparticle description had broken down and the ambiguity would be of no physical relevance.

Interestingly, for the HTL model, the difference in the flow equation parameter b seems to completely lift the ambiguity problem: the characteristic curves are well behaved and do not intersect anywhere, as can be seen in Fig. 3.6. Unfortunately, the pressure still turns negative for some region in the T, μ plane for the HTL model, so that clearly also this model breaks down for certain T, μ . On the other hand, one can turn this breakdown of the quasiparticle models into a virtue by assuming that the deconfinement transition occurs near the line $T = T(\mu)$ where the pressure vanishes. Therefore, an estimate for the “critical” transition line for arbitrary μ becomes calculable within the quasiparticle models, (see chapter 4 for details).

3.5 The pressure at finite chemical potential

Solving the flow equation provides one with an effective coupling in the whole T, μ plane, so that – via the explicit form of the quasiparticle masses – the contributions p_g and p_q to the full pressure (2.20,3.9) are fixed. It remains to calculate the residual interaction B , which is most easily done by integrating Eq.(2.27) along the characteristic curves of the flow equation (2.26). The result for the full pressure is shown in a 3D-plot in Fig. 3.7.

As will be discussed in more detail in chapter 4, this result is in fairly good

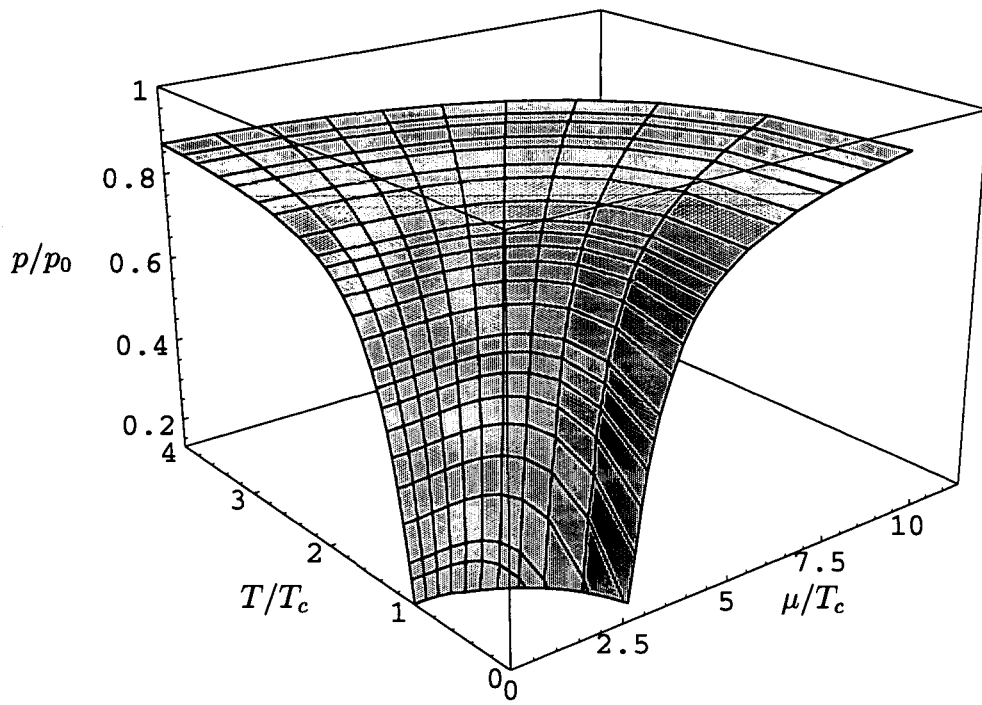


Figure 3.7: The full pressure of the HTL quasiparticle model normalized to the free pressure p_0 in the T, μ plane.

agreement with various lattice approaches. On the other hand, IPP and REBHAN [75] have found that in the exactly solvable large- N_f model of QCD the pressure has a conspicuous "kink" near $\mu \simeq \pi T$, signalling an abrupt change of the pressure for larger chemical potentials. This kind of behavior is not reproduced in the quasiparticle model approach for 2 flavors; on the contrary, it turns out that the quasiparticle model pressure is well described by its small- μ behavior even for large values of the chemical potential, as will be discussed in more detail in chapter 4. However, it is by no means clear that results obtained in the large- N_f case are also relevant in general for the physically interesting situations of $N_f = 2$ or $N_f = 3$, although for special cases their effect may well be considerable, as has recently been demonstrated [76].

3.6 Summary

In this chapter I have introduced the entropy of the quark gluon plasma through the so-called Φ -derivable formalism. A 2-loop approximation for the functional Φ that allows the entropy to be written as an effectively one-loop quantity was presented, and it was pointed out that because of problems concerning renormalization and gauge-dependencies it is useful to introduce the notion of *approximate self-consistency*. Since using the HTL self-energies together with the respective Dyson's equations for the propagators introduced in chapter 2 corresponds to such an approximately self-consistent approximation to the full quark-gluon plasma entropy, this expression was used as a basis for an HTL quasiparticle model, and it was shown that this model corresponds to an extension of the simple quasiparticle model introduced in chapter 2.

Fitting two flavor lattice data for the pressure it was found that at vanishing chemical potential the HTL model constitutes only a small correction to the simple quasiparticle model, so it seems that the plasmon effect which plays such a devastating role in strict perturbation theory is not destabilizing the quasiparticle implementation. Moreover, an explicit solution to the flow equation for the coupling shows that while the simple quasiparticle model solution becomes ambiguous in some region in the T, μ plane, one does not encounter any such problems for the HTL model.

Finally, I investigated the pressure at finite chemical potential and discussed its general behavior in view of recent exact results for the large-flavor limit of QCD.

Chapter 4

The QCD EOS for arbitrary μ and completion of plasmon effect

Having demonstrated in the last chapter that lattice data at vanishing chemical potential can be accurately described by quasiparticle models with an effective coupling, I now concentrate on the quantitative predictions one can make by mapping lattice data to nonzero chemical potential. More precisely, first the quasiparticle model results at low chemical potential will be compared to those obtained through lattice calculations and strictly perturbative methods, and then the case of high chemical potential and low temperatures, where nearly all other methods eventually break down, will be investigated. However, I will ignore the effect of color superconductivity, which should become important at very small temperatures only, assuming that because of the comparatively small energy gap it constitutes only a minor modification to the thermodynamic pressure in the region of interest [44]. The results in this chapter are based on Ref. [77]; however, here I will be able to go into more detail and also add some new results.

In the previous chapters, I have introduced the HTL quasiparticle model that includes $1/4$ of the full plasmon effect at vanishing chemical potential, which is a factor of $\sqrt{2}$ more than in the simple quasiparticle model that uses only the asymptotic HTL masses. Motivated by the rather successful generalization of the simple to the HTL quasiparticle model I will try to improve the accuracy of the HTL quasiparticle model further by setting up a model that includes even more of the perturbative plasmon effect. In principle, for this task one would need the complete (momentum-dependent) next-to-leading order corrections to the self-energies, which up to now no one had the strength to calculate; however, it has been shown in Ref. [27, 28] that – as far as the plasmon effect is concerned – the contribution to the thermodynamic quantities of these next-to-leading order corrections may be approximated by their averaged contribution to the asymptotic masses. Therefore, this opens the possibility of setting up a model that contains the *full* plasmon effect at $\mu = 0$, albeit at the price of introducing another unknown parameter, as will be discussed in the following.

4.1 NLO quasiparticle models

Denoting the momentum-dependent next-to-leading ($\alpha_s^{3/2}$) order corrections to the self-energies as $\delta\Pi_T(\omega, k)$ and $\delta\Sigma_+$ (the other branches do not receive contributions at this order), respectively, the averaged corrections to the asymptotic masses (2.9, 2.18) have been calculated to be [27, 28]

$$\bar{\delta}m_\infty^2 = \frac{\int dk k n'(k) \text{Re} \delta\Pi_T(\omega = k)}{\int dk k n'(k)} = -2\alpha_s NT m_D \quad (4.1)$$

and similarly

$$\bar{\delta}M_\infty^2 = \frac{\int dk k (f'_+(k) + f'_-(k)) \text{Re} 2k\delta\Sigma_+(\omega = k)}{\int dk k (f'_+(k) + f'_-(k))} = -\frac{(N^2 - 1)}{N} \alpha_s T m_D. \quad (4.2)$$

For the values of the coupling α_s considered here, these corrections are so large that they give tachyonic masses when treated strictly perturbatively. In Ref. [28] it has been proposed to incorporate these corrections through a quadratic gap equation which works well as an approximation in the exactly solvable scalar $O(N \rightarrow \infty)$ -model, where strict perturbation theory would lead to identical difficulties. However, for the fermionic asymptotic masses, in order to have the correct scaling of Casimir factors in the exactly solvable large- N_f limit of QCD [78], a corresponding gap equation has to remain linear in the fermionic mass squared. Choosing the correction therein to be determined by the solution to the gluonic gap leads to [79, 29]

$$\bar{m}_\infty^2 = m_\infty^2 - 2\sqrt{2}\alpha_s NT \bar{m}_\infty \quad (4.3)$$

$$\bar{M}_\infty^2 = M_\infty^2 - \frac{\sqrt{2}\alpha_s (N^2 - 1) T}{N} \bar{m}_\infty, \quad (4.4)$$

where m_∞^2 and M_∞^2 are the leading-order gluonic and fermionic asymptotic masses as given in (2.9) and (2.18). This in fact avoids tachyonic masses for the fermions as long as $N_f \leq 3$.¹

Finally, since the averaged quantities \bar{m}_∞^2 and \bar{M}_∞^2 are the effective masses at hard momenta only, a cutoff scale $\Lambda = \sqrt{2\pi T m_D c_\Lambda}$ is introduced that separates soft from hard momenta. The quasiparticle pressure for this model, which in the following will be referred to as NLA-model, then separates into a soft and a hard component for both gluons and fermions. The soft contributions are given by expressions similar to Eq.(3.11), but with Λ as upper limit for the momentum

¹For $N_f = 3$ the solutions to the above approximate gap equations happen to coincide with those obtained in the original version of two independent quadratic gap equations of Ref. [28]. For the case $N_f = 2$ considered here, the differences are fairly small. For $N_f > 3$, however, the necessity to avoid tachyonic masses would restrict the range of permissible coupling strength α_s .

integration. For the hard contributions, the momentum integrations run from Λ to ∞ and the mass pre-factors in the HTL self-energies (2.3,2.16) are replaced by their asymptotic counterparts, $m_D^2 \rightarrow 2\bar{m}_\infty^2$ and $M^2 \rightarrow \frac{1}{2}\bar{M}_\infty^2$.

The single free parameter c_Λ in Λ can be varied around 1 to obtain an idea of the “theoretical error” of the model. In the following the range $c_\Lambda = \frac{1}{4}$ to $c_\Lambda = 4$ will be considered; note that $c_\Lambda = \infty$ corresponds to the HTL-model (which has been used as cross-check) since all hard corrections are ignored. On the other hand, $c_\Lambda = 0$ would assume that (4.3) and (4.4) represent good approximations for the NLO corrections to the spectral properties of soft excitations. However, the few existing results, in particular on NLO corrections to the Debye mass [80] and the plasma frequency [81], appear to be rather different so that it seems safer to leave the soft sector unchanged by keeping a finite c_Λ .

4.2 Fitting lattice data at $\mu = 0$

Going through the program of fitting the entropy expressions from the models under consideration to lattice data [17] for $N_f = 2$ as described in chapter 3, one finds the following values for the fit parameters T_s and λ :

	simple	HTL	$c_\Lambda = 4$	$c_\Lambda = 1$	$c_\Lambda = 1/4$
T_s/T_c	-0.89	-0.89	-0.89	-0.84	-0.61
λ	17.1	19.4	18.64	11.43	3.43

It can be seen that the results for the simple, HTL and NLA quasiparticle model with $c_\Lambda = 4$ are very close. The fits to the entropy data all lie in a narrow band for all the models considered [77], resembling the fits for the simple and HTL quasiparticle models shown in Fig. 3.2. The fitted effective coupling α_s for the various models is shown in Fig. 4.1; for comparison, also the 2-loop perturbative running coupling in $\overline{\text{MS}}$ is shown, where the renormalization scale is varied between πT and $4\pi T$ and $T_c = 0.49\Lambda_{\overline{\text{MS}}}$. As can be seen from the plot, the results for the effective coupling are well within the range of the 2-loop perturbative running coupling (for the case $c_\Lambda = 1/4$ and renormalization scale πT the results even seem to be identical, which is, however, probably only a coincidence). The result for the coupling obtained in the semi-classical approach of Ref. [82]² is also shown in Fig. 4.1.

In general, one can see that the effective coupling becomes bigger when c_Λ gets smaller; this is because the hard masses (for equal values of the coupling) are smaller than the soft masses, which makes the entropy increase when the hard parts become more important. Accordingly, the coupling has to rise in order for

²For finite μ and constant temperatures, however, the coupling obtained in [82] rises while the quasiparticle model results indicate a decrease of the coupling (which is consistent with the standard QCD running coupling with renormalization scale proportional to $\sqrt{T^2 + (\mu/\pi)^2}$).

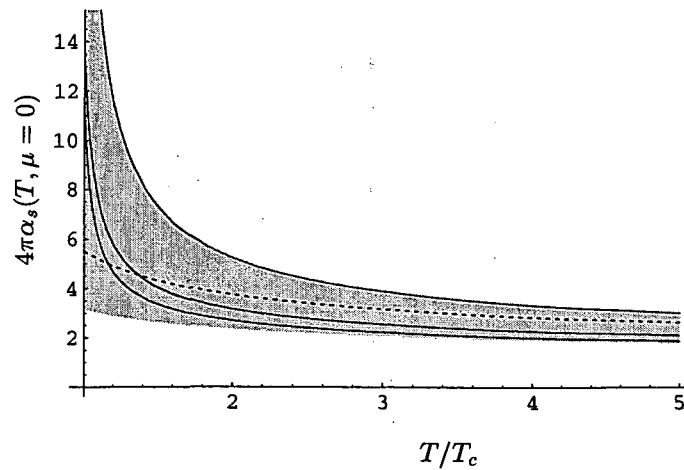


Figure 4.1: Effective coupling: NLA model results for $c_\Lambda = 4, 1$ and $1/4$ (full lines from bottom to top), 2-loop perturbative coupling in \overline{MS} (gray band) and result from Ref. [82] (dashed line).

the entropy to match the data (therefore, for the extreme case $c_\Lambda = 0$ one finds huge values of the effective coupling constant).

The fact that the fitted effective coupling agrees so well with the band of the 2-loop perturbative running coupling suggests that also simply using the perturbative running coupling as an input might lead to results for the thermodynamic pressure that are not very different; this approach will be tested in chapter 5.

Once the effective coupling is known for $\mu = 0$ one can proceed to fix the remaining integration constant B_0 as indicated in chapter 3. Setting $P(T_c) = 0.536(1) T_c^4$ one finds

	simple	HTL	$c_\Lambda = 4$	$c_\Lambda = 1$	$c_\Lambda = 1/4$
B_0/T_c^4	1.1	0.82	0.73	0.6	0.47

The fits for the model pressure for the various models also turn out to lie in a narrow band [77] resembling the HTL and simple quasiparticle model result shown in Fig. 3.4. Therefore, also the NLA quasiparticle model can be used to accurately describe lattice data for the entropy and pressure at vanishing chemical potential. In contrast to what was found from the comparison between the HTL and simple quasiparticle model, the fit parameters indicate that at least for $c_\Lambda < 1$ the NLA model differs considerably from the other models. Unfortunately, it is hard to say if this difference is due to the full inclusion of the plasmon effect in the NLA model and thereby represents a better approximation of the underlying physics than the HTL model, or rather to the fact that only the *averaged* NLO corrections to the self-energies were taken into account and the deviations of this model signal the onset of the breakdown of applicability, which probably

occurs³ at $c_\Lambda \ll 1$. In any case, the results for physical quantities from the NLA models with $1/4 < c_\Lambda < 4$ turn out to fulfill the requirement that they represent again small corrections to the HTL and simple quasiparticle model results, giving further confidence that the stability of quasiparticle models is unaffected by the plasmon effect.

4.3 Results for small chemical potential

The NLA model flow equations for the effective coupling can be solved along the lines of the HTL and simple model in chapter 3; the shape of the characteristics resembles those of the other models and the crossing of characteristics found in the simple quasiparticle model also does not occur in the NLA models (similar to what has been found for the HTL-model).

4.3.1 Susceptibilities

Once the flow equations of the various models have been solved, it is straightforward to calculate the quark-number susceptibilities at $\mu = 0$,

$$\chi(T) = \left. \frac{\partial^2 p}{\partial \mu^2} \right|_{\mu=0} \quad (4.5)$$

The result – normalized to the tree level result $\chi_0 = \frac{NN_f}{3} T^2$ – is compared to lattice data for $N_f = 2$ [83] and $N_f = 2 + 1$ [39] in Fig. 4.2. As can be seen, there is a very good agreement between the model predictions and the lattice data (which is completely independent from the one used in determining the model fit parameters). The result from a strictly perturbative calculation [84] (not shown) also is consistent with the results of Fig. 4.2 at larger temperatures, although the uncertainty in the latter is much bigger than that of the quasiparticle model results (see also chapter 5).

Calculating the pressure at finite chemical potential $p(T, \mu)$ as described in chapter 3, one is able to numerically extract the higher order susceptibility

$$\bar{\chi}(T) = \left. \frac{\partial^4 p}{\partial \mu^4} \right|_{\mu=0} \quad (4.6)$$

by doing a least-square fit to the model pressure

$$p_m(T, \mu) = p(T, 0) + \frac{\chi(T)}{2} \mu^2 + \frac{\bar{\chi}(T)}{4!} \mu^4. \quad (4.7)$$

³This hypothesis is strengthened by the fact that although the NLA model with $c_\Lambda = 0$ can be made to describe the lattice data at $\mu = 0$, the values of the fit parameters for this model do not resemble anymore those of the other quasiparticle models given above, and its subsequent extension to finite chemical potential gives results that are at odds with respect to the other models as well as lattice calculations.

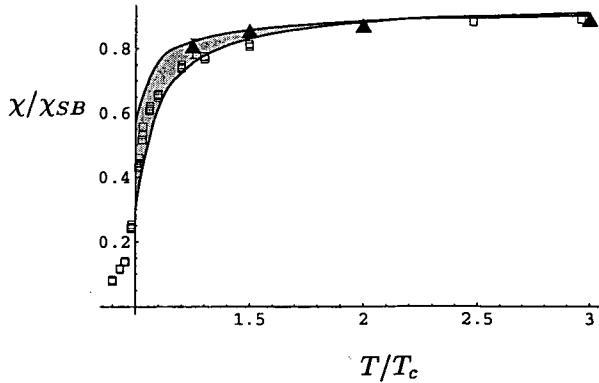


Figure 4.2: Susceptibilities from NLA models (light gray band), from lattice data for $N_f = 2$ [83] (triangles) and for 2+1 flavors [39] (boxes).

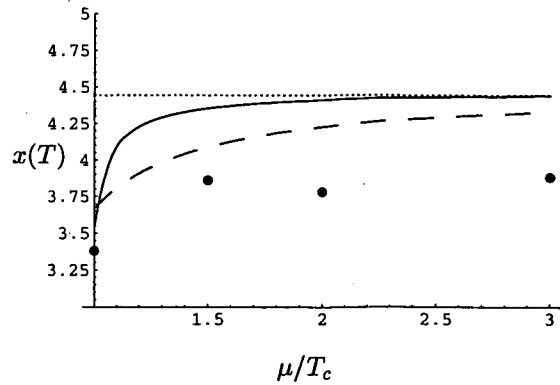


Figure 4.3: The tree-level result $\sqrt{2}\pi$ (dotted line) for the quantity $x(T)$ compared to the HTL model result (full line), lattice results from Ref. [41] as well as results from strict perturbation theory [36] (dashed line).

Parameterizing

$$\bar{\chi}(T) = \frac{\chi(T)}{2T^2} \frac{4!}{x(T)} \quad (4.8)$$

one obtains the result shown in Fig. 4.3. In this figure, also the lattice results for the corresponding quantity in Ref. [41] (which however have not been extrapolated to the continuum limit) and strictly perturbative results [36, 85] (for the specific renormalization scale $\bar{\mu} = 8.112T$ [86]) are shown, indicating general agreement between the different approaches.

A measure of how well Eq.(4.7) describes the quasiparticle result for the pressure can be obtained by considering the quantity $\delta p = p(T, \mu) - p_m(T, \mu)$, shown in Fig. 4.4: in the region considered ($\mu < 10T_c$) the biggest deviations occur for temperatures near T_c ; at $T = T_c$ there is a maximum deviation of 8% near $\mu \simeq 3.5 T_c$, while for temperatures $T > 1.3 T_c$ the deviations stay below 3×10^{-3} .

In fact, this agrees with the result of FODOR and KATZ [39], who found that a scaling relation Eq.(4.7) without the μ^4 coefficient works rather well for small $\mu \lesssim T_c$.

4.3.2 Lines of constant pressure

Once the data for the pressure at finite chemical potential has been calculated, it is also straightforward to extract lines of constant pressure $p(T, \mu) = p(T_0, 0)$. Clearly, the line $p(T, \mu) = p(T_c, 0)$ is of special interest, since it is believed that close to this line the transition from the hadronic to the quark-gluon plasma phase is occurring. For small μ , a quantity that can be compared to recent lattice results

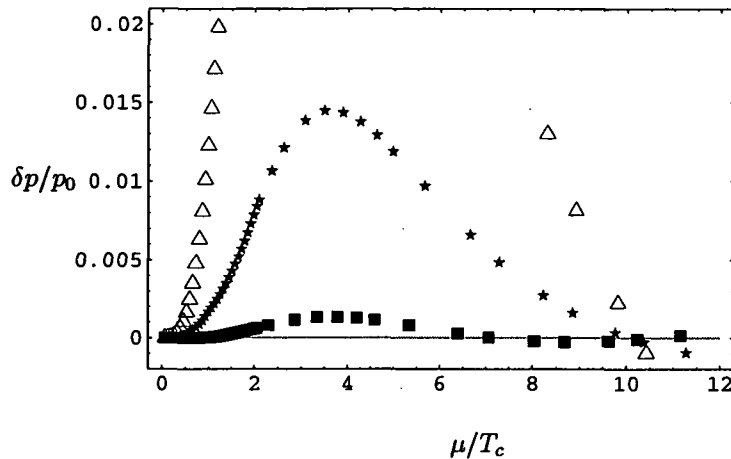


Figure 4.4: Deviations of the quasiparticle pressure from the model pressure Eq.(4.7) as a function of μ scaled with the free pressure p_0 : shown is HTL model data for $T = T_c$ (triangles), $T = 1.1T_c$ (stars) and $T = 1.3T_c$ (boxes). For higher temperatures, the deviations are even smaller than those for $T = 1.3T_c$. The result for $T = T_c$ reaches to a maximum of about 8%.

is the slope $T_c \frac{dT}{d\mu^2}$ of this constant pressure line, which is readily calculated for the quasiparticle models:

	simple	HTL	$c_\Lambda = 4$	$c_\Lambda = 1$	$c_\Lambda = 1/4$
$T_c \frac{dT}{d\mu^2}$	-0.0634(1)	-0.06818(8)	-0.06810(6)	-0.06329(34)	-0.041(9)

One finds that – as anticipated – the simple and HTL quasiparticle models as well as the NLA models for $c_\Lambda > 1$ give results that lie rather close to each other whereas for $c_\Lambda = 1/4$ the NLA model result is already somewhat off the other values. In Fig. 4.5 the quasiparticle model results are compared to recent lattice data for $2 + 1$ flavors [39] and 2 flavors [35]. One can see that the band for the $2 + 1$ flavor lattice calculation (resulting from fitting the data with a second-order (upper limit) and fourth-order (lower limit) polynomial in μ as proposed in [87]) is in very good agreement with the simple, HTL, and NLA $c_\Lambda > 1$ calculations, whereas for the NLA $c_\Lambda = 1/4$ model the slope is somewhat flatter. The lattice study for 2 flavors (dashed lines in Fig. 4.5) predicts a slope of $T_c \frac{dT}{d\mu^2} = -0.107(22)$, which is significantly steeper.

Although there is no perfect match between all the various lattice and quasiparticle model results for the constant pressure slope, the deviations are small enough that there is overall consistency between the different approaches. Indeed, it is plausible that the remaining disagreement is due to the fact that none of the lattice data have been rigorously extrapolated to the continuum limit, so that both the data and the fits of the quasiparticle models are still likely to change somewhat when this will be done eventually.

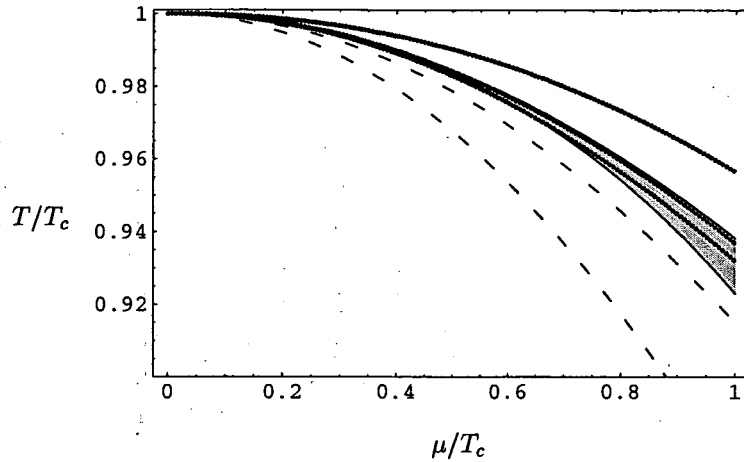


Figure 4.5: Lines of constant pressure: NLA models for $N_f = 2$ from $c_\Lambda = 4$, $c_\Lambda = 1$ and $c_\Lambda = 1/4$ (dotted lines from lowest to highest); lattice data for $N_f = 2 + 1$ [39] (light gray band) and $N_f = 2$ [35] (long dashed-lines).

4.4 Large chemical potential

Extending the lines of constant pressure from the different models to very small temperatures one obtains a crude estimate of the deconfinement transition line in this region of phase space (assuming that color superconductivity has only a minor effect, as argued above). Denoting with μ_c the chemical potential where (for vanishing temperature) the pressure at vanishing temperature equals the pressure at $\mu = 0$, $P(0, \mu_c) = P(T_c, 0)$, one finds (assuming $T_c = 172$ MeV for easier comparison)

	simple	HTL	$c_\Lambda = 4$	$c_\Lambda = 1$	$c_\Lambda = 1/4$
μ_c	548 MeV	533 MeV	536 MeV	558 MeV	584 MeV
μ_0	525 MeV	509 MeV	511 MeV	537 MeV	567 MeV

Here μ_0 denotes the value of μ where the pressure vanishes, which may be taken as a definite lower bound for the critical chemical potential within the respective models.

In general, these results are in agreement with the estimates for μ_c from Refs. [87, 43]; for the QP models considered, the lowest and highest results for μ_c are obtained for the HTL model and the NLA model with $c_\Lambda = 1/4$, respectively, while the μ_c of the simple QP model lies between the NLA $c_\Lambda = 4$ and $c_\Lambda = 1$ model values. However, even the lowest result for μ_c turns out to exceed the value for the critical chemical potential expected in Ref. [88, 44].

The quasiparticle results for the pressure at $T/T_c \simeq 0.01$ has been compared to the result of the perturbative pressure at vanishing temperature in Fig. 4.6. The latter is originally due to FREDMAN, MCLERRAN and BALUNI [50, 49] but

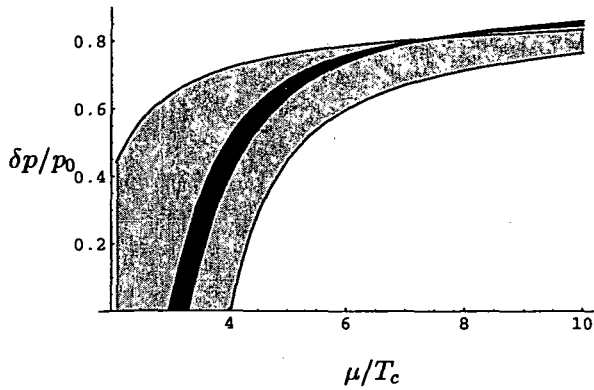


Figure 4.6: The pressure at vanishing T : shown are perturbative results (light gray band) and NLA models for c_Λ from 1/4 to 4 (dark band).

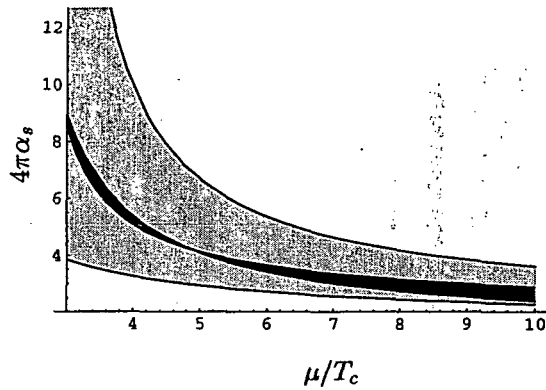


Figure 4.7: Effective coupling from NLA models with $c_\Lambda = 4$ to 1/4 (dark band) and perturbative 2-loop running coupling (light gray band).

has been recalculated more precisely by VUORINEN [36],

$$p(T=0, \mu) = \frac{\mu^4 N_f}{4\pi^2} \left\{ 1 - 2 \frac{\alpha_s}{\pi} - \left[18 - 11 \ln 2 - 0.53583 N_f + N_f \ln \frac{N_f \alpha_s}{\pi} \right. \right. \\ \left. \left. + \left(11 - \frac{2}{3} N_f \right) \ln \frac{\bar{\mu}}{\mu} \right] \left(\frac{\alpha_s}{\pi} \right)^2 + O(\alpha_s^3 \ln \alpha_s) \right\}, \quad (4.9)$$

where in this [89] form $\bar{\mu}$ again denotes the renormalization scale in the $\overline{\text{MS}}$ renormalization scheme. The perturbative result has been evaluated using the standard two-loop running coupling Eq.(1.6) with $\Lambda_{\overline{\text{MS}}} = T_c/0.49$ [12] and renormalization scale varied from μ to 3μ , as has been considered in Ref. [88]. It can be seen in Fig. 4.6 that while in general the quasiparticle model and perturbative results are consistent, the variation in the latter (due to the uncertainty in the renormalization scale $\bar{\mu}$) is much larger than the narrow band obtained from the evaluation of the different quasiparticle models. The perturbative two-loop running coupling at vanishing temperature itself is shown in Fig. 4.7 as a function of chemical potential, compared to the result of the effective coupling for the quasiparticle models.

4.4.1 EOS for cold deconfined matter

By calculating the number density at $T/T_c \simeq 0.01$ and using the results for the pressure one obtains an equation of state for cold deconfined matter. As is the case for the simple quasiparticle model [43], one finds that also for the HTL and NLA models the energy density ϵ is well fitted by the linear relation

$$\epsilon(p) = 4\tilde{B} + \alpha p$$

with

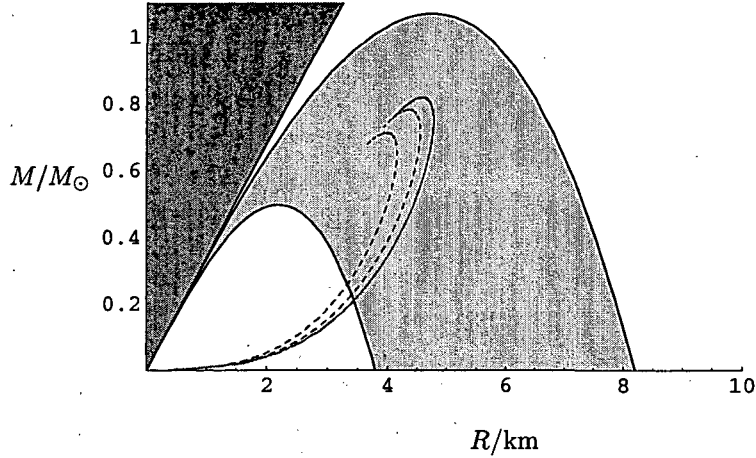


Figure 4.8: Mass-radius relations of non-rotating quark-stars: shown are the results using the EOS from the HTL (full line) and NLA models (dashed lines). Also shown are the inferred mass-radius relations of RX J1856.5-3754 from Ref. [90, 91], a possible candidate for a quark star. The dark shaded region is excluded by the condition $R > 2GM$.

	simple	HTL	$c_\Lambda = 4$	$c_\Lambda = 1$	$c_\Lambda = 1/4$
$4\bar{B}/T_c^4$	12.3 (6)	11.1(8)	12.3(8)	14.7(9)	19.2(1.6)
α	3.26(5)	3.23(5)	3.22(4)	3.22(4)	3.17(4)

The value of $\alpha \simeq 3.2$ for $N_f = 2$ seems to be model independent, in contrast to the bag constant $\bar{B}^{1/4}$, which varies between 314 and 360 MeV.

4.5 Application 1: Quark stars

As a first application I will use the above equation of state for cold deconfined matter to determine the mass-radius relations of non-rotating quark-stars. If these stars exist, they would differ from ordinary neutrons stars by being more compact and therefore considerably smaller than current neutron-star models allow [44], as I will show in the following.

Starting from Einstein's equations

$$R_{\mu\nu} - \frac{1}{2}g_{\mu\nu}R = 8\pi T_{\mu\nu}(\epsilon(p), p) \quad (4.10)$$

where $R_{\mu\nu}$, $g_{\mu\nu}$ and R denote the Ricci and metric tensor and Ricci scalar, respectively. Using the Schwarzschild solution for the metric of a spherically symmetric and static star one readily finds the familiar Tolman-Oppenheimer-Volkoff equa-

tions [92, 93, 45],

$$\frac{dp(r)}{dr} = -\frac{G [\epsilon(r) + p(r)] [M(r) + 4\pi r^3 p(r)]}{r^2 \left(1 - \frac{2GM(r)}{r}\right)}, \quad (4.11)$$

where

$$M(r) = 4\pi \int_0^r \epsilon(r) r^2 dr \quad (4.12)$$

and G is Newton's constant. The equations are easily solved by specifying a central pressure or density and calculating the size and mass of the corresponding star using the equations of state from the previous section. The results are shown in Fig. 4.8, where it can be seen that the quasiparticle model EOS allows for quark-stars with masses of $\sim 0.8M_\odot$ and radii of less than 5 km (which is similar to the results found in Refs. [44, 43, 94]). Current neutron star models – which are consistent with the pulsar data [44] – predict a maximum mass in the range of 1.4 to 2 solar masses with radii ranging from 10 to 15 km, so if pure quark-stars exist, they should in principle be distinguishable from ordinary neutron stars by observation. Interestingly, several observations of neutron star candidates possessing properties that are in apparent contradiction with current neutron star models exist, most prominently the object RX J1856.5-3754, whose inferred mass-radius relation (see Ref. [90, 91]) is also shown in Fig. 4.8. The exciting possibility that with the observation of RX J1856.5-36754 one has a direct confirmation of the existence of quark-stars is still a matter of ongoing debate, as there are propositions claiming that the available data can be described by an ordinary neutron star; future observations are therefore needed to settle the issue of the exact nature of RX J1856.5-36754.

Finally, it should be kept in mind that the outermost layers of such a possible quark star consist of hadronic matter, giving rise to what is usually named a “hybrid star”. The details of the star structure will depend sensitively on the hadronic equation of state [43], which unfortunately does not match on naturally to the EOS of the quark-gluon plasma phase calculated above [44]. Therefore, to make clear predictions for the phenomenology of compact stars one has to find a way to describe the intermediate range of densities in the equation of state, possibly by considering effective field theory models [95].

4.6 Application 2: Expansion of the quark-gluon plasma

As a second application, I shall now describe the longitudinal expansion of the matter produced in a central collision of identical nuclei, using Bjorken's relativistic hydrodynamic model and the quasiparticle EOS for the quark-gluon plasma

calculated above. The starting point is the energy-momentum tensor of a relativistic fluid with local energy density $\epsilon(x)$ and pressure $p(x)$,

$$T_{\mu\nu} = (\epsilon + p)U_\mu U_\nu - g_{\mu\nu}p, \quad (4.13)$$

where U^μ is the four-velocity of the fluid obeying $U^2 = 1$. Energy, momentum as well as the baryon number $N^\mu = nU^\mu$ of the system should be conserved, therefore

$$\partial^\mu T_{\mu\nu} = 0, \quad \partial^\mu N_\mu = 0. \quad (4.14)$$

Introducing proper time τ and space-time rapidity η defined as

$$\tau = \sqrt{t^2 - z^2}, \quad \eta = \frac{1}{2} \ln \frac{t+z}{t-z} \quad (4.15)$$

and neglecting the effect of the transverse expansion as well as assuming that the properties of the fluid are invariant under Lorentz boosts in the z -direction this implies [96]

$$\epsilon = \epsilon(\tau), \quad p = p(\tau), \quad T = T(\tau), \quad U_\mu = \frac{1}{\tau}(t, 0, 0, z). \quad (4.16)$$

With the use of the expressions

$$\partial_\mu \tau = U_\mu, \quad \partial_\nu U_\mu = \frac{1}{\tau}(\tilde{g}_{\mu\nu} - U_\mu U_\nu) \quad (4.17)$$

and $\tilde{g}_{\mu\nu} = (1, 0, 0, 1)$, the conservation equations can be brought into the form

$$u^\mu \partial_\mu \left(\frac{s}{n} \right) = 0, \quad \partial_\mu N^\mu = 0, \quad (4.18)$$

implying that the entropy density s per number density n is conserved by the longitudinal expansion.

Using the quasiparticle model EOS one can calculate the curves of constant s/n in the T, μ -plane, shown in Fig. 4.9. Surprisingly, the curves are very well approximated by straight lines having slopes consistent with the tree-level approximation

$$\frac{s}{n} \simeq \frac{T^3 \left(\frac{32\pi^2}{45} + \frac{28\pi^2}{30} \right)}{2\mu T^2} = \frac{T}{\mu} \frac{74\pi^2}{90}, \quad (4.19)$$

as can be seen in Fig. 4.9; only at very large μ the tree level approximation seemingly starts to break down.

Provided one has knowledge about the value of T, μ that the system reaches at freeze-out (e.g. by analyzing experimental data using thermal model descriptions of particle production [97]) as well as an estimate of the initial energy density created after heavy-ion collision, the above results allow an estimate of the initial temperature and chemical potential. For example, BRAUN-MUNZINGER *et al.*

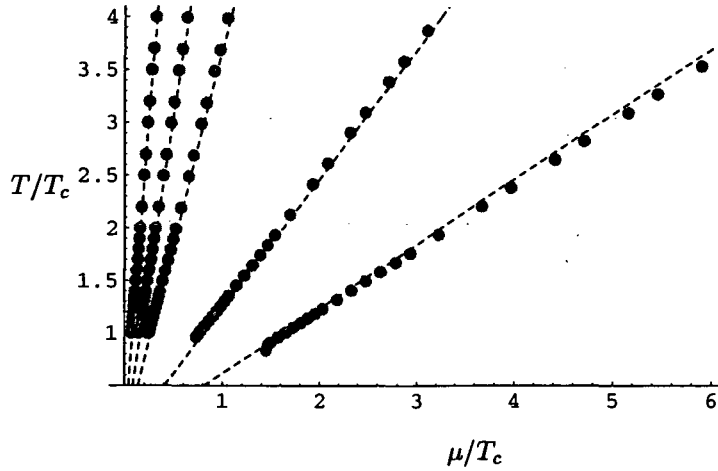


Figure 4.9: Curves of constant $s/n = 100, 50, 30, 10, 5$ for the HTL model (dots). Also shown are the tree-level results (dashed straight lines) for the corresponding values of s/n .

obtained $(T, \mu) \simeq (174\text{MeV}, 15\text{MeV})$ as freeze-out values for the central Au-Au collisions at RHIC with $\sqrt{s} = 130\text{GeV}$, which corresponds to a value of $s_0/n_0 \simeq 100$. Assuming furthermore an initial energy density of $\epsilon_0 = 20\text{GeV}/\text{fm}^3 \simeq 175T_c^4$ [97] and again $T_c = 172\text{MeV}$ one obtains $(T_0, \mu_0) = (344\text{MeV}, 27\text{MeV})$ as initial temperature and chemical potential. Consequently, one can calculate the time behavior of the system by e.g. integrating Eq.(4.18),

$$n = \frac{n_0 \tau_0}{\tau}, \quad (4.20)$$

where $n_0 = n(T(\mu_0), \mu_0)$ and τ_0 is expected to be on the order of $\tau_0 \simeq 1\text{fm}/c$. In this model, one finds that the system freeze-out time is given by $\tau_f \simeq 12\text{fm}/c$. It is clear however, that the above result is only a rough estimate of the time the system remains in a quark-gluon plasma phase since one has to take into account viscous effects of the fluid as well as the transversal expansion of the system that cannot be neglected at late times.

4.7 Summary

In this chapter, I have set up a possible extension of the HTL quasiparticle model that includes the full plasmon effect, however at the price of having to introduce another parameter. The values of the parameters used to fit the quasiparticle models to the $N_f = 2$ lattice data were given and it was shown that the resulting running coupling turns out to be comparable to the 2-loop perturbative coupling. I then investigated the quark-number susceptibilities at vanishing chemical potential and showed that they agree very well with independent lattice data; for

the HTL model, it was also shown that the higher-order derivatives represent the trend of another independent lattice study. Furthermore, it turned out that the quasiparticle pressure can be very well described by these $\mu = 0$ susceptibilities, even up to rather large values of chemical potential. Moreover, I calculated the lines of constant pressure starting from the critical temperature at $\mu = 0$, which were shown to be compatible with lattice studies in the validity region of the latter. Extrapolating these results to large chemical potentials and small temperatures I obtained an equation of state for cold dense matter which should represent an improvement over existing perturbative results. As a first application, I then derived the mass-radius relationship of so-called quark-stars, finding results that fit nicely with the values inferred for RX J1856.5-3754, a possible candidate for a quark star. As a second application, I calculated the expansion of a quark-gluon plasma created after a heavy-ion collision in the Bjorken model, finding that the system cools along nearly straight lines in the T, μ -diagram. Finally, I estimated the time that the system remains in the quark-gluon plasma phase using freeze-out values of the temperature and chemical potential inferred for Au-Au collisions at RHIC.

Chapter 5

Results independent of the lattice

In the last chapters I used an effective coupling to describe lattice data at vanishing chemical potential which eventually gave a plausible equation of state for arbitrary chemical potentials. Although this approach seems to work very well it is somewhat unsatisfactory to be limited to available lattice data and a phenomenological ansatz for an effective coupling. Therefore, I want to investigate in this chapter how the results of the previous chapters are modified if one renounces all lattice input save one number, namely the ratio $T_c/\Lambda_{\overline{MS}}$, which for $N_f = 2$ I take to be given by 0.49, as was used before. Instead of the effective coupling I will use the standard two-loop running coupling of Eq.(1.6) with $\bar{\mu}$ ranging between πT and $4\pi T$ at $\mu = 0$, therefore testing the theoretical error of the model predictions. Furthermore, since the quasiparticle models represent an implementation of the thermodynamic quantities which is correct at least to leading perturbative order, one is then able to make predictions of these quantities “uncontaminated” by lattice artifacts using the machinery of the previous sections. I will then compare these predictions to both perturbational approaches and lattice results (whenever available) as well as those obtained in the previous chapters.

5.1 Setup

Using the HTL and NLA quasiparticle models for the pressure and the two-loop perturbative coupling, the expression for the entropy becomes that of BLAIZOT *et.al* [28]. Evaluating the entropy as a function of T by using $T_c/\Lambda_{\overline{MS}} = 0.49$ for $N_f = 2$ (which differs from the value used in the original reference) one can compare the result to lattice data for $N_f = 2$ from Ref. [17] (used for the fits in the previous sections) and Ref. [18] in Fig. 5.1a. As can be seen, the NLA model results are in general agreement with the lattice data (especially since a rigorous extrapolation of the lattice data to the continuum limit is still missing) while the HTL model seems to predict slightly too small values for the entropy.

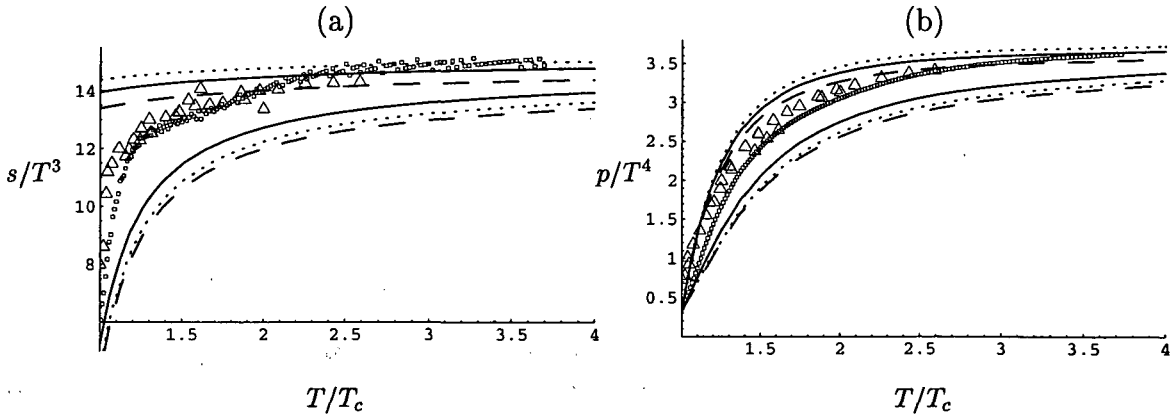


Figure 5.1: Two-flavor entropy (a) and pressure (b) for HTL (long-dashed lines) and NLA quasiparticle models (full lines for $c_\Lambda = 1$, dotted lines for $c_\Lambda = 2, \frac{1}{2}$), where the renormalization scale has been taken to be $\bar{\mu} = 4\pi T$ and $\bar{\mu} = \pi T$, respectively. Also shown are $N_f = 2$ lattice results from Refs. [17] (triangles) and [18] (boxes), respectively.

The pressure of the respective models is then given by Eq.(3.9), where B_0 is fixed in such a way that the pressure at $T = T_c$ is equal to the pressure of a free gas of 3 massless flavors of pions,

$$p(T_c, 0)/T_c^4 = \frac{\pi^2}{30} \simeq 0.329. \quad (5.1)$$

This completes the setup of the model. The resulting pressure at $\mu = 0$ as a function of the temperature is shown in Fig. 5.1b; although the model pressure is not as close to the lattice data as in the previous chapters where a phenomenological fit of the coupling was used, it is still remarkable that the resulting band turns out to cover the lattice results and not much more while the lattice input has been minimized to one number.

5.2 Results

The characteristic curves again take shapes resembling ellipses as was the case in the previous chapters. Calculating the quark-number susceptibilities one finds the results shown in Fig. 5.2. As can be seen, the agreement with lattice data is still fairly good at high temperatures, whereas at temperatures comparable to T_c the variations from varying $\bar{\mu}$ by a factor of 2 around $2\pi T$ get rather large. Note however that the results from the NLA models for the susceptibilities clearly differ from those obtained originally by BLAIZOT *et al.* [98]. The discrepancy is due to the fact that here the fermionic contributions were divided into soft and hard part similar to the gluonic contributions while in the original reference the fermions have been treated differently. As a consequence of treating the fermionic sector as in Ref. [77], the NLA model susceptibilities for $N_f = 2$ lie only slightly

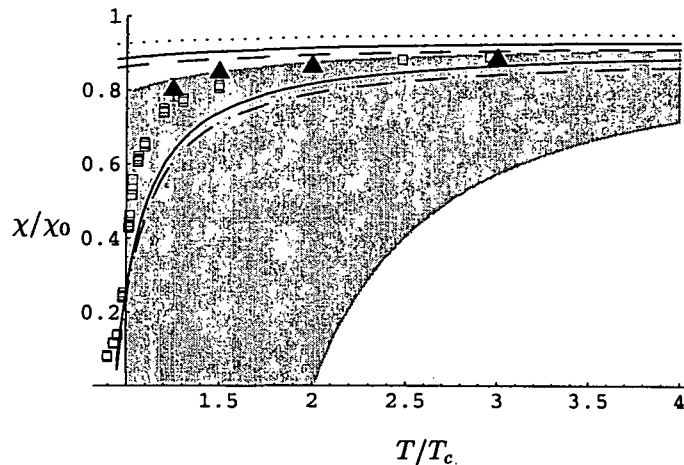


Figure 5.2: Two-flavor susceptibilities for HTL (long-dashed lines) and NLA quasiparticle models (full lines for $c_\Lambda = 1$, dotted lines for $c_\Lambda = 4, \frac{1}{4}$), where the renormalization scale has been taken to be $\bar{\mu} = 4\pi T$ and $\bar{\mu} = \pi T$, respectively. Also shown are $N_f = 2$ lattice results from Ref. [83] (full triangles) and [39] (open boxes), respectively. The gray band corresponds to results from strict perturbation theory to order $\alpha_s^3 \ln \alpha$ [84] (see text for details).

higher than the HTL results, as shown in Fig. 5.2. Therefore, the NLA results are in good agreement with existing lattice data [83, 39] while the original NLO results did not have any overlap with the data. I also show the results for the quark-number susceptibilities from strict perturbation theory to order $\alpha_s^3 \ln \alpha$, by VUORINEN [84, 85] in Fig. 5.2; the band shown corresponds to varying $\bar{\mu} = \pi T$ to $\bar{\mu} = 4\pi T$ while the unknown α_s^3 coefficient is taken close to zero [85].

When calculating the slope of the lines of constant pressure one obtains $T_c \frac{dT}{d\mu^2} \simeq -0.055 / -0.065$ for the HTL quasiparticle model for $\bar{\mu} = \pi T$ (first value) and $\bar{\mu} = 4\pi T$ (second value). The variations for the NLA model are slightly larger since one also has to consider the variation in the coefficient c_Λ ; one finds $T_c \frac{dT}{d\mu^2} \simeq -0.052 / -0.065$ for the NLA model when varying $\bar{\mu}$ as above and c_Λ by a factor of 2 around 1. Therefore, also the slopes of constant pressure turn out to be very similar to what was found in chapter 4, indicating that the agreement between these results and lattice calculations for $N_f = 2$ is a quite robust prediction of the quasiparticle models and in fact nearly independent of the fit data used in the previous chapters.

Extrapolating the $N_f = 2$ quasiparticle results to the region of small temperatures one can calculate an estimate for the critical density where $p(0, \mu_0) = 0$. Again varying $\bar{\mu}$ one finds for the HTL model $\mu_0 \simeq 3.49T_c$ and $\mu_0 = 2.93T_c$ for $\bar{\mu} = \pi T$ and $\bar{\mu} = 4\pi T$, respectively. For the NLA model the results turn out to be very similar, with the only difference being that the upper prediction of μ_0 is slightly increased to $\mu_0 \simeq 3.52T_c$. Comparing these to the results from the fitted

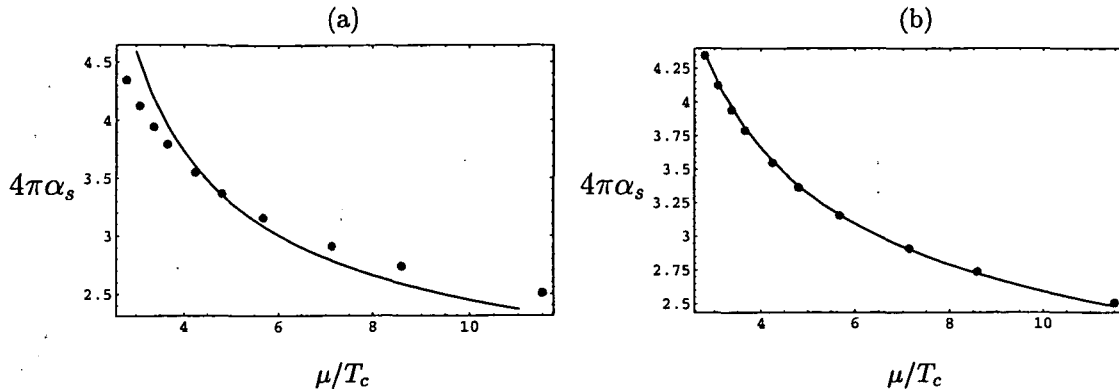


Figure 5.3: Two-loop (a) and one loop (b) fits (full line) to the quasiparticle model coupling at $T = 0$ (points).

quasiparticle models one finds that for $\bar{\mu} = \pi T$ the estimates for μ_0 are noticeably higher in the models not fitted to lattice data at $\mu = 0$, while for larger values of $\bar{\mu}$ the results become very similar (i.e. for $\bar{\mu} = 4\pi T$ the HTL model result is only about 2% lower than in chapter 4).

Finally, it is also interesting to investigate closer what form the coupling constant takes in the region $T \ll \mu$. For example, one can try to describe $\alpha_s(T = 0, \mu)$ by the standard two-loop result with $\bar{\mu} = y\mu$, where y is to be determined by a least-square fit. This approach turns out to be not too successful, as can be seen in the exemplary plot of Fig. 5.3a, where such a fit has been tried on the HTL model result. Remarkably, the situation is very different when using the *one-loop* form for the running coupling Eq.(1.4) instead of the two-loop result. For the one-loop coupling, the fits with $\bar{\mu} = y\mu$ typically look like the one shown in Fig. 5.3b, both for the HTL model as well as for the NLA models. Moreover, it turns out that the fit constant c is always proportional to the scale used at $\mu = 0$, i.e. when the renormalization scale was $\bar{\mu} = 4\pi T$ at $\mu = 0$ the scale that fits the coupling best at $T = 0$ is given by $\bar{\mu} \simeq 4\pi\mu 0.37$ while for an original scale of $\bar{\mu} = \pi T$ one finds $\bar{\mu} \simeq \pi\mu 0.33$ at $T = 0$.

5.2.1 Notes on changing $T_c/\Lambda_{\overline{MS}}$

As stressed before, the above results depend only on one external parameter, namely the value of $T_c/\Lambda_{\overline{MS}}$. It is therefore interesting to investigate how the results derived above will change when this parameter turns out to be smaller or bigger than 0.49. To this effect it is sufficient to see that the running coupling only depends on the scale through $\bar{\mu}/\Lambda_{\overline{MS}}$ and accordingly

$$\frac{\bar{\mu}}{\Lambda_{\overline{MS}}} = \frac{\bar{\mu}}{T_c} \frac{T_c}{\Lambda_{\overline{MS}}}. \quad (5.2)$$

Increasing the value of $T_c/\Lambda_{\overline{MS}}$ therefore amounts to increasing the ratio renormalization scale over critical temperature. As an effect, the entropy and the sus-

ceptibilities will rise, whereas the slopes of constant pressure will become more negative. Finally, the estimate for the critical density will also take smaller values.

5.3 Summary

In this chapter I investigated the results from various quasiparticle models when using only one number, namely the value of $T_c/\Lambda_{\overline{MS}}$ as an input. It turns out that the pressure and the quark number susceptibilities at $\mu = 0$ are still described fairly well. The results for the slopes of constant pressure are close to what has been found in the previous chapters as long as $\bar{\mu}$ is not much smaller than $2\pi T$, as is the case for the estimates of the critical density at $T = 0$. Furthermore, it turns out that the resulting coupling at $T = 0$ can be very well described by the standard one-loop running coupling. I conclude by pointing out how the results derived in this chapter have to be modified when $T_c/\Lambda_{\overline{MS}}$ changes from the value adopted here.

Chapter 6

The anisotropic quark-gluon plasma

In the previous chapters I have limited myself to the consideration of isotropic systems. However, as pointed out in the introduction, the only system above the deconfinement transition one can (probably) study on earth, namely that of a fireball following an ultrarelativistic heavy-ion collision, is rather anisotropic in nature. Therefore, it is interesting to investigate which effects the presence of an anisotropy has on the dynamics of the system and which differences one can expect when comparing to the usually studied isotropic case. Note that I will consider only systems which are anisotropic in *momentum space*, therefore taking a snapshot of the system at some short time after the collision and before the system had time to convert the anisotropy from momentum space to configuration space. Although eventually one would require a full treatment including anisotropies in configuration space, I will show that one can learn a lot about anisotropic systems by considering momentum anisotropies alone; moreover, a treatment of configuration space anisotropies would involve a full non-equilibrium quantum field theoretical description of the system, which despite recent progress is not available yet.

In this chapter, I will therefore analyze the collective modes of high-temperature QCD in the case when there is an anisotropy in the momentum-space distribution function. I will present results (published in Ref. [99]) for a class of anisotropic distribution functions which can be obtained by stretching or squeezing an isotropic distribution function along one direction, thereby preserving a cylindrical symmetry in momentum space.

6.1 Gluon self-energy in an anisotropic system

Generalizing the classification of quasiparticles in an isotropic quark-gluon plasma in chapter 2 one first derives the HTL resummed gluon self-energy in an anisotropic system within semi-classical transport theory [56, 57, 58], which has been shown to be equivalent to the HTL diagrammatic approach [100]. Within semi-classical

transport theory partons are described by their phase-space densities and their time evolution is given by Vlasov-type transport equations [101, 102]. Concentrating on the physics at the soft scale, $k \sim \alpha_s^{1/2} T \ll T$, the magnitude of the field fluctuations at this scale is $A \sim \alpha_s^{1/4} T$ and derivatives are of the scale $\partial_x \sim \alpha_s^{1/2} T$. With this power-counting a systematic truncation of the terms contributing to the transport equations for soft momenta can be realized.

At leading order in the coupling constant the color current J^μ induced by a soft gauge field A^μ with four-momentum $K = (\omega, \mathbf{k})$ can be obtained by performing a covariant gradient expansion of the quark and gluon Wigner functions in mean-field approximation. The result is

$$J_{\text{ind}}^{\mu,a}(X) = (4\pi\alpha_s)^{1/2} \int \frac{d^3p}{(2\pi)^3} V^\mu (2N\delta n^a(p, X) + N_f(\delta f_+^a(p, X) - \delta f_-^a(p, X))), \quad (6.1)$$

where $V^\mu = (1, \mathbf{k}/\omega)$ is the velocity of the hard plasma constituents, $\delta n^a(p, X)$ is the fluctuating part of the gluon density, and $\delta f_+^a(p, X)$ and $\delta f_-^a(p, X)$ are the fluctuating parts of the quark and anti-quark densities, respectively. Note that δn^a transforms as a vector in the adjoint representation ($\delta n \equiv \delta n^a T^a$) and δf_\pm^a transforms as a vector in the fundamental representation ($\delta f_\pm \equiv \delta f_\pm^a t^a$).

Neglecting the collision terms which only enter at subleading order, the quark and gluon density matrices above satisfy the following transport equations:

$$[V \cdot D_X, \delta f_\pm(p, X)] = \mp (4\pi\alpha_s)^{1/2} V_\mu F^{\mu\nu}(p, X) \partial_\nu f_\pm(\mathbf{p}), \quad (6.2)$$

$$[V \cdot D_X, \delta n(p, X)] = -(4\pi\alpha_s)^{1/2} V_\mu F^{\mu\nu}(p, X) \partial_\nu n(\mathbf{p}), \quad (6.3)$$

where $D_X = \partial_X + i(4\pi\alpha_s)^{1/2} A(X)$ is the covariant derivative and $n(\mathbf{p})$ and $f_\pm(\mathbf{p})$ are the initial anisotropic gluon and quark distribution functions (which in the isotropic limit would correspond to the Bose-Einstein and Fermi-Dirac distribution functions, respectively).

Solving the transport equations (6.2) and (6.3) for the fluctuations δn and δf_\pm gives the induced current via Eq.(6.1),

$$J_{\text{ind}}^\mu(X) = 4\pi\alpha_s \int \frac{d^3p}{(2\pi)^3} V^\mu V^\alpha \partial_{(p)}^\beta h(\mathbf{p}) \times \int d\tau U(X, X - V\tau) F_{\alpha\beta}(X - V\tau) U(X - V\tau, X), \quad (6.4)$$

where $U(X, Y)$ is a gauge parallel transporter defined by the path-ordered integral

$$U(X, Y) = \mathcal{P} \exp \left[-i(4\pi\alpha_s)^{1/2} \int_X^Y dZ_\mu A^\mu(Z) \right], \quad (6.5)$$

$F_{\alpha\beta} = \partial_\alpha A_\beta - \partial_\beta A_\alpha - i(4\pi\alpha_s)^{1/2} [A_\mu, A_\nu]$ is the gluon field strength tensor, and

$$h(\mathbf{p}) = 2Nn(\mathbf{p}) + N_f(f_+(\mathbf{p}) + f_-(\mathbf{p})) \quad (6.6)$$

is a particular combination of the gluon and quark distribution functions. Neglecting terms of subleading order in α_s (implying $U \rightarrow 1$ and $F_{\alpha\beta} \rightarrow \partial_\alpha A_\beta - \partial_\beta A_\alpha$) and performing a Fourier transform of the induced current to momentum space one obtains

$$J_{\text{ind}}^\mu(K) = 4\pi\alpha_s \int \frac{d^3p}{(2\pi)^3} V^\mu \partial_{(p)}^\beta h(\mathbf{p}) \left(g_{\gamma\beta} - \frac{V_\gamma K_\beta}{K \cdot V + i\epsilon} \right) A^\gamma(K), \quad (6.7)$$

where ϵ is a small parameter that has to be sent to zero in the end.

From this expression of the induced current the self-energy is obtained through the relation

$$\Pi^{\mu\nu}(K) = \frac{\delta J_{\text{ind}}^\mu(K)}{\delta A_\nu(K)}, \quad (6.8)$$

which gives the gluon self-energy of an anisotropic system,

$$\Pi_{\mu\nu}(K) = 4\pi\alpha_s \int \frac{d^3p}{(2\pi)^3} V_\mu \partial_{(p)}^\beta h(\mathbf{p}) \left(g_{\nu\beta} - \frac{V_\nu K_\beta}{K \cdot V + i\epsilon} \right). \quad (6.9)$$

Note that this result can also be obtained using diagrammatic methods if one assumes that the distribution function is symmetric under $\mathbf{p} \rightarrow -\mathbf{p}$ [100]. Furthermore, in the isotropic limit $h(\mathbf{p}) \rightarrow h_{\text{iso}}(p)$, one recovers the well-known HTL gluon self-energy from Eq.(6.9).

After a little bit of algebra one finds that this tensor is symmetric, $\Pi^{\mu\nu}(K) = \Pi^{\nu\mu}(K)$, and transverse, $K^\mu \Pi^{\mu\nu}(K) = 0$, if the distribution function vanishes on a two-sphere at infinity, $\lim_{p \rightarrow \infty} h(\mathbf{p}) = 0$, since e.g.

$$K^\mu \Pi_{\mu 0} = -4\pi\alpha_s k_j \int \frac{d^3p}{(2\pi)^3} \partial^j h(\mathbf{p}). \quad (6.10)$$

Therefore, only the spatial components of the self-energy are needed for the dispersion relations of the quasi-gluons, which can be shown as follows: in the linear approximation the equations of motion for the gauge fields can be obtained by expressing the induced current in terms of the self-energy

$$J_{\text{ind}}^\mu(K) = \Pi^{\mu\nu}(K) A^\nu(K), \quad (6.11)$$

and plugging this into Maxwell's equations

$$-iK_\mu F^{\mu\nu}(K) = J_{\text{ind}}^\nu(K) + J_{\text{ext}}^\nu(K), \quad (6.12)$$

to obtain

$$[K^2 g^{\mu\nu} - K^\mu K^\nu + \Pi^{\mu\nu}(K)] A_\nu(K) = -J_{\text{ext}}^\mu(K), \quad (6.13)$$

where J_{ext}^ν is an external current. Using the gauge covariance of the self-energy in the HTL-approximation one can write this in terms of a physical electric field

by specifying a particular gauge. Using the temporal axial gauge ($A_0 = 0$) which has already been used in the isotropic case in chapter 2 one obtains

$$[(k^2 - \omega^2)\delta^{ij} - k^i k^j + \Pi^{ij}(K)]E^j(K) = (\Delta^{-1}(K))^{ij}E^j(K) = i\omega J_{\text{ext}}^i(K). \quad (6.14)$$

Inverting the propagator allows one to determine the response of the system to the external source

$$E^i(K) = i\omega \Delta^{ij}(K)J_{\text{ext}}^j(K). \quad (6.15)$$

The dispersion relations for the collective modes can then be obtained as in chapter 2, by finding the poles of the propagator $\Delta^{ij}(K)$.

6.1.1 Tensor decomposition

Since an anisotropic system possesses a preferred spatial direction¹, the gluon propagator cannot simply be decomposed into a transversal and longitudinal part as was the case for the isotropic system treated in chapter 2; therefore one needs to construct a new tensor basis.

As mentioned above, the gluon self-energy is symmetric and transverse; as a result not all components of $\Pi^{\mu\nu}$ are independent and one can restrict the considerations to the spatial part of $\Pi^{\mu\nu}$, denoted Π^{ij} . One therefore needs to construct a basis for a symmetric 3-tensor that – apart from the momentum k^i – also depends on a fixed anisotropy three-vector \hat{n}^i , with $\hat{n}^2 = 1$. Following Ref. [64] one first defines the projection operator

$$A^{ij} = \delta^{ij} - k^i k^j / k^2, \quad (6.16)$$

and uses it to construct $\tilde{n}^i = A^{ij}\hat{n}^j$ which obeys $\tilde{n} \cdot k = 0$. With this one can construct the remaining three symmetric 3-tensors

$$B^{ij} = k^i k^j / k^2 \quad (6.17)$$

$$C^{ij} = \tilde{n}^i \tilde{n}^j / \tilde{n}^2 \quad (6.18)$$

$$D^{ij} = k^i \tilde{n}^j + k^j \tilde{n}^i. \quad (6.19)$$

The basis spanned by the four tensors **A**, **B**, **C**, and **D** therefore allows one to decompose any symmetric 3-tensor **T** into

$$\mathbf{T} = a \mathbf{A} + b \mathbf{B} + c \mathbf{C} + d \mathbf{D}; \quad (6.20)$$

furthermore, the inverse of any such tensor is then given as

$$\mathbf{T}^{-1} = a^{-1} \mathbf{A} + \frac{(a+c)\mathbf{B} - a^{-1}(bc - \tilde{n}^2 k^2 d^2)\mathbf{C} - d\mathbf{D}}{b(a+c) - \tilde{n}^2 k^2 d^2}, \quad (6.21)$$

¹If I were to consider a system where also the cylindrical symmetry is lost there would be two preferred spatial directions and the tensor basis for this system would accordingly be more complicated, but still can be constructed by the method proposed here.

as a short amount of algebra reveals. With the above tensor decomposition one is now able to decompose the propagator into modes similar to what is done in the isotropic case. For this, one first needs to decompose the self-energy into "self-energy structure functions", which are the equivalents of the transversal and longitudinal parts of the self-energy in the isotropic case.

6.1.2 Self-energy structure functions

From Eq.(6.9) the spatial part of the general gluon self-energy tensor is found to be

$$\Pi^{ij}(K) = -4\pi\alpha_s \int \frac{d^3p}{(2\pi)^3} v^i \partial^j h(\mathbf{p}) \left(\delta^{jl} + \frac{v^j k^l}{K \cdot V + i\epsilon} \right). \quad (6.22)$$

Since the collision term was set to zero, the distribution function $h(\mathbf{p})$ is completely arbitrary at this point, so in order to proceed one needs to assume a specific form for the distribution function. In what follows I will require that $h(\mathbf{p})$ can be obtained from an (arbitrary) isotropic distribution function by the rescaling of one direction in momentum space,

$$h(\mathbf{p}) = h_\xi(\mathbf{p}) = N(\xi) h_{\text{iso}} \left(\sqrt{\mathbf{p}^2 + \xi(\mathbf{p} \cdot \hat{\mathbf{n}})^2} \right), \quad (6.23)$$

where $\hat{\mathbf{n}}$ is the direction of the anisotropy, $\xi > -1$ is a parameter reflecting the strength of the anisotropy and $N(\xi)$ is a normalization constant². Note that $\xi > 0$ corresponds to a contraction of the distribution in the $\hat{\mathbf{n}}$ direction (shown in Fig. 6.1) whereas $-1 < \xi < 0$ corresponds to a stretching of the distribution in the $\hat{\mathbf{n}}$ direction.

The normalization constant $N(\xi)$ has been introduced to preserve the relation

$$\frac{d^3n}{d^3k} = h(\mathbf{p}) \quad (6.24)$$

between number density n and the momentum-space distribution function also in the case where the latter is anisotropic. $N(\xi)$ is then simply determined by requiring n to be the same both for isotropic and anisotropic systems,

$$\int \frac{d^3p}{(2\pi)^3} h_{\text{iso}}(p) = \int \frac{d^3p}{(2\pi)^3} h_\xi(\mathbf{p}) = N(\xi) \int \frac{d^3p}{(2\pi)^3} h_{\text{iso}} \left(\sqrt{\mathbf{p}^2 + \xi(\mathbf{p} \cdot \hat{\mathbf{n}})^2} \right) \quad (6.25)$$

and can be evaluated to be

$$N(\xi) = \sqrt{1 + \xi} \quad (6.26)$$

²In the original reference [99] this normalization constant has been set to one since it does not affect the collective modes qualitatively. However, the correct value has to be used in order to make quantitative predictions of physical observables (e.g. applying the results of this chapter to the calculation of the heavy quark energy loss in chapter 7).

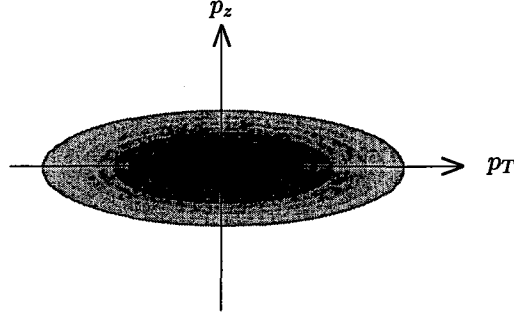


Figure 6.1: Contour plot of an anisotropic version Eq.(6.23) of the Fermi-Dirac distribution function with positive anisotropy parameter. The anisotropy vector is taken to be along the p_z -direction.

by performing a change of variables to \tilde{p}

$$\tilde{p}^2 = p^2 (1 + \xi(\mathbf{v} \cdot \hat{\mathbf{n}})^2) . \quad (6.27)$$

The same change of variables then also allows one to simplify (6.22) since then it is possible to integrate out the $|\tilde{p}|$ -dependence, giving

$$\Pi^{ij}(K) = m_D^2 \sqrt{1 + \xi} \int \frac{d\Omega}{4\pi} v^i \frac{v^l + \xi(\mathbf{v} \cdot \hat{\mathbf{n}})n^l}{(1 + \xi(\mathbf{v} \cdot \hat{\mathbf{n}})^2)^2} \left(\delta^{jl} + \frac{v^j k^l}{K \cdot V + i\epsilon} \right) , \quad (6.28)$$

where

$$m_D^2 = -\frac{2\alpha_s}{\pi} \int_0^\infty dp p^2 \frac{dh_{\text{iso}}(p^2)}{dp} , \quad (6.29)$$

which corresponds to Eq.(2.4). Using the tensor basis from above, one can then decompose the self-energy into four structure functions

$$\Pi^{ij} = \alpha A^{ij} + \beta B^{ij} + \gamma C^{ij} + \delta D^{ij} , \quad (6.30)$$

which are determined by taking the contractions

$$\begin{aligned} k^i \Pi^{ij} k^j &= k^2 \beta , \\ \tilde{n}^i \Pi^{ij} k^j &= \tilde{n}^2 k^2 \delta , \\ \tilde{n}^i \Pi^{ij} \tilde{n}^j &= \tilde{n}^2 (\alpha + \gamma) , \\ \text{Tr} \Pi^{ij} &= 2\alpha + \beta + \gamma . \end{aligned} \quad (6.31)$$

Since the form of the structure functions is somewhat unwieldy, the integral expressions following from Eq.(6.31) have been relegated to appendix B.

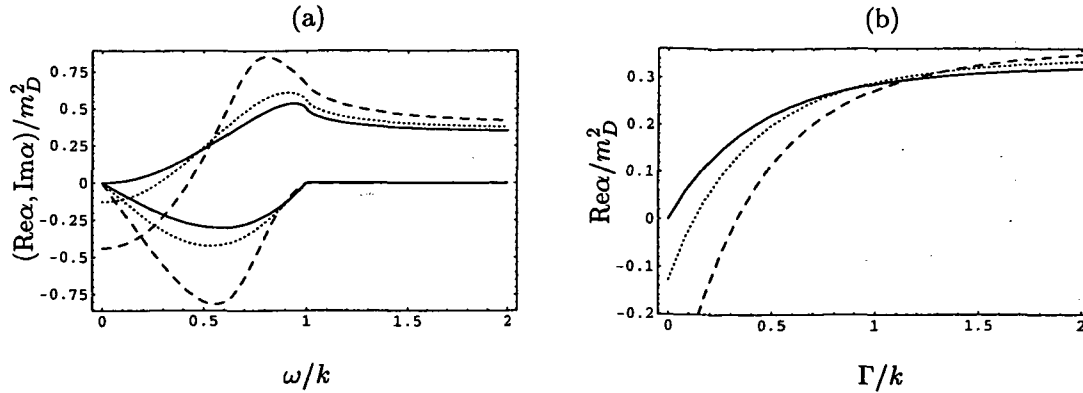


Figure 6.2: Real and imaginary parts of α/m_D^2 as a function of real ω/k (a) and (b) the real part of α/m_D^2 for $\omega/k = i\Gamma/k$ with $\theta_n = \pi/4$ and $\xi = \{0, 1, 10\}$ (full line, dotted line and dashed line, respectively) in both cases.

6.1.3 Evaluation of the structure functions

The four structure functions $\alpha, \beta, \gamma, \delta$ depend on the Debye mass m_D , the frequency and spatial momentum ω and k , the strength of the anisotropy ξ and the angle between the spatial momentum and the anisotropy direction $\hat{\mathbf{k}} \cdot \hat{\mathbf{n}} = \cos \theta_n$. For symmetry reasons one can restrict $0 < \theta_n < \frac{\pi}{2}$ in the following. In the isotropic limit ($\xi \rightarrow 0$) the structure functions α and β reduce to the isotropic HTL self-energies and γ and δ vanish,

$$\begin{aligned} \alpha(K, 0) &= \Pi_T(K), \\ \beta(K, 0) &= -\frac{\omega^2}{k^2} \Pi_L(K), \\ \gamma(K, 0) &= 0, \\ \delta(K, 0) &= 0, \end{aligned} \quad (6.32)$$

where $\Pi_T(K)$ and $\Pi_L(k)$ are given by Eq.(2.3). Note that for finite ξ the analytic structure of $\alpha, \beta, \gamma, \delta$ is the same as for Π_L, Π_T in the isotropic case, namely there is a cut in the complex ω plane which can be chosen to run along the real ω axis from $-k < \omega < k$. For real-valued ω the structure functions are complex for all $\omega < k$ (corresponding to the Landau damping regime of chapter 2) and real for $\omega > k$ while for imaginary-valued ω all four structure functions are real-valued. As an example, a plot of the structure function α for real and imaginary values of ω , $\xi = \{0, 1, 10\}$, and $\theta_n = \pi/4$ is shown in Fig. 6.2.

Using these structure functions it is then possible to write the inverse propagator $\Delta^{-1}(K)$ in terms of the above tensor basis

$$\Delta^{-1}(K) = (k^2 - \omega^2 + \alpha)\mathbf{A} + (\beta - \omega^2)\mathbf{B} + \gamma\mathbf{C} + \delta\mathbf{D}. \quad (6.33)$$

Applying the inversion formula (6.21) one obtains a decomposition for the gluon

propagator into modes

$$\Delta(K) = \Delta_A \mathbf{A} + (k^2 - \omega^2 + \alpha + \gamma) \Delta_G \mathbf{B} + [(\beta - \omega^2) \Delta_G - \Delta_A] \mathbf{C} - \delta \Delta_G \mathbf{D}, \quad (6.34)$$

where

$$\Delta_A^{-1}(K) = k^2 - \omega^2 + \alpha, \quad (6.35)$$

$$\Delta_G^{-1}(K) = (k^2 - \omega^2 + \alpha + \gamma)(\beta - \omega^2) - k^2 \tilde{n}^2 \delta^2. \quad (6.36)$$

In the following it is convenient to use the form

$$\Delta(K) = \Delta_A [\mathbf{A} - \mathbf{C}] + \Delta_G [(k^2 - \omega^2 + \alpha + \gamma) \mathbf{B} + (\beta - \omega^2) \mathbf{C} - \delta \mathbf{D}], \quad (6.37)$$

so that the poles of the propagator correspond to the poles of Δ_A and Δ_G , respectively.

6.1.4 The quark propagator in an anisotropic system

Using the equivalence of semi-classical kinetic theory and the HTL diagrammatic approach one can derive the quark propagator in an anisotropic system similar to the gluon propagator above. However, unlike the gluon propagator the quark propagator in an anisotropic system can be shown to behave very similar to its isotropic counterpart [103]. Consequently, the quark collective modes will look very similar to those derived in chapter 2 and therefore the quark propagator in an anisotropic system will not be treated here explicitly.

6.2 Collective modes of an anisotropic quark-gluon plasma

The dispersion relations for the gluonic modes in an anisotropic quark-gluon plasma are determined by setting $\Delta_A^{-1} = 0$ and $\Delta_G^{-1} = 0$ and then solving these equations using Eqs.(6.35,6.36). A subsequent comparison to the results of chapter 2 will show the qualitative differences with respect to the isotropic case.

6.2.1 Static limit

As a first test of how the momentum-space anisotropy in the distribution functions affects the properties of the system one can consider the response of the system to static electric and magnetic fluctuations. For this test, one needs to examine the limit $\omega \rightarrow 0$ of the propagators (6.35) and (6.36): approaching along the real ω axis one finds that to leading order $\alpha \sim \gamma \sim O(\omega^0)$, $\beta \sim O(\omega^2)$, and $\delta \sim O(i\omega)$;

therefore, one can define the four mass scales

$$\begin{aligned} m_\alpha^2 &= \lim_{\omega \rightarrow 0} \alpha, \\ m_\beta^2 &= \lim_{\omega \rightarrow 0} -\frac{k^2}{\omega^2} \beta, \\ m_\gamma^2 &= \lim_{\omega \rightarrow 0} \gamma, \\ m_\delta^2 &= \lim_{\omega \rightarrow 0} \frac{\tilde{n} k^2}{\omega} \text{Im } \delta, \end{aligned} \quad (6.38)$$

which will be used in the following. The static limit of the propagators Δ_A Eq.(6.35) and Δ_G Eq.(6.36) in terms of these masses is then given by the expressions

$$\Delta_A^{-1} = k^2 + m_\alpha^2 \quad (6.39)$$

$$\Delta_G^{-1} = -\frac{\omega^2}{k^2} [(k^2 + m_\alpha^2 + m_\gamma^2)(k^2 + m_\beta^2) - m_\delta^4]. \quad (6.40)$$

Furthermore, Δ_G^{-1} can be factorized into

$$\Delta_G^{-1} = -\frac{\omega^2}{k^2} (k^2 + m_+^2)(k^2 + m_-^2), \quad (6.41)$$

where

$$2m_\pm^2 = \mathcal{M}^2 \pm \sqrt{\mathcal{M}^4 - 4(m_\beta^2(m_\alpha^2 + m_\gamma^2) - m_\delta^4)}, \quad (6.42)$$

and

$$\mathcal{M}^2 = m_\alpha^2 + m_\beta^2 + m_\gamma^2. \quad (6.43)$$

In the isotropic limit $\xi \rightarrow 0$, most of the mass parameters vanish, $m_\alpha^2 = m_\gamma^2 = m_\beta^2 = m_-^2 \rightarrow 0$, while m_+^2 becomes equal to the Debye mass squared, $m_+^2 \rightarrow m_D^2$, so that one recovers the results obtained in chapter 2. For finite ξ it is possible to evaluate all four masses defined above analytically (the results for m_α and m_β are listed in Appendix B), but since the resulting expressions are quite unwieldy it is more straightforward to use a numerical evaluation. As an example, the angular dependence of m_α^2 , m_+^2 , and m_-^2 at fixed $\xi = 10$ and $\xi = -0.9$ is plotted in Fig. 6.3. In the case $\xi > 0$ (Fig. 6.3a), one can see that the scale m_+^2 is bigger than m_D^2 for small θ_n while being smaller than m_D^2 for θ_n near $\pi/2$; indeed one finds that this corresponds to the screening of electrostatic modes in the isotropic limit, the only difference being an angular dependence of the screening length for nonzero ξ .

Non-vanishing scales m_α^2 and m_-^2 , however, should naively correspond to a screening of magnetostatic modes, which is absent in isotropic systems. Indeed, the fact that anisotropic systems allow for non-vanishing magnetostatic screening masses was already found by COOPER *et al.* [104]; however, COOPER *et al.*

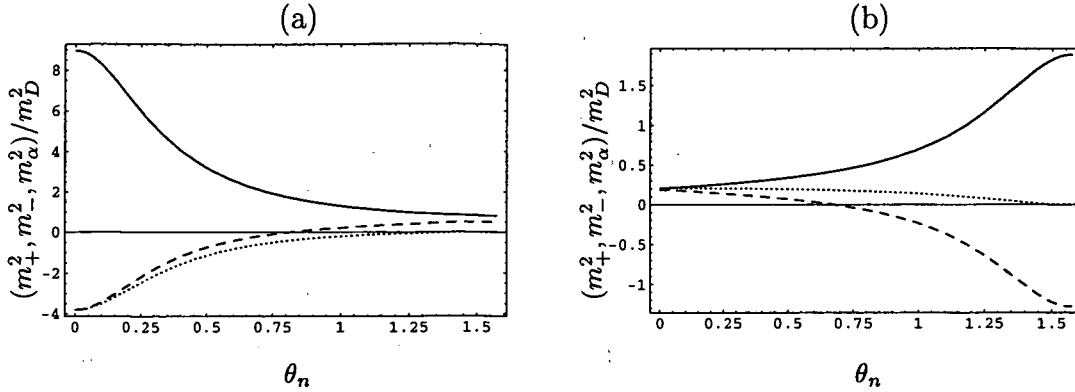


Figure 6.3: Angular dependence of m_α^2 , m_+^2 , and m_-^2 (dotted line, full line and dashed line, respectively) at fixed (a) $\xi = 10$ and (b) $\xi = -0.9$.

neglected to consider the fact that the resulting mass squares might be negative (as is the case for small θ_n in Fig. 6.3a) and would therefore not correspond to a screening of the magnetic interaction.

More precisely, the fact that these quantities are negative indicates that for $\xi > 0$ the system possesses an instability to transverse and “mixed” external perturbations associated with m_α^2 and m_-^2 , respectively, as has now been verified by BIRSE et al. [105] and discussed in a more general context by ARNOLD, LENAGHAN and MOORE [62]. As can be seen in Fig. 6.3a the transverse instability is present for any $\theta_n \neq \pi/2$ while the mixed instability is only present for $\theta_n < \theta_c^{\text{mixed}}$ with θ_c^{mixed} depending on the value of ξ .

For the case $\xi < 0$, which is shown in Fig. 6.3b, the θ_n -dependence of the scales m_+^2 and m_-^2 is exactly reversed with respect to the case $\xi > 0$, as one would expect naively from Eq.(6.23). The scale m_α^2 , however, which was strictly negative for $\xi > 0$, now turns out to be strictly positive in the case of $\xi < 0$, so the transverse instability vanishes in the case of $\xi < 0$. For $\theta_n \gtrsim \pi/4$ the mixed instability is still present, since the scale m_-^2 is again negative.

The role of these unstable modes will be treated later on in more detail.

6.2.2 Stable modes

In the non-static case, a factorization of Δ_G^{-1} similar to Eq.(6.41) can be achieved, which allows the determination of the dispersion relations for all of the collective modes in the system.

Considering first the stable collective modes which correspond to poles of the propagator at real-valued $\omega > k$ one factorizes Δ_G^{-1} as

$$\Delta_G^{-1} = (\omega^2 - \Omega_+^2)(\omega^2 - \Omega_-^2), \quad (6.44)$$

where

$$2\Omega_\pm^2 = \bar{\Omega}^2 \pm \sqrt{\bar{\Omega}^4 - 4((\alpha + \gamma + k^2)\beta - k^2\bar{n}^2\delta^2)}, \quad (6.45)$$

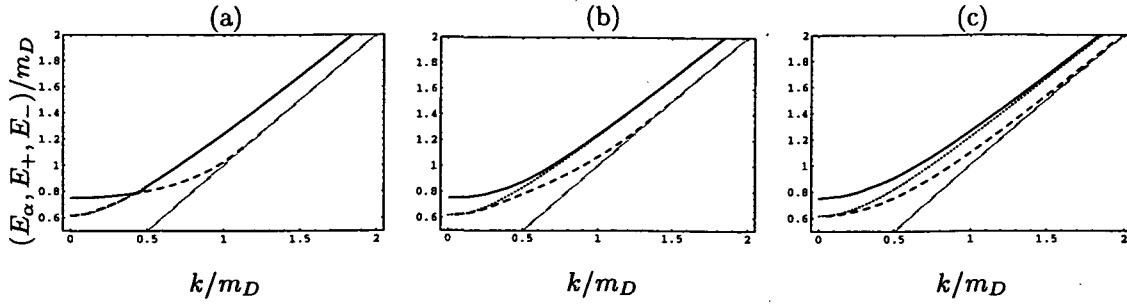


Figure 6.4: Angular dependence of E_α (dotted line), E_+ (full line), and E_- (dashed line) for $\xi = 10$, and $\theta_n = \{0, \pi/4, \pi/2\}$ (plots (a), (b) and (c), respectively).

and

$$\bar{\Omega}^2 = \alpha + \beta + \gamma + k^2. \quad (6.46)$$

Since the quantity under the square root in (6.45) can be written as $(\alpha - \beta + \gamma + k^2)^2 + 4k^2\tilde{n}^2\delta^2$ (which is always positive for real $\omega > k$), there are at most two stable modes coming from Δ_G , while the remaining stable collective mode comes from the zero of Δ_A^{-1} .

The dispersion relations for all of the collective modes are then given by the solutions to

$$E_\pm^2 = \Omega_\pm^2(E_\pm), \quad (6.47)$$

$$E_\alpha^2 = k^2 + \alpha(E_\alpha). \quad (6.48)$$

In the isotropic limit (6.32) one finds the correspondence $E_\alpha = E_+ = E_T$ and $E_- = E_L$. Accordingly, for finite ξ , there are three stable quasiparticle modes with dispersion relations that depend on the angle of propagation with respect to the anisotropy vector, θ_n . The resulting dispersion relations for all three modes for the case $\xi = 10$, and $\theta_n = \{0, \pi/4, \pi/2\}$ are plotted in Fig. 6.4.

6.2.3 Unstable modes

For non-zero ξ the propagator also has poles along the imaginary ω axis³, that correspond to exponentially growing or decaying field amplitudes, depending on the sign of the imaginary part. The exponentially growing solutions correspond to the unstable modes of the system with $\omega \rightarrow i\Gamma$ and Γ the real-valued solution to the equations

$$\begin{aligned} \Delta_G^{-1} &= (\Gamma^2 + \Omega_+^2)(\Gamma^2 + \Omega_-^2) = 0, \\ \Delta_A^{-1} &= (\Gamma^2 + k^2 + \alpha) = 0. \end{aligned} \quad (6.49)$$

³Checking for poles at complex ω can be done numerically; however, no poles have been found.

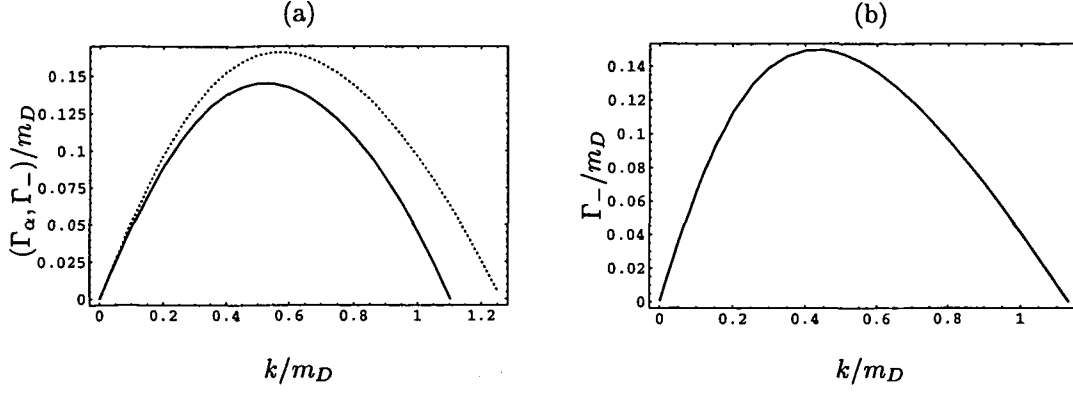


Figure 6.5: $\Gamma_\alpha(k)$ (dotted line) and $\Gamma_-(k)$ as a function of k with (a) $\xi = 10$ and $\theta_n = \pi/8$ and (b) $\xi = -0.9$ and $\theta_n = \pi/2$.

It turns out that in contrast to the stable modes there is at most one solution for $\Delta_G^{-1}(\omega = i\Gamma) = 0$ since numerically one finds that $\Omega_+^2 > 0$ for all $\Gamma > 0$, while $\Delta_A^{-1}(\omega = i\Gamma) = 0$ has only solutions for $\xi > 0$. Therefore, the system possesses one or two unstable modes depending on the sign of the anisotropy parameter.

In Fig. 6.5a a plot of the growth rates $\Gamma_\alpha(k)$ and $\Gamma_-(k)$ with $\xi = 10$ and $\theta_n = \pi/8$ is shown, reflecting the presence of two unstable modes; in Fig. 6.5b $\Gamma_-(k)$ is shown for $\xi = -0.9$ and $\theta_n = \pi/2$.

6.3 Small ξ limit

In the small- ξ limit it is possible to obtain analytic expressions for all of the structure functions order-by-order in ξ , which provide a well-defined test case to the otherwise numerically conducted analysis. To linear order in ξ one finds

$$\begin{aligned}
 \alpha &= \Pi_T(z) + \xi \left[\frac{z^2}{12} (3 + 5 \cos 2\theta_n) m_D^2 - \frac{1}{6} (1 + \cos 2\theta_n) m_D^2 \right. \\
 &\quad \left. + \frac{1}{4} \Pi_T(z) ((3 + 3 \cos 2\theta_n) - z^2 (3 + 5 \cos 2\theta_n)) \right], \\
 z^{-2} \beta &= -\Pi_L(z) + \xi \left[\frac{1}{6} (1 + 3 \cos 2\theta_n) m_D^2 - \frac{\Pi_L(z)}{2} (\cos 2\theta_n (2 - 3z^2) + 1 - z^2) \right], \\
 \gamma &= \frac{\xi}{3} (3\Pi_T(z) - m_D^2) (z^2 - 1) \sin^2 \theta_n, \\
 \delta &= \frac{\xi}{3k} (4z^2 m_D^2 + 3\Pi_T(z) (1 - 4z^2)) \cos \theta_n, \tag{6.50}
 \end{aligned}$$

where $z = \omega/k$ and again $\hat{\mathbf{k}} \cdot \hat{\mathbf{n}} = \cos \theta_n$.

6.3.1 Static Limit

Using the linear expansions from above and the well-known static limits $\Pi_L \rightarrow m_D^2$ and $\Pi_T \rightarrow -i\pi\omega/(4k)$ one obtains analytic expressions for the mass scales (6.38),

$$\begin{aligned}\hat{m}_\alpha^2 &= -\frac{\xi}{6}(1 + \cos 2\theta_n), \\ \hat{m}_\beta^2 &= 1 + \frac{\xi}{6}(3 \cos 2\theta_n + 2), \\ \hat{m}_\gamma^2 &= \frac{\xi}{3} \sin^2 \theta_n, \\ \hat{m}_\delta^2 &= -\xi \frac{\pi}{4} \sin \theta_n \cos \theta_n,\end{aligned}\tag{6.51}$$

where $\hat{m}^2 = m^2/m_D^2$. Using these one obtains expansions to linear order in ξ for m_\pm^2 defined in (6.42)

$$\begin{aligned}\hat{m}_+^2 &= 1 + \frac{\xi}{6}(3 \cos 2\theta_n + 2), \\ \hat{m}_-^2 &= -\frac{\xi}{3} \cos 2\theta_n.\end{aligned}\tag{6.52}$$

Clearly, the mass scales in the small- ξ limit have the same qualitative behavior as their exact counterparts, as one can see by comparing the above expressions to Fig. 6.3. Therefore, one gains confidence that the small- ξ limit conserves the basic features of the full anisotropic problem while having the advantage of being analytically tractable.

6.3.2 Collective modes

The collective modes in the small- ξ limit are most easily found by an expansion of Eq.(6.34),

$$\begin{aligned}\Delta_A^{-1} &= k^2 - \omega^2 + \alpha = 0 \\ \Delta_G^{-1} &= (k^2 - \omega^2 + \alpha + \gamma)(\beta - \omega^2) = 0,\end{aligned}\tag{6.53}$$

where α , β , and γ are given by (6.50) and δ^2 can be ignored in the expansion since it is of order $O(\xi^2)$. Solving the above equations one finds that again both the stable and unstable modes in the small- ξ limit correspond qualitatively to the full problem. Note that there is again only one unstable mode coming from Δ_G^{-1} since $\beta(i\Gamma) > 0$ for all $\Gamma > 0$.

6.4 Large ξ limit

Another case where one is able to calculate analytic results for the structure functions is the limit $\xi \rightarrow \infty$. By considering the action of the distribution

Eq.(6.23) on some smooth test function $\Phi(\mathbf{p})$,

$$F = \lim_{\xi \rightarrow \infty} \int \frac{d^3 p}{(2\pi)^3} h_\xi(\mathbf{p}) \Phi(\mathbf{p}) \quad (6.54)$$

and choosing $\mathbf{p} \cdot \hat{\mathbf{n}}$ to be parallel to the p_z -axis one can rescale $\cos \theta \rightarrow \frac{\cos \theta}{\sqrt{\xi}}$ so that the limit $\xi \rightarrow \infty$ can be performed,

$$F = \int \frac{p^2 dp d\phi}{(2\pi)^3} \int_{-\infty}^{\infty} d \cos \theta h_{\text{iso}} \left(p \sqrt{1 + \cos^2 \theta} \right) \Phi \begin{pmatrix} p \cos \phi \\ p \sin \phi \\ 0 \end{pmatrix}. \quad (6.55)$$

This means that in the limit $\xi \rightarrow \infty$ Eq.(6.23) takes the form

$$\lim_{\xi \rightarrow \infty} h_\xi(\mathbf{p}) \rightarrow \delta(\hat{\mathbf{p}} \cdot \hat{\mathbf{n}}) \int_{-\infty}^{\infty} dx h_{\text{iso}} \left(p \sqrt{1 + x^2} \right), \quad (6.56)$$

which corresponds to the extreme anisotropic case considered by ARNOLD, LENAGHAN and MOORE [62]. As a consequence, one can make use of this form by partially integrating Eq.(6.22)

$$\Pi^{ij}(K) = 4\pi\alpha_s \int \frac{d^3 p}{(2\pi)^3} \frac{h_\xi(\mathbf{p})}{p} \left[\delta^{ij} - \frac{k^i v^j + k^j v^i}{-K \cdot V - i\epsilon} + \frac{(-\omega^2 + k^2) v^i v^j}{(-K \cdot V - i\epsilon)^2} \right] \quad (6.57)$$

and applying the techniques from Ref. [62] to obtain analytic expressions for the structure functions in the large ξ limit. Using

$$4\pi\alpha_s \int \frac{d^3 p}{(2\pi)^3} \frac{h_\xi(\mathbf{p})}{p} = m_D^2 \frac{\pi}{4} \quad (6.58)$$

one immediately finds

$$\Pi^{ij}(K) = \frac{m_D^2 \pi}{4} \int_0^{2\pi} \frac{d\phi}{2\pi} \left[\delta^{ij} - \frac{k^i v^j + k^j v^i}{-K \cdot V - i\epsilon} + \frac{(-\omega^2 + k^2) v^i v^j}{(-K \cdot V - i\epsilon)^2} \right]. \quad (6.59)$$

The remaining average over angles can easily be done, obtaining the structure functions through the contractions Eq.(6.31), giving

$$\begin{aligned} \alpha &= \frac{m_D^2 \pi}{4} \left[-\cot^2 \theta_n + \frac{\hat{\omega}}{\sin^2 \theta_n} \left(\hat{\omega} + \frac{1 - \hat{\omega}^2}{\sqrt{\hat{\omega}^2 - \sin^2 \theta_n}} \right) \right] \\ \beta &= \frac{m_D^2 \pi}{4} \hat{\omega}^2 \left[-1 + \hat{\omega} \frac{\hat{\omega}^2 + \cos 2\theta_n}{(\hat{\omega}^2 - \sin^2 \theta_n)^{3/2}} \right] \\ \gamma &= \frac{m_D^2 \pi}{4} \frac{1 - \hat{\omega}^2}{4 \sin^2 \theta_n} \left[6 + 2 \cos 2\theta_n + \hat{\omega} \frac{3 - 6\hat{\omega}^2 - 2(1 + \hat{\omega}^2) \cos 2\theta_n - \cos 4\theta_n}{(\hat{\omega}^2 - \sin^2 \theta_n)^{3/2}} \right] \\ \delta &= \frac{m_D^2 \pi}{4k} \frac{\cos \theta_n}{\sin^2 \theta_n} \hat{\omega} \left[\hat{\omega} + \frac{-(1 - \hat{\omega}^2)^2 + (1 - 2\hat{\omega}^2) \cos^2 \theta_n}{(\hat{\omega}^2 - \sin^2 \theta_n)^{3/2}} \right]. \end{aligned} \quad (6.60)$$

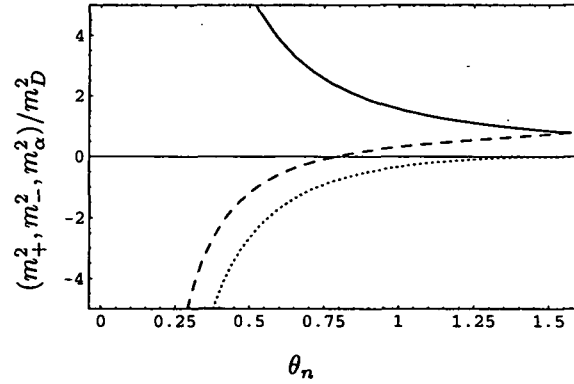


Figure 6.6: Angular dependence of the mass-scales m_α^2, m_+^2, m_-^2 (dotted line, full line and dashed line, respectively) in $\xi \rightarrow \infty$ limit.

It is then straightforward to extract the static limit of these structure functions, giving the mass scales m_α^2, m_+^2, m_-^2 in the large- ξ limit. The result is plotted in Fig. 6.6 as a function of the angle θ_n . As can be seen, the mass scales diverge at $\theta_n = 0$, whereas m_-^2 and m_+^2 coincide at $\theta_n = \pi/2$ and m_α^2 vanishes. Also, one recovers the results from ARNOLD, LENAGHAN and MOORE [62] that the scale m_-^2 is only negative for $\sin \theta_n < 1/\sqrt{2}$ (corresponding to the presence of the electric instability in this reference) and the various growth rates of the unstable modes. Finally, one can show that the expressions of the structure functions for general ξ converge towards the above analytic results when ξ becomes large.

6.5 $\xi \rightarrow -1$ limit

To get some insight in the case of $\xi \rightarrow -1$ where the distribution function Eq.(6.23) becomes extremely elongated one can again consider its action on a test function $\Phi(\mathbf{p})$,

$$F = \lim_{\xi \rightarrow -1} \int \frac{d^3 p}{(2\pi)^3} h_\xi(\mathbf{p}) \Phi(\mathbf{p}). \quad (6.61)$$

Performing a simple scaling $p_z \rightarrow \frac{p_z}{\sqrt{1+\xi}}$ one obtains the interesting result

$$F = \lim_{\xi \rightarrow -1} \int \frac{d^2 p_\perp d\phi}{(2\pi)^3} \int_{-\infty}^{\infty} dp_z h_{\text{iso}} \left(\sqrt{p_\perp^2 + p_z^2} \right) \Phi \left(\frac{\mathbf{p}_\perp}{\sqrt{1+\xi}} \right) \quad (6.62)$$

indicating that the argument of the test function Φ is pushed to very large values, where Φ is usually taken to be vanishing. However, one can get a bit more insight by compactifying momentum space to a sphere and considering the coordinate map

$$\mathbf{p} \rightarrow \frac{\mathbf{p}'}{p'^2}, \quad (6.63)$$

with the volume element transforming to

$$d^3 p \rightarrow \frac{d^3 p'}{p'^6}. \quad (6.64)$$

One then considers the action of the distribution function on a test function Φ' in the primed coordinate system,

$$F = \lim_{\xi \rightarrow -1} N(\xi) \int \frac{d^3 p'}{(2\pi)^3 p'^6} h_{\text{iso}} \left(\frac{\sqrt{\mathbf{p}'^2 + \xi(\mathbf{p}' \cdot \hat{\mathbf{n}})^2}}{p'^2} \right) \Phi'(\mathbf{p}'). \quad (6.65)$$

Taking again $\hat{\mathbf{p}}' \cdot \hat{\mathbf{n}} = \cos \theta'$ one scales

$$p' \rightarrow p' \sqrt{1 + \xi \cos^2 \theta'} \quad (6.66)$$

to obtain

$$F = \lim_{\xi \rightarrow -1} \int \frac{d^3 p'}{(2\pi)^3 p'^6} \frac{1}{(1 + \xi \cos^2 \theta')^{3/2}} h_{\text{iso}} \left(\frac{1}{p'} \right) \Phi'(p' \sqrt{1 + \xi \cos^2 \theta'}). \quad (6.67)$$

Since the isotropic distribution function consisting of Bose-Einstein and Fermi-Dirac statistical factors lifts the possible singularity at $p' = 0$, the only "dangerous" term in the integrand is $1 + \xi \cos^2 \theta$ which becomes zero for $\xi \rightarrow -1$ and small angles θ' . Substituting therefore $\cos^2 \theta = 1 - (1 + \xi)\chi$ one can perform the limit $\xi \rightarrow -1$, obtaining

$$F = \int \frac{dp' d\phi d\chi}{(2\pi)^3} \frac{1}{p'^4} \frac{1}{(1 + \chi)^{3/2}} h_{\text{iso}} \left(\frac{1}{p'} \right) \Phi'(0) = 4\pi \Phi'(0) \int_0^\infty dp p^2 h_{\text{iso}}(p). \quad (6.68)$$

Therefore, in the limit $\xi \rightarrow -1$, Eq.(6.23) simply is given by

$$\lim_{\xi \rightarrow -1} h_\xi(\mathbf{p}) d^3 p \rightarrow \delta^3(\mathbf{p}') d^3 p' 4\pi \int_0^\infty dp p^2 h_{\text{iso}}(p), \quad (6.69)$$

which upon insertion into Eq.(6.57) shows that in this limit the self-energy and consequently all structure functions vanish. Therefore, the limit $\xi \rightarrow -1$ unfortunately does not correspond to the interesting physical situation of a line momentum distribution but rather to the free limit.

6.6 Discussion of instabilities

The existence of unstable modes in an anisotropic quark-gluon plasma (first studied by MRÓWCZYŃSKI in a series of papers [56, 57, 58]) may play an important role in the dynamical evolution of the quark-gluon plasma, since their exponential growth can lead to a more rapid thermalization and isotropization of the plasma.

Recently, MRÓWCZYŃSKI and RANDRUP [61] have performed a phenomenological estimate of the growth rate of the instabilities for scenarios relevant to the quark-gluon plasma produced at RHIC or LHC, using however a different implementation of the anisotropy than Eq.(6.23). They found that the degree of amplification of the instabilities is not expected to dominate the dynamics of the quark-gluon plasma, but instead their effect would be comparable to the contribution from elastic Boltzmann collisions. However, they also pointed out that if a large number of unstable modes would be excited then their combined effect on the overall dynamics could well be significant. More recently, ARNOLD, LENAGHAN and MOORE [62] investigated the case corresponding to the $\xi \rightarrow \infty$ limit from above, arguing that it drastically modifies the scenario of "bottom-up thermalization" advocated by BAIER, MUELLER, SCHIFF and SON [51], which would then have to be replaced by a different scheme.

Furthermore, the presence of instabilities will in general prohibit the calculation of physical quantities in a perturbative framework, since they correspond to unregularized singularities of the propagator. This problem as well as special exception to it will be discussed in more detail in chapter 7.

Because of these findings, it is probably fair to say that a more intensive study of the instabilities of anisotropic systems and especially their saturation and effect on the thermalization will be of great interest in the near future.

6.7 Summary

In this chapter I calculated the gluon self-energy in a system that has an anisotropy in momentum space. I presented a tensor basis that can be used to write the gluon self-energy as the sum of four "structure functions" and showed that in the isotropic limit two of these structure functions vanish while the others correspond to the longitudinal and transversal part of the self-energy of chapter 2. Considering the static limit of the self-energy it was found that for anisotropic systems there is in general a non-vanishing magnetostatic mass-scale, but since the associated mass squared is negative, this corresponds to the existence of unstable modes.

Furthermore, solving the dispersion relations three stable and either one or two unstable modes were found, depending on whether the distribution function is stretched or squeezed. I also considered the limit of weak anisotropies and two cases where the anisotropy gets extremely strong, deriving analytic expressions for the structure functions which serve as verification of the general result and provide the basis for further analytic studies. I conclude by reviewing the current knowledge about the effects of the unstable modes on the thermalization of the quark-gluon plasma produced in heavy-ion collisions.

Chapter 7

Energy loss of a heavy parton

In this chapter I will make use of the resummed self-energies derived for isotropic and anisotropic systems obtained in chapters 2 and 6 to calculate the collisional energy loss of a heavy parton in a deconfined QCD plasma. In the context of heavy-ion collisions, a theoretical understanding of the heavy parton energy loss in a quark-gluon plasma is important for a proper comparison with experimental results, e.g. for the inclusive electron spectrum (measured recently at RHIC [106]) and for jet suppression rates. In the following I will focus on the collisional energy loss (for a review on the radiative energy loss see e.g. [107, 108]) using the technique of BRAATEN and THOMA [109, 110] which gives the complete leading-order result for this quantity.

The main idea behind this technique is to consider independently the contributions from soft (involving momenta $q \sim m_D$) and hard ($q \sim T$) gluon exchange, which are separated by some arbitrary momentum scale q^* that cuts off the UV and IR divergences of the soft/hard contributions, respectively. Moreover, it was found that in the weak-coupling limit $\alpha_s \ll 1$ the condition $m_D \ll q^* \ll T$ could be used to expand the resulting integral expressions for the soft and hard contributions further, giving an analytic result for the energy loss independent of the separation scale q^* . However, in the case of QCD where the coupling becomes quite large, this approach may give unphysical results for energy loss, as will be shown later on.

It turns out that when not expanding the integral expressions with respect to the condition $m_D \ll q^* \ll T$, in the isotropic case both the hard and soft contributions to the energy loss *always* stay positive, even for very large coupling, as has been shown in QED [111]. However, this comes at the expense of giving up independence of the complete result on the scale q^* , which then has to be fixed somehow. Fortunately, it turns out that in the weak coupling limit the scale dependence becomes very small, too, so that unless q^* is taken to be very large ($q^* \gg T$) or very small ($q^* \ll m_D$) one recovers the result found by BRAATEN and THOMA. When the coupling is increased one can then still fix q^* by the “principle of minimal sensitivity”, which means that q^* is chosen such that the

energy loss (and therefore also the variation with respect to q^*) is minimized. As will be shown, this procedure eliminates the unphysical result of negative energy loss and also provides an estimate on the theoretical uncertainty of the result by varying q^* by a fixed amount around the minimizing value.

Moreover, it will be shown that the technique by BRAATEN and THOMA can also be applied to anisotropic systems. This is in fact non-trivial since the presence of plasma instabilities in general could render the calculation of the soft part divergent; however, the collisional energy loss turns out to be protected by an interesting mechanism dubbed "dynamical shielding" [111], rendering the calculation safe at least to leading order, as will be shown in the following.

7.1 Soft contribution and effect of instabilities

The soft contribution to the collisional energy loss can be calculated using classical field theory methods. Starting from the classical expression for the parton energy loss per unit of time given by

$$\left(\frac{dW}{dt}\right)_{\text{soft}} = \text{Re} \int d^3\mathbf{x} \mathbf{J}_{\text{ext}}^a(X) \cdot \mathbf{E}_{\text{ind}}^a(X), \quad (7.1)$$

where a is a color index, $X = (t, \mathbf{x})$, and \mathbf{J}_{ext} is the current induced by a test parton propagating with velocity \mathbf{v} :

$$\begin{aligned} \mathbf{J}_{\text{ext}}^a(X) &= Q^a \mathbf{v} \delta^{(3)}(\mathbf{x} - \mathbf{v}t), \\ \mathbf{J}_{\text{ext}}^a(Q) &= (2\pi) Q^a \mathbf{v} \delta(\omega - \mathbf{q} \cdot \mathbf{v}), \end{aligned} \quad (7.2)$$

with $Q = (\omega, \mathbf{q})$ and Q^a being the color charge. Using

$$E_{\text{ind}}^{i,a}(Q) = i\omega (\Delta^{ij}(Q) - \Delta_0^{ij}(Q)) J_{\text{ext}}^{j,a}(Q), \quad (7.3)$$

where Δ_0^{ij} denotes the free propagator, and Fourier transforming to coordinate space one obtains

$$E_{\text{ind}}^{i,a}(X) = iQ^a \int \frac{d^3\mathbf{q}}{(2\pi)^3} (\mathbf{q} \cdot \mathbf{v}) (\Delta^{ij}(Q) - \Delta_0^{ij}(Q)) v^j e^{i(\mathbf{q} \cdot \mathbf{x} - (\mathbf{q} \cdot \mathbf{v})t)}, \quad (7.4)$$

where $Q = (\mathbf{q} \cdot \mathbf{v}, \mathbf{q})$. Using the above equation one finds for the soft contribution Eq.(7.1) to the heavy parton energy-loss

$$-\left(\frac{dW}{dt}\right)_{\text{soft}} = Q^2 \text{Im} \int \frac{d^3\mathbf{q}}{(2\pi)^3} (\mathbf{q} \cdot \mathbf{v}) v^i [\Delta^{ij}(Q) - \Delta_0^{ij}(Q)] v^j. \quad (7.5)$$

7.1.1 Dynamical shielding of instabilities

In the case of an anisotropic system unstable modes are present that manifest themselves by poles of the propagator in the static limit $\lim_{\omega \rightarrow 0} \Delta_{ij}^{-1} = 0$, as has been discussed in chapter 6. To simplify the argument, one can use the tensor decomposition of the propagator in chapter 6 and concentrate on the poles of Δ_A given in Eq.(6.34) only, while the poles of Δ_G can be treated in a similar way. Schematically the soft contribution to the energy loss Eq.(7.5) is then given as

$$\left(\frac{dW}{dx}\right)_{A, \text{soft}} \sim \text{Im} \int d\Omega \int q dq \frac{\hat{\omega}}{(q^2 - q^2 \hat{\omega}^2 + \alpha)}. \quad (7.6)$$

Since the structure function α for $\xi > 0$ is negative-valued,

$$\lim_{\omega \rightarrow 0} \alpha(\omega, q) = M^2(-1 + iD\hat{\omega}) + \mathcal{O}(\omega^2), \quad (7.7)$$

in the static limit the integrand in Eq.(7.6) seems to contain an unregulated singularity at $q = M$, which therefore renders the result divergent. Thus the presence of instabilities in a system is believed to generically prohibit the calculation of quantities in a perturbative framework since those quantities will be plagued by unregulated divergencies [112].

The schematic integrand for the energy loss in Eq.(7.6), however, turns out to be "shielded" from this singularity, as can be seen by taking the limit

$$\lim_{\hat{\omega} \rightarrow 0} \lim_{q \rightarrow M} \frac{\hat{\omega}}{q^2 - q^2 \hat{\omega}^2 + M^2(-1 + iD\hat{\omega})} \rightarrow \frac{1}{M^2(\hat{\omega} + iD)} \rightarrow -\frac{i}{M^2 D}. \quad (7.8)$$

This limit exists as long as the coefficient D in Eq.(7.7) is non-vanishing, being somewhat similar to dynamical screening of the magnetic sector of finite temperature QCD. Therefore, the integral Eq.(7.6) may safely be performed, as long as $D \neq 0$.

Proof of dynamical shielding I: small ξ

Since dynamical shielding relies crucially on the fact that the imaginary part of the structure function is of $O(\omega)$ when the real part is negative-valued, a simple proof of this assumption valid for the weak-anisotropy or small- ξ regime will be given here. For Δ_A the proof is straightforward since $\text{Im} \Delta_A^{-1} = \text{Im} \alpha$ and from Eqs.(6.50) one finds

$$\lim_{\hat{\omega} \rightarrow 0} \alpha = m_D^2 \left[-\frac{\xi}{6}(1 + \cos 2\theta_n) - \frac{i\pi}{4} \hat{\omega} \left(1 + \frac{3\xi}{4}(1 + \cos 2\theta_n) \right) \right]. \quad (7.9)$$

From this expression it is clear that the imaginary value cannot change sign for any positive value of ξ , whereas for negative value of ξ , the static limit of α is

positive-valued, so no instability exists in Δ_A . To prove that Δ_G is also safe, one first uses its small- ξ decomposition Eq.(6.53) to see that only the $\alpha + \gamma$ term can become negative-valued. Using once again the expressions in Eq.(6.50) one finds after a little bit of algebra

$$\lim_{\hat{\omega} \rightarrow 0} \alpha + \gamma = m_D^2 \left[-\frac{\xi}{6}(-2 + 4 \cos^2 \theta_n) - \frac{i\pi}{4} \hat{\omega} \left(1 + \frac{\xi}{4}(-4 + 10 \cos^2 \theta_n) \right) \right]. \quad (7.10)$$

For $\xi > 0$ the instability is present for $\cos^2 \theta_n > \frac{1}{2}$, while the imaginary part may change its sign only for $\cos^2 \theta_n < \frac{4}{10}$; for $\xi < 0$, the instability occurs for $\cos^2 \theta_n < \frac{1}{2}$ while even for the "worst case" $\xi = -1$ the imaginary part can only change its sign for $\cos^2 \theta_n > \frac{8}{10}$, so also the Δ_G contribution to the energy loss is protected by dynamical shielding. This completes the proof for the case of small ξ .

Proof of dynamical shielding II: large ξ

Also for very large ξ it can be shown analytically that the energy loss calculation is protected by dynamical shielding. Considering the Δ_A contribution first one can make use of the analytic expressions in Eq.(6.60) to find

$$\lim_{\hat{\omega} \rightarrow 0} \alpha = \frac{m_D^2 \pi}{4} \left[-\cot^2 \theta_n - \frac{i\hat{\omega}}{\sin^3 \theta_n} \right], \quad (7.11)$$

where again it can immediately be seen that the $O(\omega)$ contribution to the imaginary part never vanishes. For Δ_G it turns out that a factorization similar to the small- ξ case is possible,

$$\Delta_G(\hat{\omega}, q) = \hat{\omega}^2 (q^2 + q_+^2)(q^2 + q_-^2), \quad (7.12)$$

where

$$\begin{aligned} q_+^2 &= \frac{m_D^2 \pi}{16 \sin^2 \theta_n} \left[2(1 + \cos^2 \theta_n) + 2\sqrt{\cos^4 \theta_n + 4 \cos^2 \theta_n} \right] + O(\hat{\omega}) \\ q_-^2 &= \frac{m_D^2 \pi}{16 \sin^2 \theta_n} \left[4 - 2 \cos^2 \theta_n - 2\sqrt{\cos^4 \theta_n + 4 \cos^2 \theta_n} + \right. \\ &\quad \left. + \frac{i\hat{\omega}}{(4 + \cos^2 \theta_n) \sin \theta_n} \left(8 + 2 \cos^2 \theta_n - 3\sqrt{2}\sqrt{(8 + 2 \cos^2 \theta_n) \cos^2 \theta_n} \right) \right] \end{aligned} \quad (7.13)$$

As can be seen, $q_+^2 > 0$ in the whole region $0 < \theta_n < \frac{\pi}{2}$, so one can limit the considerations to q_-^2 . There a little bit of algebra shows that $q_-^2 < 0$ for $\cos^2 \theta_n > \frac{1}{2}$, while on the other hand the imaginary part changes sign at $\cos^2 \theta_n = \frac{1}{2}$, so all angles $\theta_n \neq \frac{\pi}{4}$ are protected through dynamical shielding, while for the angle $\theta_n = \frac{\pi}{4}$ the singularity at $q = 0$ of Δ_G is rendered harmless by the volume element of the integration. This completes the proof for the case of large ξ .

7.1.2 Application of dynamical shielding

Unfortunately a proof that shows that dynamical shielding protects the soft contribution to the energy loss of naked singularities is rather difficult for general ξ . Numerical evidence however suggests that dynamical shielding also works for general ξ , which is not covered by the above proofs. Therefore, one can be reasonably confident that the singularities coming from the unstable modes are rendered safe everywhere and one may proceed to evaluate the soft contribution to the energy loss.

Using the tensor basis derived in chapter 6 to invert the propagator in Eq.(7.5) and taking the contractions

$$\begin{aligned} v^i A^{ij} v^j &= v^2 - (\hat{\mathbf{q}} \cdot \mathbf{v})^2, \\ v^i B^{ij} v^j &= (\hat{\mathbf{q}} \cdot \mathbf{v})^2, \\ v^i C^{ij} v^j &= (\tilde{\mathbf{n}} \cdot \mathbf{v})^2 / \tilde{n}^2, \\ v^i D^{ij} v^j &= 2(\mathbf{q} \cdot \mathbf{v})(\tilde{\mathbf{n}} \cdot \mathbf{v}), \end{aligned} \quad (7.14)$$

one obtains

$$\begin{aligned} - \left(\frac{dW}{dx} \right)_{\text{soft}} &= \frac{Q^2}{v} \text{Im} \int \frac{d^3 \mathbf{q}}{(2\pi)^3} \omega \left(\Delta_A(Q) - \frac{1}{q^2 - \omega^2} \right) \left[v^2 - \frac{\omega^2}{q^2} - \frac{(\tilde{\mathbf{n}} \cdot \mathbf{v})^2}{\tilde{n}^2} \right] \\ &+ \omega \Delta_G(Q) \left[\frac{\omega^2}{q^2} (q^2 - \omega^2 + \alpha + \gamma) + (\beta - \omega^2) \frac{(\tilde{\mathbf{n}} \cdot \mathbf{v})^2}{\tilde{n}^2} - 2\delta\omega(\tilde{\mathbf{n}} \cdot \mathbf{v}) \right] \\ &+ \frac{1}{\omega(q^2 - \omega^2)} \left[\frac{\omega^2}{q^2} (q^2 - \omega^2) - \omega^2 \frac{(\tilde{\mathbf{n}} \cdot \mathbf{v})^2}{\tilde{n}^2} \right], \end{aligned} \quad (7.15)$$

where $dW/dx = v^{-1} dW/dt$ and $\omega = \mathbf{q} \cdot \mathbf{v}$. After some algebraic transformations involving scaling out the momentum one obtains

$$\begin{aligned} \left(\frac{dW}{dx} \right)_{\text{soft}} &= \frac{Q^2}{v} \text{Im} \int \frac{d^3 \mathbf{q}}{(2\pi)^3} \frac{\hat{\omega}}{q(1 - \hat{\omega}^2)} \left[\frac{-\alpha}{(q^2 - q^2 \hat{\omega}^2 + \alpha)} (v^2 - \hat{\omega}^2 - \frac{(\tilde{\mathbf{n}} \cdot \mathbf{v})^2}{\tilde{n}^2}) \right. \\ &\left. + \frac{q^2 \mathcal{A} + \mathcal{B}}{q^4 \mathcal{C} + q^2 \mathcal{D} + \mathcal{E}} \right], \end{aligned} \quad (7.16)$$

where

$$\begin{aligned} \mathcal{A} &= (1 - \hat{\omega}^2)^2 \beta + \hat{\omega}^2 \frac{(\tilde{\mathbf{n}} \cdot \mathbf{v})^2}{\tilde{n}^2} (\alpha + \gamma) - 2\hat{\omega}(1 - \hat{\omega}^2)(\tilde{\mathbf{n}} \cdot \mathbf{v})\hat{\delta}, \\ \mathcal{B} &= \left((\alpha + \gamma)\beta - \tilde{\mathbf{n}}^2 \hat{\delta}^2 \right) \left(1 - \hat{\omega}^2 - \frac{(\tilde{\mathbf{n}} \cdot \mathbf{v})^2}{\tilde{n}^2} \right), \\ \mathcal{C} &= -\hat{\omega}^2(1 - \hat{\omega}^2), \\ \mathcal{D} &= -\hat{\omega}^2(\alpha + \gamma) + (1 - \hat{\omega}^2)\beta \\ \mathcal{E} &= (\alpha + \gamma)\beta - \tilde{\mathbf{n}}^2 \hat{\delta}^2, \end{aligned} \quad (7.17)$$

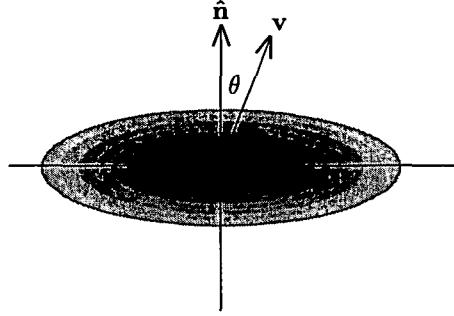


Figure 7.1: Sketch of the directional dependence of the energy loss: $\hat{\mathbf{n}}$ is the direction of the anisotropy, \mathbf{v} the velocity of the parton and θ the angle between these.

with $\hat{\omega} = \hat{\mathbf{q}} \cdot \mathbf{v}$ and $\hat{\delta} = q\delta$. Since all the momentum dependence has been made explicit and possible singularities coming from the instabilities are known to be shielded one can perform the q integration, obtaining

$$-\left(\frac{dW}{dx}\right)_{\text{soft}} = \frac{Q^2}{v} \text{Im} \int \frac{d\Omega_q}{(2\pi)^3} \frac{\hat{\omega}}{(1-\hat{\omega}^2)} \left[-\alpha \frac{(v^2 - \hat{\omega}^2 - \frac{(\hat{\mathbf{n}} \cdot \mathbf{v})^2}{\hat{\mathbf{n}}^2})}{2(1-\hat{\omega}^2)} \ln \frac{q^{*2}(1-\hat{\omega}^2) + \alpha}{\alpha} + F(q^*) - F(0) \right], \quad (7.18)$$

where

$$F(q) = \frac{A}{4C} \ln(-4C(Cq^4 + Dq^2 + \mathcal{E})) + \frac{AD - 2BC}{4C\sqrt{D^2 - 4C\mathcal{E}}} \ln \frac{\sqrt{D^2 - 4C\mathcal{E}} + D + 2Cq^2}{\sqrt{D^2 - 4C\mathcal{E}} - D - 2Cq^2}, \quad (7.19)$$

and a UV momentum cutoff q^* has been introduced on the q integration.

7.1.3 Behavior of the soft part

To get some idea on how the soft part behaves as a function of the parameters it is useful to consider once again the limit of small ξ in Eq.(7.18). It turns out that in this limit one obtains

$$-\left(\frac{dW}{dx}\right)_{\text{soft, small-}\xi} = - \left[\left(\frac{dW}{dx}\right)_{\text{soft, iso}} + \xi \left(\left(\frac{dW}{dx}\right)_{\text{soft, } \xi_1} + \frac{(\mathbf{v} \cdot \hat{\mathbf{n}})^2}{v^2} \left(\frac{dW}{dx}\right)_{\text{soft, } \xi_2} \right) \right], \quad (7.20)$$

with

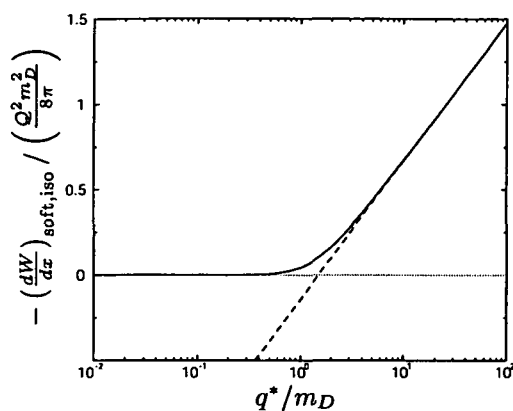


Figure 7.2: Soft contribution to the energy loss (full line) as a function of q^*/m_D for $v = 0.5$ compared to the Braaten-Thoma result (dashed line).

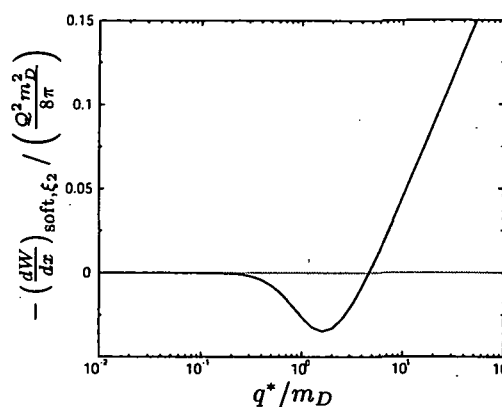


Figure 7.3: The contribution $-(dW/dx)_{\text{soft},\xi_2}$ as a function of q^*/m_D for $v = 0.5$.

$$-\left(\frac{dW}{dx}\right)_{\text{soft,iso}} = \frac{Q^2}{v^2} \text{Im} \int_{-v}^v \frac{d\hat{\omega}}{(2\pi)^2} \hat{\omega} \left[-\frac{v^2 - \hat{\omega}^2}{2(1 - \hat{\omega}^2)^2} \Pi_T \ln \frac{(1 - \hat{\omega}^2)q^{*2} + \Pi_T}{\Pi_T} - \frac{\Pi_L}{2} \ln \frac{q^{*2} - \Pi_L}{-\Pi_L} \right] \quad (7.21)$$

being the isotropic result for general q^* (calculated originally by Thoma and Gyulassy [113]). Note that Eq.(7.21) corresponds to the Braaten-Thoma result when expanding the logarithms under the assumption $q^* \gg m_D$. The respective results are compared in Fig. 7.2: while the results are identical for large q^*/m_D the Braaten-Thoma result becomes negative for small q^*/m_D whereas the unexpanded result obtained through numerical integration is positive for all values of q^*/m_D .

The effects of the anisotropy are encoded in the functions $(dW/dx)_{\text{soft},\xi_1}$ and $(dW/dx)_{\text{soft},\xi_2}$ which resemble that of $(dW/dx)_{\text{soft,iso}}$, but since they consist of many more terms than the isotropic contribution they will not be listed here explicitly. The direction of the heavy parton enters the small- ξ result only through the explicit term $(\mathbf{v} \cdot \hat{\mathbf{n}})^2/v^2$. The function $-(dW/dx)_{\text{soft},\xi_2}$ which multiplies this term and therefore controls the directional dependence of the soft part is plotted in Fig. 7.3. As can be seen in this figure, the function is negative for small q^*/m_D but becomes positive for large q^*/m_D . Since the function will eventually be evaluated at some q^*/m_D that minimizes the overall energy loss depending on the velocity and the coupling constant, the directional trend of the soft part reverses once this value of q^*/m_D crosses the point where $(dW/dx)_{\text{soft},\xi_2} = 0$. Therefore, one expects the energy loss to be peaked along $\hat{\mathbf{n}}$ for some couplings and velocities, while being peaked transverse to $\hat{\mathbf{n}}$ for others (see sketch in Fig. 7.1).

For general ξ it turns out that the results obtained in the small ξ limit still hold qualitatively although quantitatively the predictions differ considerably once

ξ becomes large. Fortunately, in the limit $\xi \rightarrow \infty$ one can again use the analytic results for the structure functions of chapter 6 as a verification of quantitative results.

7.2 Hard Contribution

The hard contribution can be separated into two parts: one contribution coming from the scattering of the heavy parton on quarks in the plasma and another one that takes into account the scattering on gluons (corresponding to the tree-level diagrams shown in Fig.7.4). Assuming the velocity of the parton to be much higher than the ratio of the plasma temperature to the energy of the parton, $v \gg T/E$, the contribution coming from quark-quark scattering can be reduced to [110]

$$-\left(\frac{dW}{dx}\right)_{\text{hard}}^{Qq} = \frac{2(4\pi)^3 N_f \alpha_s^2}{3v} \int \frac{d^3\mathbf{k}}{(2\pi)^3} \frac{f_\xi(\mathbf{k})}{k} \int \frac{d^3\mathbf{k}'}{(2\pi)^3} \frac{1-f_\xi(\mathbf{k}')}{k'} \delta(\omega - \mathbf{v} \cdot \mathbf{q}) \\ \times \Theta(q - q^*) \frac{\omega}{(\omega^2 - q^2)^2} \left[2(k - \mathbf{v} \cdot \mathbf{k})^2 + \frac{1-v^2}{2}(\omega^2 - q^2) \right], \quad (7.22)$$

after performing the Dirac traces and evaluating the sum over spins while the contribution coming from quark-gluon scattering gives

$$-\left(\frac{dW}{dx}\right)_{\text{hard}}^{Qg} = \frac{(4\pi)^3 \alpha_s^2}{2v} \int \frac{d^3\mathbf{k}}{(2\pi)^3} \frac{n_\xi(\mathbf{k})}{k} \int \frac{d^3\mathbf{k}'}{(2\pi)^3} \frac{1+n_\xi(\mathbf{k}')}{k'} \delta(\omega - \mathbf{v} \cdot \mathbf{q}) \Theta(q - q^*) \\ \times \omega \left[\frac{(1-v^2)^2}{(k - \mathbf{v} \cdot \mathbf{k})^2} + 8 \frac{(k - \mathbf{v} \cdot \mathbf{k})^2 + \frac{1-v^2}{2}(\omega^2 - q^2)}{(\omega^2 - q^2)^2} \right]. \quad (7.23)$$

Here $f_\xi(\mathbf{k})$ and $n_\xi(\mathbf{k})$ are the anisotropic versions of the tree-level Fermi-Dirac and Bose-Einstein distribution functions at zero chemical potential and $\omega = k' - k$ while $\mathbf{q} = \mathbf{k}' - \mathbf{k}$. Note also that q^* acts as IR cutoff for the q integration. Since the integrand is odd under the interchange $\mathbf{k} \leftrightarrow \mathbf{k}'$ the terms involving the products $f_\xi(\mathbf{k})f_\xi(\mathbf{k}')$ and $n_\xi(\mathbf{k})n_\xi(\mathbf{k}')$ vanish since they are symmetric. Redefining the origin of the \mathbf{k}' integration so that it becomes an integration over \mathbf{q} one obtains

$$-\left(\frac{dW}{dx}\right)_{\text{hard}}^{Qq} = \frac{16N_f \alpha_s^2}{3v} \int \frac{d^3\mathbf{k}}{(2\pi)^3} \frac{f_\xi(\mathbf{k})}{k} \int_{q^*}^{\infty} q^2 dq \int d\Omega_q \frac{\delta(\omega - \mathbf{v} \cdot \mathbf{q})}{|\mathbf{q} + \mathbf{k}|} \\ \times \frac{\omega}{(\omega^2 - q^2)^2} \left[2(k - \mathbf{v} \cdot \mathbf{k})^2 + \frac{1-v^2}{2}(\omega^2 - q^2) \right], \\ -\left(\frac{dW}{dx}\right)_{\text{hard}}^{Qg} = \frac{4\alpha_s^2}{v} \int \frac{d^3\mathbf{k}}{(2\pi)^3} \frac{n_\xi(\mathbf{k})}{k} \int_{q^*}^{\infty} q^2 dq \int d\Omega_q \frac{\delta(\omega - \mathbf{v} \cdot \mathbf{q})}{|\mathbf{q} + \mathbf{k}|} \\ \times \omega \left[\frac{(1-v^2)^2}{(k - \mathbf{v} \cdot \mathbf{k})^2} + 8 \frac{(k - \mathbf{v} \cdot \mathbf{k})^2 + \frac{1-v^2}{2}(\omega^2 - q^2)}{(\omega^2 - q^2)^2} \right], \quad (7.24)$$

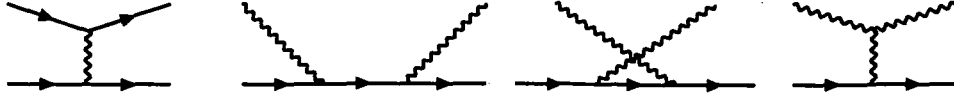


Figure 7.4: Tree-level Feynman diagrams for the scattering processes $Qq \rightarrow Qq$ (first diagram) and $Qg \rightarrow Qg$ (remaining diagrams).

where now $\omega = |\mathbf{q} + \mathbf{k}| - k$.

Choosing \mathbf{v} to be the z -axis for the \mathbf{q} and \mathbf{k} integration one can rewrite the delta-function as

$$\delta(|\mathbf{q} + \mathbf{k}| - k - \mathbf{v} \cdot \mathbf{q}) = \frac{\delta(\phi_q - \phi_0) \Theta(k + \mathbf{v} \cdot \mathbf{q}) 2|\mathbf{q} + \mathbf{k}|}{q \sqrt{4k^2 \sin^2 \theta_k \sin^2 \theta_q - (q(1 - v^2 \cos^2 \theta_q) + 2 \cos \theta_q (k \cos \theta_k - kv))^2}}, \quad (7.25)$$

where ϕ_0 is the solution of the equation

$$\cos(\phi_0 - \phi_k) = -\frac{q(1 - v^2 \cos^2 \theta_q) + 2 \cos \theta_q (k \cos \theta_k - kv)}{2k \sin \theta_k \sin \theta_q}. \quad (7.26)$$

Including a factor of 2 because of the symmetry $\phi_0 \leftrightarrow 2\pi - \phi_0$ the ϕ_q integration is straightforward. Moreover, the q integration can be done by scaling $k = qz$ as well as $\omega = qv \cos \theta_q$, since then

$$n_\xi(\mathbf{k}) \rightarrow \sqrt{1 + \xi n(qz \sqrt{1 + (\hat{\mathbf{q}} \cdot \hat{\mathbf{n}})^2})} \quad (7.27)$$

and one only needs to consider the integrals over Fermi-Dirac and Bose-Einstein distributions,

$$\int_{xT}^{\infty} dq q f(q) = T^2 \frac{x \ln(1 + \exp(-x)) - \text{Li}_2(-\exp(-x))}{x^2} = T^2 F_1(x) \quad (7.28)$$

$$\int_{xT}^{\infty} dq q n(q) = T^2 \frac{-x \ln(1 - \exp(-x)) + \text{Li}_2(\exp(-x))}{x^2} = T^2 F_2(x), \quad (7.29)$$

where $x = \frac{q^*}{T} \sqrt{1 + \xi(n_x \sin \theta_k \cos \phi_k + n_z \cos \theta_k)^2}$, with $n_z = \hat{\mathbf{n}} \cdot \hat{\mathbf{v}}$ and $1 = n_x^2 + n_z^2$. The hard contributions to the energy loss then take the form

$$-\left(\frac{dW}{dx}\right)_{\text{hard}}^{Qq} = \frac{8\alpha_s^2 N_f(\hat{q}^*)^2 T^2 \sqrt{1 + \xi}}{3\pi^3 v} \int_0^{\infty} zdz \int_{-1}^1 d \cos \theta_k \left[\int_0^{2\pi} d\phi_k F_1(x) \right] \int_{-1}^1 d \cos \theta_q \times \mathcal{T} \frac{v \cos \theta_q}{(v^2 \cos^2 \theta_q - 1)^2} \left[2z^2(1 - v \cos \theta_k)^2 + \frac{1 - v^2}{2}(v^2 \cos^2 \theta_q - 1) \right],$$

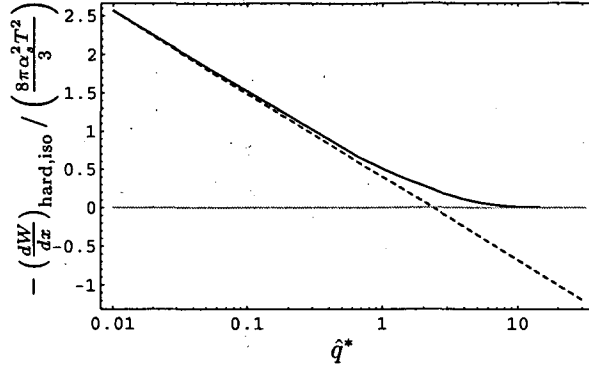


Figure 7.5: Hard contribution to the isotropic energy loss for $N_f = 2$ (full line) as a function of \hat{q}^* for $v = 0.5$ compared to the Braaten-Thoma result (dashed line).

$$\begin{aligned}
 - \left(\frac{dW}{dx} \right)_{\text{hard}}^{Qg} &= \frac{2\alpha_s^2 (\hat{q}^*)^2 T^2 \sqrt{1+\xi}}{\pi^3 v} \int_0^\infty z dz \int_{-1}^1 d \cos \theta_k \left[\int_0^{2\pi} d\phi_k F_2(x) \right] \\
 &\quad \int_{-1}^1 d \cos \theta_q \times \mathcal{T} v \cos \theta_q \left[\frac{(1-v^2)^2}{z^2 (1-v \cos \theta_k)^2} \right. \\
 &\quad \left. + 8 \frac{z^2 (1-v \cos \theta_k)^2 + \frac{1-v^2}{2} (v^2 \cos^2 \theta_q - 1)}{(v^2 \cos^2 \theta_q - 1)^2} \right], \tag{7.30}
 \end{aligned}$$

where \mathcal{T} denotes the unwieldy expression

$$\mathcal{T} = \Theta(z+v \cos \theta_q) \frac{\Theta(4z^2 \sin^2 \theta_k \sin^2 \theta_q - (1-v^2 \cos^2 \theta_q + 2 \cos \theta_q z (\cos \theta_k - v))^2)}{\sqrt{4z^2 \sin^2 \theta_k \sin^2 \theta_q - (1-v^2 \cos^2 \theta_q + 2 \cos \theta_q z (\cos \theta_k - v))^2}}. \tag{7.31}$$

The remaining integrations have to be performed numerically.

7.2.1 Behavior of the hard part

Similar to what has been done for the soft part it is possible to gain some insight on the parametric dependence of the hard contribution by considering the anisotropy to be weak ($\xi \ll 1$) [111]. One can then compare the unexpanded isotropic ($\xi = 0$) result to the Braaten-Thoma result, shown in Fig. 7.5. As one can see, the two results are identical for small $\hat{q}^* = q^*/T$ while for larger \hat{q}^* the Braaten-Thoma result becomes negative and the unexpanded result Eq.(7.30) is positive for all values of \hat{q}^* .

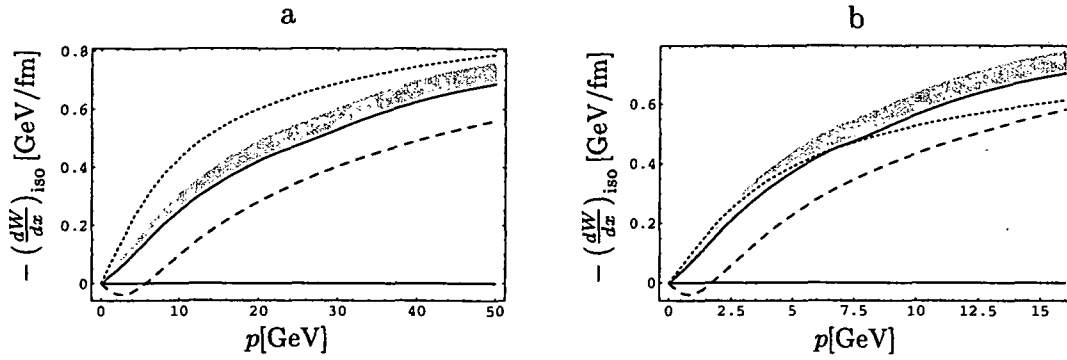


Figure 7.6: Energy loss of a beauty (a) and charm quark (b) as a function of momentum p for $T = 250\text{MeV}$ and $\alpha_s = 0.3$. Shown are the respective results from Ref. [114] (dotted line) and Ref. [110] (dashed line) as well as the evaluation of Eq.(7.32) (full line) with a variation of q^* (gray band).

7.3 Isotropic results

In the isotropic limit, the total collisional energy loss of a heavy parton is obtained by adding Eq.(7.21) and Eq.(7.30) with $\xi = 0$,

$$-\left(\frac{dW}{dx}\right)_{\text{iso}} = -\left[\left(\frac{dW}{dx}\right)_{\text{soft,iso}} + \left(\frac{dW}{dx}\right)_{\text{hard,iso}}\right]. \quad (7.32)$$

It is a function of the strong coupling α_s , the particle velocity v , the temperature T and the momentum separation scale q^* . As has already been discussed above, the q^* dependence of the result is found to become weak for small values of the coupling limit α_s (similar to what has been found in QED [111]), corresponding to the original result by BRAATEN and THOMA [110]; for larger values of the coupling one fixes $q^* = q^{\text{pms}}$ using the principle of minimum sensitivity,

$$\frac{d}{dq^*} \left(\frac{dW}{dx}\right)_{\text{iso}} \Big|_{q^*=q_{\text{pms}}^*} = 0. \quad (7.33)$$

Note that $-\left(\frac{dW}{dx}\right)_{\text{iso}} \Big|_{q^*=q_{\text{pms}}^*}$ always serves as a lower bound on the result for the energy loss. To get an estimate of how strongly the result depends on this special value of q^* , one can e.g. vary q_{pms}^* by a certain factor c_{q^*} and evaluate the energy loss at $q_{\text{pms}}^* c_{q^*}$ and q_{pms}^*/c_{q^*} . This factor c_{q^*} is in principle arbitrary, but should be such that the resulting q^* is neither much smaller than m_D , nor much bigger than $2\pi T$; in the following, I have chosen $c_{q^*} = 2$ to be consistent with what has been done in QED [111], although for QCD this probably overestimates the resulting variations in the energy loss since for realistic couplings $q_{\text{pms}}^*/c_{q^*} \leq m_D$.

However, whereas the choice $c_{q^*} = 2$ represents a very conservative choice on the variations of the leading-order energy loss, it should be noted that no estimate on the next-to-leading order (NLO) corrections to the energy loss has

been made here. Therefore, it should be kept in mind that for QCD with large realistic coupling the inclusion of these NLO corrections might give energy loss results that are not covered by the variations of q^* in the leading-order result, so these variations should be interpreted with care.

In Fig. 7.6a,b various results for the energy loss of a heavy parton in an isotropic quark-gluon plasma are compared: shown are the results from BJORKEN [114], BRAATEN and THOMA [110], as well as Eq.(7.32) at $q^* = q_{\text{pms}}^*$ together with its variation using $c_q = 2$. For the compilations a temperature of $T = 250\text{MeV}$ and a coupling constant of $\alpha_s = 0.3$ was adopted; Fig. 7.6a shows the energy loss of a beauty quark with mass $M_Q \simeq 5\text{GeV}$ while in Fig. 7.6b the energy loss of a charm quark with mass $M_Q \simeq 1.5\text{GeV}$ is plotted, both as a function of their momenta

$$p = \frac{vM_Q}{\sqrt{1-v^2}}. \quad (7.34)$$

7.3.1 Limitations

Since Eq.(7.32) has been derived for an infinitely heavy parton, it breaks down for thermal velocities $v \sim \sqrt{T/M_Q}$ because a quark with $v = 0$ can only gain energy from collisions with other particles in the heat bath. A semi-quantitative estimate of the velocity where the energy loss becomes negative has been done in Ref. [110] by repeating the above calculation in the limit $v \rightarrow 0$ and for weak couplings, finding $v \sim \sqrt{3T/M_Q}$ (which corresponds to $p = 1.5\text{GeV}$ and $p = 2.1\text{GeV}$ for charm and beauty quarks, respectively). Similarly, Eq.(7.32) also breaks down for ultrarelativistic energies $E \gg M_Q^2/T$, with the cross-over energy having been determined to be $E_{\text{cross}} \simeq 1.8M_Q^2/T$ (corresponding to $v > 0.995$ for both charm and beauty quarks). However, note that the reason that the Braaten-Thoma result turns negative for a momentum of $p \simeq 5.7\text{GeV}$ for the beauty and $p \simeq 1.71\text{GeV}$ for the charm quark (as is indicated in Fig. 7.6a,b) is not due to this physical reason but rather due to a failure of the extrapolation from the weak coupling limit to realistic couplings [110]. For the unexpanded result Eq.(7.32), this unphysical behavior does not occur and one can therefore expect it to be valid for velocities down to the original estimate $v \sim \sqrt{3T/M_Q}$.

7.4 Anisotropic results

The full result for the heavy parton energy loss in an anisotropic system with strength ξ is given by adding the soft contribution from Eq.(7.18) and the hard contributions from Eq.(7.30),

$$-\left(\frac{dW}{dx}\right) = -\left[\left(\frac{dW}{dx}\right)_{\text{soft}} + \left(\frac{dW}{dx}\right)_{\text{hard}}\right]. \quad (7.35)$$

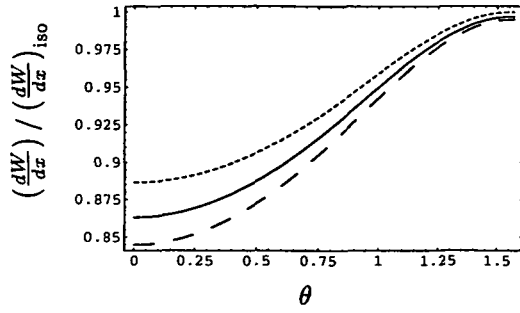


Figure 7.7: Anisotropic energy loss at $v = 0.5$, $\xi = 1.0$ for $\alpha_s = 0.2, 0.3, 0.4$ (dotted, full and dashed line, respectively) as a function of the angle θ (normalized to the isotropic result).

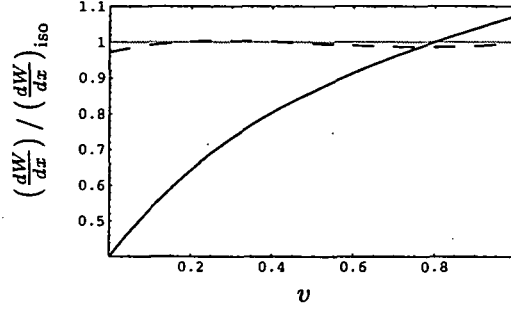


Figure 7.8: Anisotropic energy loss for $\xi = 1.0$, $\alpha_s = 0.3$ and $\theta = 0$ (full line) compared to $\theta = \pi/2$ (dashed line) as a function of velocity (normalized to the isotropic result).

It depends on q^* , T and v as was the case for the isotropic energy loss, but in general also on the angle of the particle direction with respect to the anisotropy vector $\cos \theta = \hat{v} \cdot \hat{n}$ (sketched in Fig. 7.1). The angular dependence of the energy loss at $\xi = 1$ normalized to the isotropic energy loss Eq.(7.32) is shown in Fig. 7.7 for $v = 0.5$ and different couplings $\alpha_s = 0.2, 0.3, 0.4$; as can be seen, for all couplings considered the energy loss turns out to be smaller along \hat{n} than transverse to it. However, as already noted in the earlier discussion on the soft contribution to the energy loss, this dependence may change as a function of the velocity v , as can be seen in Fig. 7.8, where the energy loss Eq.(7.35) evaluated at $\theta = 0$ and $\theta = \pi/2$ has been plotted for $\alpha_s = 0.3$. From this figure it becomes clear that the energy loss is peaked at $\theta = \pi/2$ for velocities smaller than v_0 while it is peaked at $\theta = 0$ for $v > v_0$, where $v_0 \simeq 0.7$ for $\xi = 1$ and $\alpha_s = 0.3$. Note that in Figs. 7.7, 7.8 the variational bands obtained by varying q^* exhibit the same trend but lie about 30% higher than the curves shown.

Note that for simplicity here it was assumed that quark and gluon distribution functions have momentum-space anisotropies of the same strength. In general, this assumption is quite probably not fulfilled, so a more realistic result for the energy loss will depend on the quark and gluon anisotropies separately.

7.5 Effects of finite chemical potential

Taking finite chemical potential into account, the soft contribution Eq.(7.18) remains unchanged in form with the only difference being the change of the Debye mass

$$m_D^2 \rightarrow 4\pi\alpha_s \left(\frac{6 + N_f T^2}{6} + \frac{N_f \mu^2}{2\pi^2} \right), \quad (7.36)$$

in the structure functions according to Eq.(2.4). For the hard contribution, only the quark-quark scattering term changes, so one has to replace

$$f_{\xi}(\mathbf{k})(1 - f_{\xi}(\mathbf{k}')) \rightarrow \frac{1}{4}(f_{+,\xi}(\mathbf{k}) + f_{-,\xi}(\mathbf{k}))(1 - (f_{+,\xi}(\mathbf{k}) + f_{-,\xi}(\mathbf{k}))) \quad (7.37)$$

in Eq.(7.22). Again, all terms involving products of distribution functions can be shown not to contribute to the energy loss, so one recovers Eq.(7.30) with the function $F_1(x)$ being replaced by

$$F_1(x) \rightarrow \frac{1}{2T^2} \int_{xT}^{\infty} dq q (f_+(q) + f_-(q)), \quad (7.38)$$

which can be calculated analytically similar to Eq.(7.28). A subsequent evaluation of the collisional energy loss at finite chemical potential in the weak coupling limit has been done in Ref. [115]. There it was found that the effects played by the quark chemical potential are rather small unless μ/T gets large.

7.6 Summary

In this chapter I have calculated the complete leading-order collisional energy loss of a heavy parton propagating through an anisotropic quark-gluon plasma. The calculation was based on results for the collective modes in an anisotropic plasma of chapter 6 and it was demonstrated that the unstable modes found for such a system would in principle cause the result to be divergent. However, it has been shown that the collisional energy loss is protected by the mechanism of dynamical shielding, for which a proof in two analytically tractable regimes (weak and extremely strong anisotropy) was given. As a side result, in the isotropic limit the original result for the energy loss was shown to have a correction which cured the problem of unphysical energy loss results for heavy partons.

The results were applied for beauty and charm quarks and the applicability of the calculation was discussed. Also, it was shown that for anisotropic systems the collisional energy loss has an angular dependence which is expected to increase for larger couplings and stronger anisotropies, possibly having phenomenological implications. Finally, a refinement of the calculation involving different momentum-space anisotropies for the quark and gluon distribution functions was suggested and the effects of finite chemical potential were discussed.

Chapter 8

Conclusions and outlook

In this work, I have investigated the quasiparticle description of certain observables in the hot and dense quark-gluon plasma. More precisely, the quasiparticle excitations and in general the collective modes of systems with isotropic as well as anisotropic momentum-space distribution functions were analyzed in the HTL approximation, with a special emphasis on the gluonic excitations.

For isotropic systems, an HTL quasiparticle model for the thermodynamic pressure based on the two-loop Φ -derivable approximation for the entropy was proposed, which improves on an existing simpler model by taking into account the full momentum dependence of the HTL self-energies. It was shown that these quasiparticle models can be used to accurately describe two-flavor lattice results for the pressure, entropy and quark-number susceptibilities at zero chemical potential by adopting an effective running coupling including two fit parameters. An extension of these quasiparticle models to finite chemical potential (naturally given by a flow equation for the strong coupling as a consequence of the stationarity condition for the quark and gluon propagators) was also shown to be consistent with independent lattice studies in the region of applicability of the latter. Therefore, these results demonstrate that quasiparticle models can qualitatively reproduce lattice results for the major bulk thermodynamic quantities above the phase transition, at least when supplied by a phenomenologically inspired effective strong coupling as an input. Quantitatively the differences with respect to lattice studies were found to be small but non-vanishing, although it is probably fair to say that currently the variations in the latter due to different implementations of fermions and incomplete continuum-extrapolations are comparable in magnitude. Encouragingly, the inclusion of the plasmon effect which has devastating effects on a strictly perturbative calculation for the pressure turns out to lead to small corrections when incorporated through a quasiparticle model, as has been shown here.

Therefore, quasiparticle models in general and the HTL model in particular provide a simple, physically intuitive and rather accurate description of the quark-gluon plasma, both at zero and also at non-vanishing chemical potential.

Moreover, motivated by this success at small chemical potential, estimates of quantities at large chemical potential, such as the critical chemical potential at very small temperature, can and have been calculated. Although these results represent only estimates based on the physics at small μ and are therefore likely to change somewhat once techniques more accurate for the high density regime will be developed, the quasiparticle model calculations give precise and robust predictions in contrast to lattice studies which (as yet) cannot reach this domain of high density at all or strictly perturbative results that suffer from large renormalization scheme dependences.

However, further refinements are possible: as a first step, a complete determination of the next-to-leading order corrections to the self-energies would eliminate the dependence of the NLA model on the free parameter c_Λ , allowing a precise inclusion of the full plasmon term in the model, thereby greatly increase its accuracy. The next (ambitious) step would be to aim for a fully self-consistent calculation of the one-loop self-energies, which in turn would make the quasiparticle model completely self-contained, since both the form of the gap-equations as well as the running coupling would result from such a calculation. Unfortunately, while the first step is fairly straightforward, the second step probably still has to await progress concerning gauge-dependencies and the renormalization procedure of e.g. the two-loop Φ -derivable approximation for QCD. Nevertheless, the results of such calculations would be highly interesting since it is possible that knowledge about such fully non-perturbative quasiparticle-like excitations might be sufficient to offer something that is very close to a full description of the isotropic quark-gluon plasma.

For anisotropic systems, however, the situation is fairly different: the reason for this is that systems with an anisotropy in momentum space possess unstable modes that correspond to exponentially growing gauge field amplitudes. The presence of these unstable modes is believed to have important consequences both on the dynamical evolution of the quark-gluon plasma as well as on more practical issues as the de-facto breakdown of calculations using a perturbative framework, as has been demonstrated. However, owing to the fact that in QCD the (re-)discovery of these instabilities has only occurred very recently, many important questions remain largely unanswered and indeed are subject to active ongoing research. For example, there are indications that certain observables exist that are protected from the breakdown of perturbative calculations, as has been shown explicitly here for the collisional energy loss of a heavy parton. However, it is currently unknown if there are any other observables that are either dynamically shielded or otherwise protected from the singularities coming from the unstable modes, so further studies in this direction are mandatory to have a better understanding of the effects of the QCD plasma instabilities. Also the saturation mechanism of the instabilities deserves closer investigation: while for QED non-perturbative effects on the hard particles are responsible for halting the growth of the unstable modes, for QCD the non-Abelian interaction between

the soft fields might saturate this growth already earlier. Moreover, a detailed understanding of the role that the instabilities play in modifying the bottom-up thermalization scheme is still missing and would probably be very important for the early system evolution following a heavy-ion collision. Summarizing, the full implications of unstable modes in the anisotropic quark-gluon plasma have not yet been worked out, but current knowledge suggests that these might have (measurable?) consequences on the physics tested at RHIC and especially the LHC once it becomes operable, since there the momentum-space anisotropies are probably very strong.

In conclusion, calculations based on the analysis of collective modes offer qualitative as well as quantitative predictions relevant for QCD at high temperature (and non-vanishing chemical potential) both for isotropic and anisotropic systems. However, whereas for isotropic systems quasiparticle models for thermodynamic quantities are well-developed and have been tested in many occasions, anisotropic systems are less well understood and their theoretical treatment has only been tested in the case of QED. Moreover, current calculations (although non-perturbative in character because of implicit resummations) are essentially limited to including only leading-order correction terms completely, so the quantitative (as well as qualitative?) effects of higher order corrections might still be substantial for QCD where the coupling gets large. Nevertheless – pending the development of new methods – quasiparticle descriptions of hot and dense QCD allow predictions in a range of situations where other approaches from first principles become either ambiguous, very complicated or break down altogether, thus making the former an invaluable tool in the study of the new form of matter called the quark-gluon plasma.

Appendix A

Coefficients for the HTL coupling flow equation

In order to rewrite Eq.(3.17) into the form of Eq.(2.26), quite some algebra is necessary. For convenience, I therefore reproduce here the final coefficients a_T , a_μ and b which may be directly used to solve the flow equation. I find

$$\begin{aligned}
 a_T &= \frac{2NN_f C}{N^2 - 1 T}, \\
 a_\mu &= -\frac{\mathcal{A}}{T^2} - \frac{2NN_f B}{N^2 - 1 T^2}, \\
 \frac{b}{4\pi\alpha_{s,\text{eff}}} &= \frac{2NN_f C}{N^2 - 1 T} \frac{4\pi\alpha_{s,\text{eff}}}{M^2} \frac{N^2 - 1}{8N} T - \frac{\mathcal{A}}{T^2} \frac{4\pi\alpha_{s,\text{eff}}}{m_D^2} \frac{N_f}{\pi^2} \mu \\
 &\quad - \frac{2NN_f B}{N^2 - 1 T^2} \frac{4\pi\alpha_{s,\text{eff}}}{M^2} \frac{N^2 - 1}{8N} \frac{\mu}{\pi^2}, \tag{A.1}
 \end{aligned}$$

where

$$\begin{aligned}
 \mathcal{A} &= \int \frac{d^3k}{(2\pi)^3} \left\{ \left[\frac{2}{\pi} \int_0^k d\omega dn(\omega)(-\omega) \frac{2(k^2 - \omega^2)(\text{Im}\Pi_T)^3}{[(k^2 - \omega^2 + \text{Re}\Pi_T)^2 + (\text{Im}\Pi_T)^2]^2} \right. \right. \\
 &\quad \left. \left. + \frac{2}{\pi} \int_0^k d\omega dn(\omega)(-\omega) \frac{k^2(\text{Im}\Pi_L)^3}{[(k^2 + \text{Re}\Pi_L)^2 + (\text{Im}\Pi_L)^2]^2} \right] \right. \\
 &\quad \left. - 2E_T^2 dn(E_T) \frac{E_T^2 - k^2}{|m_D^2 E_T^2 - (E_T^2 - k^2)^2|} - E_L^2 dn(E_L) \frac{E_L^2 - k^2}{|k^2 - E_L^2 + m_D^2|} \right\}, \tag{A.2}
 \end{aligned}$$

$$\begin{aligned}
 \mathcal{B} &= \int \frac{d^3k}{(2\pi)^3} \left\{ \left[\frac{2}{\pi} \int_0^k d\omega [df_+(\omega)(-\omega + \mu) - df_-(\omega)(\omega + \mu)] \right. \right. \\
 &\quad \left. \left. \times \frac{(k - \omega)(\text{Im}\Sigma_+)^3}{[(k - \omega + \text{Re}\Sigma_+)^2 + (\text{Im}\Sigma_+)^2]^2} \right. \right. \\
 &\quad \left. \left. + \frac{2}{\pi} \int_0^k d\omega [df_+(\omega)(-\omega + \mu) - df_-(\omega)(\omega + \mu)] \frac{(k + \omega)(\text{Im}\Sigma_-)^3}{[(k + \omega + \text{Re}\Sigma_-)^2 + (\text{Im}\Sigma_-)^2]^2} \right] \right\}.
 \end{aligned}$$

88 APPENDIX A. COEFFICIENTS FOR THE HTL COUPLING FLOW EQUATION

$$\begin{aligned}
 & +(E_+ - k) [df_+(E_+)(-E_+ + \mu) - df_-(E_+)(E_+ + \mu)] \frac{E_+^2 - k^2}{2M^2} \\
 & +(E_- + k) [df_+(E_-)(-E_- + \mu) - df_-(E_-)(E_- + \mu)] \frac{E_-^2 - k^2}{2M^2} \Big\}, \quad (A.3)
 \end{aligned}$$

$$\begin{aligned}
 C = & \int \frac{d^3k}{(2\pi)^3} \left\{ \left[\frac{2}{\pi} \int_0^k d\omega (-df_+(\omega) + df_-(\omega)) \frac{(k - \omega)(\text{Im}\Sigma_+)^3}{[(k - \omega + \text{Re}\Sigma_+)^2 + (\text{Im}\Sigma_+)^2]^2} \right. \right. \\
 & \left. \left. + \frac{2}{\pi} \int_0^k d\omega [-df_+(\omega) + df_-(\omega)] \frac{(k + \omega)(\text{Im}\Sigma_-)^3}{[(k + \omega + \text{Re}\Sigma_-)^2 + (\text{Im}\Sigma_-)^2]^2} \right] \right. \\
 & \left. + (E_+ - k) [-df_+(E_+) + df_-(E_+)] \right. \\
 & \left. + (E_- + k) [-df_+(E_-) + df_-(E_-)] \right\}. \quad (A.4)
 \end{aligned}$$

In the above equations I have used the abbreviations

$$\begin{aligned}
 dn(\omega) &= \frac{-\exp \omega/T}{(\exp \omega/T - 1)^2} \\
 df_{\pm}(\omega) &= \frac{-\exp(\omega \pm \mu)/T}{(\exp(\omega \pm \mu)/T + 1)^2}. \quad (A.5)
 \end{aligned}$$

Furthermore, E_T, E_L and E_+, E_- are the dispersion relations $E_T(k), E_L(k)$ and $E_+(k), E_-(k)$ for the bosonic and fermion quasiparticles shown in chapter 2, and $\Pi_T, \Pi_L, \Sigma_+, \Sigma_-$ are the bosonic and fermionic HTL self-energies also presented in this chapter.

Appendix B

Analytic expressions for structure functions

In this appendix I collect the integral and analytic expressions for the structure functions α , β , γ , and δ defined in Eq.(6.31). Choosing $\hat{\mathbf{n}} = \hat{\mathbf{z}}$ and \mathbf{k} to lie in the xz plane ($k_x/k_z = \tan \theta_n$) one has $\hat{\mathbf{v}} \cdot \hat{\mathbf{n}} = \cos \theta$ and $\mathbf{v} \cdot \mathbf{k} = vk_x \cos \phi \sin \theta + vk_z \cos \theta$. Using this parameterization the ϕ integration for all four structure functions defined by the contractions in Eq.(6.31) can be performed analytically.

$$\alpha(K, \xi) = \frac{m_D^2}{k^2 \bar{n}^2} \int \frac{d(\cos \theta)}{2} \frac{\omega + \xi k_z \cos \theta}{(1 + \xi(\cos \theta)^2)^2} \left[\omega - k_z \cos \theta + k^2 (s^2 - (\cos \theta - \frac{\omega k_z}{k^2})^2) R(\omega - k_z \cos \theta, k_x \sin \theta) \right], \quad (\text{B.1})$$

$$\beta(K, \xi) = -\frac{m_D^2 \omega^2}{k^2} \int \frac{d(\cos \theta)}{2} \frac{1}{(1 + \xi(\cos \theta)^2)^2} \times [1 - (\omega + \xi k_z \cos \theta) R(\omega - k_z \cos \theta, k_x \sin \theta)], \quad (\text{B.2})$$

$$\gamma(K, \xi) = m_D^2 \int \frac{d(\cos \theta)}{2k^2} \frac{1}{(1 + \xi \cos^2 \theta)^2} \left[\omega^2 + \xi k^2 \cos^2 \theta - 2 \frac{k^2}{k_x^2} (\omega^2 - \xi k_z^2 \cos^2 \theta) + \frac{(\omega + \xi k_z \cos \theta) k^4}{k_x^2} \left(2(\cos \theta - \frac{\omega k_z}{k^2})^2 - s^2 \right) R(\omega - k_z \cos \theta, k_x \sin \theta) \right], \quad (\text{B.3})$$

$$\delta(K, \xi) = \frac{m_D^2 \omega}{k^4 \bar{n}^2} \int \frac{d(\cos \theta)}{2} \frac{\omega + \xi k_z \cos \theta}{(1 + \xi \cos^2 \theta)^2} (k_z + (k^2 \cos \theta - \omega k_z)) \times R(\omega - k_z \cos \theta, k_x \sin \theta), \quad (\text{B.4})$$

where $s^2 = (1 - \omega^2/k^2)(k_x^2/k^2)$ and

$$R(a, b) = \int_0^{2\pi} \frac{d\phi}{2\pi} \frac{1}{a - b \cos \phi + i\epsilon} = \frac{1}{\sqrt{a+b+i\epsilon}\sqrt{a-b+i\epsilon}}. \quad (\text{B.5})$$

When a and b are real-valued R can be simplified to

$$R(a, b) = \frac{\text{sgn}(a)\Theta(a^2 - b^2)}{\sqrt{a^2 - b^2}} - \frac{i\Theta(b^2 - a^2)}{\sqrt{b^2 - a^2}}, \quad (\text{B.6})$$

with $\Theta(x)$ being the usual step-function. Note that the remaining integration over θ can also be done analytically but the results are rather unwieldy so I do not list them here.

Static Limit

In the limit $\omega \rightarrow 0$ it is possible to obtain analytic expressions for all four structure functions. The results for m_α and m_β defined in Eq.(6.38) are

$$m_\alpha^2 = -\frac{m_D^2 \sqrt{1+\xi}}{2k_x^2 \sqrt{\xi}} \left(k_z^2 \arctan \sqrt{\xi} - \frac{k_z k^2}{\sqrt{k^2 + \xi k_x^2}} \arctan \frac{\sqrt{\xi} k_z}{\sqrt{k^2 + \xi k_x^2}} \right), \quad (\text{B.7})$$

$$m_\beta^2 = m_D^2 \frac{(\sqrt{\xi} + (1+\xi) \arctan \sqrt{\xi})(k^2 + \xi k_x^2)}{2\sqrt{\xi} \sqrt{1+\xi} (k^2 + \xi k_x^2)} + m_D^2 \frac{\xi k_z \left(k_z \sqrt{\xi} + \frac{k^2(1+\xi)}{\sqrt{k^2 + \xi k_x^2}} \arctan \frac{\sqrt{\xi} k_z}{\sqrt{k^2 + \xi k_x^2}} \right)}{2\sqrt{\xi} \sqrt{1+\xi} (k^2 + \xi k_x^2)}, \quad (\text{B.8})$$

with similar results for m_γ^2 and m_δ^2 .

Bibliography

- [1] J. Gasser and H. Leutwyler, *Chiral perturbation theory to one loop*, *Ann. Phys.* **158** (1984) 142.
- [2] J. Gasser and H. Leutwyler, *Chiral perturbation theory: Expansions in the mass of the strange quark*, *Nucl. Phys.* **B250** (1985) 465.
- [3] S. Scherer, *Introduction to chiral perturbation theory*, hep-ph/0210398.
- [4] F. Karsch, *Lattice QCD at high temperature and density*, *Lect. Notes Phys.* **583** (2002) 209–249, [hep-lat/0106019].
- [5] H. Grigorian, D. Blaschke, and G. Poghosyan, *Mapping déconfinement with a compact star phase diagram*, *Nucl. Phys.* **A715** (2003) 831–834, [nucl-th/0209068].
- [6] M. Bellac, *Thermal field theory*. Cambridge University Press, Cambridge, 1996.
- [7] CP-PACS Collaboration, A. Ali Khan *et. al.*, *Phase structure and critical temperature of two flavor QCD with renormalization group improved gauge action and clover improved Wilson quark action*, *Phys. Rev.* **D63** (2001) 034502, [hep-lat/0008011].
- [8] J.I.Kapusta, *Finite-temperature field theory*. Cambridge University Press, Cambridge, 1989.
- [9] Particle Data Group Collaboration, K. Hagiwara *et. al.*, *Review of particle physics*, *Phys. Rev.* **D66** (2002) 010001.
- [10] G. Rodrigo and A. Santamaria, *QCD matching conditions at thresholds*, *Phys. Lett.* **B313** (1993) 441–446, [hep-ph/9305305].
- [11] T. van Ritbergen, J. A. M. Vermaseren, and S. A. Larin, *The four-loop beta function in quantum chromodynamics*, *Phys. Lett.* **B400** (1997) 379–384, [hep-ph/9701390].

- [12] S. Gupta, *A precise determination of $T(c)$ in QCD from scaling*, *Phys. Rev. D* **64** (2001) 034507, [hep-lat/0010011].
- [13] P. Arnold and C.-x. Zhai, *The three loop free energy for high temperature QED and QCD with fermions*, *Phys. Rev. D* **51** (1995) 1906–1918, [hep-ph/9410360].
- [14] C.-x. Zhai and B. Kastening, *The free energy of hot gauge theories with fermions through g^5* , *Phys. Rev. D* **52** (1995) 7232–7246, [hep-ph/9507380].
- [15] K. Kajantie, M. Laine, K. Rummukainen, and Y. Schroder, *The pressure of hot QCD up to $g^6 \ln(1/g)$* , *Phys. Rev. D* **67** (2003) 105008, [hep-ph/0211321].
- [16] J. P. Blaizot, E. Iancu, and A. Rebhan, *On the apparent convergence of perturbative QCD at high temperature*, *Phys. Rev. D* **68** (2003) 025011, [hep-ph/0303045].
- [17] CP-PACS Collaboration, A. Ali Khan *et. al.*, *Equation of state in finite-temperature QCD with two flavors of improved Wilson quarks*, *Phys. Rev. D* **64** (2001) 074510, [hep-lat/0103028].
- [18] F. Karsch, E. Laermann, and A. Peikert, *The pressure in 2, 2+1 and 3 flavour QCD*, *Phys. Lett. B* **478** (2000) 447–455, [hep-lat/0002003].
- [19] B. Kastening, *Perturbative finite-temperature results and Pade approximants*, *Phys. Rev. D* **56** (1997) 8107–8110, [hep-ph/9708219].
- [20] T. Hatsuda, *Pade improvement of the free energy in high temperature QCD*, *Phys. Rev. D* **56** (1997) 8111–8114, [hep-ph/9708257].
- [21] G. Cvetic and R. Kogerler, *Resummations of free energy at high temperature*, *Phys. Rev. D* **66** (2002) 105009, [hep-ph/0207291].
- [22] R. R. Parwani, *Borel resummation of the perturbative free energy of hot Yang-Mills theory*, *Phys. Rev. D* **63** (2001) 054014, [hep-ph/0010234].
- [23] R. R. Parwani, *The free-energy of hot gauge theories*, *Phys. Rev. D* **64** (2001) 025002, [hep-ph/0010294].
- [24] E. Braaten and R. D. Pisarski, *Simple effective Lagrangian for hard thermal loops*, *Phys. Rev. D* **45** (1992) 1827–1830.
- [25] J. O. Andersen, E. Braaten, and M. Strickland, *Hard-thermal-loop resummation of the free energy of a hot gluon plasma*, *Phys. Rev. Lett.* **83** (1999) 2139–2142, [hep-ph/9902327].

- [26] J. O. Andersen, E. Braaten, E. Petitgirard, and M. Strickland, *HTL perturbation theory to two loops*, *Phys. Rev. D* **66** (2002) 085016, [hep-ph/0205085].
- [27] J. P. Blaizot, E. Iancu, and A. Rebhan, *The entropy of the QCD plasma*, *Phys. Rev. Lett.* **83** (1999) 2906–2909, [hep-ph/9906340].
- [28] J. P. Blaizot, E. Iancu, and A. Rebhan, *Approximately self-consistent resummations for the thermodynamics of the quark-gluon plasma. I: Entropy and density*, *Phys. Rev. D* **63** (2001) 065003, [hep-ph/0005003].
- [29] J.-P. Blaizot, E. Iancu, and A. Rebhan, *Thermodynamics of the high-temperature quark gluon plasma*, hep-ph/0303185.
- [30] A. Peshier, *HTL resummation of the thermodynamic potential*, *Phys. Rev. D* **63** (2001) 105004, [hep-ph/0011250].
- [31] E. Braaten and E. Petitgirard, *Solution to the 3-loop Φ -derivable approximation for scalar thermodynamics*, *Phys. Rev. D* **65** (2002) 041701, [hep-ph/0106045].
- [32] H. van Hees and J. Knoll, *Renormalization in self-consistent approximations schemes at finite temperature. I: Theory*, *Phys. Rev. D* **65** (2002) 025010, [hep-ph/0107200].
- [33] J.-P. Blaizot, E. Iancu, and U. Reinosa, *Renormalizability of Φ -derivable approximations in scalar ϕ^4 theory*, hep-ph/0301201.
- [34] E. Braaten and A. Nieto, *Free energy of QCD at high temperature*, *Phys. Rev. D* **53** (1996) 3421–3437, [hep-ph/9510408].
- [35] C. R. Allton *et al.*, *The QCD thermal phase transition in the presence of a small chemical potential*, *Phys. Rev. D* **66** (2002) 074507, [hep-lat/0204010].
- [36] A. Vuorinen, *The pressure of QCD at finite temperatures and chemical potentials*, hep-ph/0305183.
- [37] Z. Fodor and S. D. Katz, *A new method to study lattice QCD at finite temperature and chemical potential*, *Phys. Lett. B* **534** (2002) 87–92, [hep-lat/0104001].
- [38] P. de Forcrand and O. Philipsen, *The QCD phase diagram for small densities from imaginary chemical potential*, *Nucl. Phys. B* **642** (2002) 290–306, [hep-lat/0205016].

- [39] Z. Fodor, S. D. Katz, and K. K. Szabo, *The QCD equation of state at nonzero densities: lattice result*, hep-lat/0208078.
- [40] M. D'Elia and M.-P. Lombardo, *Finite density QCD via imaginary chemical potential*, *Phys. Rev. D* **67** (2003) 014505, [hep-lat/0209146].
- [41] R. V. Gavai and S. Gupta, *Pressure and non-linear susceptibilities in QCD at finite chemical potentials*, hep-lat/0303013.
- [42] A. Peshier, B. Kampfer, and G. Soff, *The equation of state of deconfined matter at finite chemical potential in a quasiparticle description*, *Phys. Rev. C* **61** (2000) 045203, [hep-ph/9911474].
- [43] A. Peshier, B. Kampfer, and G. Soff, *From QCD lattice calculations to the equation of state of quark matter*, *Phys. Rev. D* **66** (2002) 094003, [hep-ph/0206229].
- [44] E. S. Fraga, R. D. Pisarski, and J. Schaffner-Bielich, *New class of compact stars at high density*, *Nucl. Phys. A* **702** (2002) 217–223, [nucl-th/0110077].
- [45] J. O. Andersen and M. Strickland, *The equation of state for dense QCD and quark stars*, *Phys. Rev. D* **66** (2002) 105001, [hep-ph/0206196].
- [46] A. Ipp, G. D. Moore, and A. Rebhan, *Comment on and erratum to 'Pressure of hot QCD at large $N(f)$ '*, *JHEP* **01** (2003) 037, [hep-ph/0301057].
- [47] R. A. Schneider and W. Weise, *On the quasiparticle description of lattice QCD thermodynamics*, *Phys. Rev. C* **64** (2001) 055201, [hep-ph/0105242].
- [48] M. A. Thaler, R. A. Schneider, and W. Weise, *Quasiparticle description of hot QCD at finite quark chemical potential*, hep-ph/0310251.
- [49] V. Baluni, *Nonabelian gauge field theories of the fermi gas*, *Phys. Lett. B* **72** (1978) 381.
- [50] B. A. Freedman and L. D. McLerran, *Fermions and gauge vector mesons at finite temperature and density. 3. the ground state energy of a relativistic quark gas*, *Phys. Rev. D* **16** (1977) 1169.
- [51] R. Baier, A. H. Mueller, D. Schiff, and D. T. Son, *'Bottom-up' thermalization in heavy ion collisions*, *Phys. Lett. B* **502** (2001) 51–58, [hep-ph/0009237].
- [52] J. Berges, S. Borsanyi, and J. Serreau, *Thermalization of fermionic quantum fields*, *Nucl. Phys. B* **660** (2003) 51–80, [hep-ph/0212404].

- [53] J. Berges and J. Cox, *Thermalization of quantum fields from time-reversal invariant evolution equations*, *Phys. Lett.* **B517** (2001) 369–374, [hep-ph/0006160].
- [54] J. Baacke and A. Heinen, *Nonequilibrium evolution of ϕ^4 theory in 1+1 dimensions in the 2PPI formalism*, *Phys. Rev.* **D67** (2003) 105020, [hep-ph/0212312].
- [55] F. Cooper, J. F. Dawson, and B. Mihaila, *Quantum dynamics of phase transitions in broken symmetry $\lambda\phi^4$ field theory*, *Phys. Rev.* **D67** (2003) 056003, [hep-ph/0209051].
- [56] S. Mrowczynski, *Plasma instability at the initial stage of ultrarelativistic heavy ion collisions*, *Phys. Lett.* **B314** (1993) 118–121.
- [57] S. Mrowczynski, *Color collective effects at the early stage of ultrarelativistic heavy ion collisions*, *Phys. Rev.* **C49** (1994) 2191–2197.
- [58] S. Mrowczynski, *Color filamentation in ultrarelativistic heavy-ion collisions*, *Phys. Lett.* **B393** (1997) 26–30, [hep-ph/9606442].
- [59] E.S.Weibel *Phys. Rev. Lett.* **2** (1959) 83.
- [60] M. W. et al., *Experimental observations of the Weibel instability in high intensity laser solid interactions*, *Central Laser Facility (UK) Annual Report* (2002).
- [61] J. Randrup and S. Mrowczynski, *Chromodynamic Weibel instabilities in relativistic nuclear collisions*, nucl-th/0303021.
- [62] P. Arnold, J. Lenaghan, and G. D. Moore, *QCD plasma instabilities and bottom-up thermalization*, *JHEP* **08** (2003) 002, [hep-ph/0307325].
- [63] A. Rebhan, *Thermal gauge field theories*, *Lect. Notes Phys.* **583** (2002) 161–208, [hep-ph/0105183].
- [64] R. Kobes, G. Kunstatter, and A. Rebhan, *Gauge dependence identities and their application at finite temperature*, *Nucl. Phys.* **B355** (1991) 1–37.
- [65] J.-P. Blaizot, E. Iancu, and R. R. Parwani, *On the screening of static electromagnetic fields in hot QED plasmas*, *Phys. Rev.* **D52** (1995) 2543–2562, [hep-ph/9504408].
- [66] A. Cucchieri, F. Karsch, and P. Petreczky, *Propagators and dimensional reduction of hot $SU(2)$ gauge theory*, *Phys. Rev.* **D64** (2001) 036001, [hep-lat/0103009].

- [67] E. Braaten and R. D. Pisarski, *Calculation of the gluon damping rate in hot QCD*, *Phys. Rev. D* **42** (1990) 2156–2160.
- [68] R. D. Pisarski, *Damping rates for moving particles in hot QCD*, *Phys. Rev. D* **47** (1993) 5589–5600.
- [69] F. Flechsig, A. K. Rebhan, and H. Schulz, *The infrared sensitivity of screening and damping in a quark - gluon plasma*, *Phys. Rev. D* **52** (1995) 2994–3002, [hep-ph/9502324].
- [70] M. I. Gorenstein and S.-N. Yang, *Gluon plasma with a medium dependent dispersion relation*, *Phys. Rev. D* **52** (1995) 5206–5212.
- [71] J. P. Blaizot, E. Iancu, and A. Rebhan, *Self-consistent hard-thermal-loop thermodynamics for the quark-gluon plasma*, *Phys. Lett. B* **470** (1999) 181–188, [hep-ph/9910309].
- [72] B. Vanderheyden and G. Baym, *Self-consistent approximations in relativistic plasmas: quasiparticle analysis of the thermodynamic properties*, hep-ph/9803300.
- [73] A. Arrizabalaga and J. Smit, *Gauge-fixing dependence of Φ -derivable approximations*, *Phys. Rev. D* **66** (2002) 065014, [hep-ph/0207044].
- [74] P. Romatschke, *Cold deconfined matter EOS through an HTL quasi-particle model*, hep-ph/0210331.
- [75] A. Ipp and A. Rebhan, *Thermodynamics of large- $N(f)$ QCD at finite chemical potential*, *JHEP* **06** (2003) 032, [hep-ph/0305030].
- [76] A. Ipp, A. Gerhold, and A. Rebhan, *Anomalous specific heat in high-density QED and QCD*, hep-ph/0309019.
- [77] A. Rebhan and P. Romatschke, *HTL quasiparticle models of deconfined QCD at finite chemical potential*, hep-ph/0304294.
- [78] G. D. Moore, *Pressure of hot QCD at large $N(f)$* , *JHEP* **10** (2002) 055, [hep-ph/0209190].
- [79] A. Rebhan, *HTL-resummed thermodynamics of hot and dense QCD: An update*, hep-ph/0301130.
- [80] A. K. Rebhan, *The non-Abelian Debye mass at next-to-leading order*, *Phys. Rev. D* **48** (1993) 3967–3970, [hep-ph/9308232].
- [81] H. Schulz, *Gluon plasma frequency: The next-to-leading order term*, *Nucl. Phys. B* **413** (1994) 353–395, [hep-ph/9306298].

- [82] R. A. Schneider, *The QCD running coupling at finite temperature and density*, hep-ph/0303104.
- [83] R. V. Gavai, S. Gupta, and P. Majumdar, *Susceptibilities and screening masses in two flavor QCD*, *Phys. Rev. D* **65** (2002) 054506, [hep-lat/0110032].
- [84] A. Vuorinen, *Quark number susceptibilities of hot QCD up to $g^6 \ln(g)$* , *Phys. Rev. D* **67** (2003) 074032, [hep-ph/0212283].
- [85] A. Vuorinen, "private communication."
- [86] K. Kajantie, M. Laine, K. Rummukainen, and M. E. Shaposhnikov, *3d $SU(N)$ + adjoint Higgs theory and finite-temperature QCD*, *Nucl. Phys. B* **503** (1997) 357–384, [hep-ph/9704416].
- [87] K. K. Szabo and A. I. Toth, *Quasiparticle description of the QCD plasma, comparison with lattice results at finite T and μ* , *JHEP* **06** (2003) 008, [hep-ph/0302255].
- [88] E. S. Fraga, R. D. Pisarski, and J. Schaffner-Bielich, *Small, dense quark stars from perturbative QCD*, *Phys. Rev. D* **63** (2001) 121702, [hep-ph/0101143].
- [89] U. Kraemmer and A. Rebhan, *Advances in perturbative thermal field theory*, hep-ph/0310337.
- [90] J. J. Drake et. al., *Is RXJ1856.5-3754 a quark star?*, *Astrophys. J.* **572** (2002) 996–1001, [astro-ph/0204159].
- [91] K. Kohri, K. Iida, and K. Sato, *Upper limit on the mass of RX J1856.5-3754 as a possible quark star*, *Prog. Theor. Phys.* **109** (2003) 765–780, [astro-ph/0210259].
- [92] J. R. Oppenheimer and G. M. Volkoff, *On massive neutron cores*, *Phys. Rev.* **55** (1939) 374–381.
- [93] H. Heiselberg and M. Hjorth-Jensen, *Phases of dense matter in neutron stars*, *Phys. Rept.* **328** (2000) 237–327, [nucl-th/9902033].
- [94] D. Blaschke, H. Grigorian, G. Poghosyan, C. D. Roberts, and S. M. Schmidt, *A dynamical, confining model and hot quark stars*, *Phys. Lett. B* **450** (1999) 207–214, [nucl-th/9801060].
- [95] E. S. Fraga, Y. Hatta, R. D. Pisarski, and J. Schaffner-Bielich, *The equation of state for cold and dense strongly interacting matter*, nucl-th/0301062.

- [96] J. D. Bjorken, *Highly relativistic nucleus-nucleus collisions: The central rapidity region*, *Phys. Rev.* **D27** (1983) 140–151.
- [97] P. Braun-Munzinger, K. Redlich, and J. Stachel, *Particle production in heavy ion collisions*, nucl-th/0304013.
- [98] J. P. Blaizot, E. Iancu, and A. Rebhan, *Quark number susceptibilities from HTL-resummed thermodynamics*, *Phys. Lett.* **B523** (2001) 143–150, [hep-ph/0110369].
- [99] P. Romatschke and M. Strickland, *Collective modes of an anisotropic quark gluon plasma*, hep-ph/0304092.
- [100] S. Mrowczynski and M. H. Thoma, *Hard loop approach to anisotropic systems*, *Phys. Rev.* **D62** (2000) 036011, [hep-ph/0001164].
- [101] H.-T. Elze and U. W. Heinz, *Quark - gluon transport theory*, *Phys. Rept.* **183** (1989) 81–135.
- [102] J.-P. Blaizot and E. Iancu, *The quark-gluon plasma: Collective dynamics and hard thermal loops*, *Phys. Rept.* **359** (2002) 355–528, [hep-ph/0101103].
- [103] S. Mrowczynski, *Quasiquarks in anisotropic systems*, *Proceedings of the SEWM 2002 meeting*, World Scientific Publ. Co. (2003) 369–373.
- [104] F. Cooper, C.-W. Kao, and G. C. Nayak, *Non-zero magnetic screening mass in QED and QCD at one loop level in non-equilibrium*, hep-ph/0207370.
- [105] M. C. Birse, C.-W. Kao, and G. C. Nayak, *Magnetic screening effects in anisotropic QED and QCD plasmas*, hep-ph/0304209.
- [106] PHENIX Collaboration, K. Adcox *et. al.*, *Measurement of single electrons and implications for charm production in Au + Au collisions at $s(NN)^{1/2} = 130$ GeV*, *Phys. Rev. Lett.* **88** (2002) 192303, [nucl-ex/0202002].
- [107] R. Baier, D. Schiff, and B. G. Zakharov, *Energy loss in perturbative QCD*, *Ann. Rev. Nucl. Part. Sci.* **50** (2000) 37–69, [hep-ph/0002198].
- [108] A. Accardi *et. al.*, *Hard probes in heavy ion collisions at the LHC: Jet physics*, hep-ph/0310274.
- [109] E. Braaten and M. H. Thoma, *Energy loss of a heavy fermion in a hot plasma*, *Phys. Rev.* **D44** (1991) 1298–1310.

- [110] E. Braaten and M. H. Thoma, *Energy loss of a heavy quark in the quark - gluon plasma*, *Phys. Rev. D* **44** (1991) 2625–2630.
- [111] P. Romatschke and M. Strickland, *Energy loss of a heavy fermion in an anisotropic QED plasma*, hep-ph/0309093.
- [112] G. Moore, “QCD Kinetic theory (lecture), Quantum fields in and out of equilibrium, University of Bielefeld, (2003).”
- [113] M. H. Thoma and M. Gyulassy, *Quark damping and energy loss in the high temperature QCD*, *Nucl. Phys. B* **351** (1991) 491–506.
- [114] J. D. Bjorken, *Energy loss of energetic partons in quark - gluon plasma: Possible extinction of high $p(t)$ jets in hadron - hadron collisions*, . FERMILAB-PUB-82-059-THY.
- [115] H. Vija and M. H. Thoma, *Braaten-Pisarski method at finite chemical potential*, *Phys. Lett. B* **342** (1995) 212–218, [hep-ph/9409246].

Paul Romatschke

Persönliche Information

- Nationalität: Österreicher
- Geburtsdatum: 22.10.1977
- Geburtsstadt: Wels, Oberösterreich
- Familienstand: ledig
- Adresse: Pilgramgasse 13/28, 1050 Wien

Ausbildung

- 1996 Matura mit Auszeichnung, *BG Brucknerstraße, Wels*
- 1998 Erste Diplomprüfung für Technische Physik mit Auszeichnung, *Technische Universität Wien*
- 1999/2000 Erasmus Austauschjahr an der *École Polytechnique Fédéral de Lausanne, Schweiz*
- 2001 Zweite Diplomprüfung für Technische Physik (Studienzweig Theoretische Physik) und Sponsion zum "Diplom-Ingenieur" mit Auszeichnung, *Technische Universität Wien*
- 2001-2003 Doktoratsstudium der technischen Wissenschaften, wissenschaftlicher Mitarbeiter am Institut für Theoretische Physik, *Technische Universität Wien*

Mitgliedschaften

- Mitglied des Österreichischen Alpenvereins
- Mitglied des Symphonischen Orchesters der Technischen Universität Wien
- Mitglied des Chores der Wirtschaftsuniversität Wien

Auszeichnungen

- Verleihung des Dr.Sepp-Käfer Begabtenförderungspreises 1996
- Gewinner des Lokalbewerbes in Wels (1995 & 1996) und des Regionalbewerbes für Oberösterreich, Salzburg und Tirol (1996) der Österreichischen Mathematik-Olympiade